4
Introductory magnetic resonance

Both electrons and atomic nuclei have quantised angular momentum, with an associated magnetic dipole moment. Just as a top precesses when its angular momentum experiences the reorienting torque due to gravity, so electrons and nuclei would be expected to precess when placed in a magnetic field, and to precess at a frequency characteristic of field strength and magnetic dipole moment. In the laboratory magnetic fields available in the 1930s, that frequency was expected to lie in the radiowave part of the electromagnetic spectrum, with the electron frequency being typically three orders of magnitude higher than for most nuclei. How might such precession be observed directly? The idea of Dutch physicist C. J. Gorter was to disturb precessing quantum magnets by resonant perturbation using electromagnetic radiation oscillating at the nuclear precession frequency. His attempt to see this effect for atomic nuclei via heating effects in the surrounding sample were unsuccessful [1, 2]. In 1938, after a visit from Gorter [3], Isador Rabi demonstrated the first evidence for nuclear magnetic resonance through the deflection of atoms in a molecular beam apparatus [4, 5]. The discovery of the magnetic resonance phenomenon in condensed matter, as an absorption of electromagnetic energy from a surrounding radiofrequency antenna, was achieved for electrons by Evgeny Zavoisky in 1944 [6], and for hydrogen nuclei, independently by Felix Bloch [7] and Edward Purcell [8] in 1945.

Of these two types of magnetic resonance, nuclear magnetic resonance (NMR) is the more ubiquitous in application. There are three reasons why 'electron magnetic resonance', more commonly known as electron spin resonance (ESR) or electron paramagnetic resonance (EPR) is a less powerful spectroscopic tool than NMR. The first is the need for an unpaired electron, a feature of free radicals or inorganic complexes possessing a transition metal ion. The second is the very short relaxation time of the resonantly-excited electron spin state, the lifetime before return to thermal equilibrium. For the electron in free radicals or transition metals, this is on the order of or less than a few microseconds, resulting in very broad spectral lines. By contrast, nuclear relaxation time may be as long as seconds, permitting sub-hertz spectral resolution and permitting complex manipulations of spins in the time domain of their quantum evolution. And finally, there are the comparative natures of the interactions of the electron and nuclear spins with their atomic and molecular environments. Each has interactions that provide insight regarding structure and dynamics, but of the two, the nuclear spin interaction, the so-called nuclear spin Hamiltonian, is arguably richer, and made the more powerful by the very high spectral resolution afforded by long nuclear relaxation times.

Translational Dynamics and Magnetic Resonance, First Edition, Paul T. Callaghan, © Paul T. Callaghan 2011.
Published in 2011 by Oxford University Press.

For unpaired electrons the microsecond or sub-microsecond relaxation times leave little opportunity for translational motion measurement. While some such measurements using electrons have been reported, and will be described in later chapters, the main focus of the book is the NMR phenomenon, where long 'relaxation times' allow for sophisticated measurements of a wide range of translational dynamics.

4.1 Introductory remarks

4.1.1 The NMR orchestra

The scope of magnetic resonance is daunting, partly because the interactions of atomic nuclei with their atomic and molecular surroundings are subtle and diverse, and partly because the ways in which the nuclei can be made to respond to those terms by virtue of externally applied electromagnetic fields is almost boundless. The designer of magnetic resonance pulse sequences has at his or her disposal the depth of complexity possible when a composer writes a score for an orchestra. Any book about magnetic resonance faces an obvious problem. Do we attempt to describe the principles governing our 'musical instruments', the nuclei and their interactions, or do we write of the 'orchestral compositions', the encyclopedic collection of possible measurements? And if we seek to do both we must confront our limitations. While we need to at least describe the musical instruments, we cannot write of all possible music.

This book addresses a very limited, though interesting, repertoire, the use of magnetic field gradients to measure translational motion. Rather than pretending to be comprehensive, Chapter 4 merely outlines some of those elements of NMR essential to understanding that repertoire, in particular the information able to be encoded in the phases of the spins and how transmission and reception of resonant radiowaves gives access to that information. To cover the principles of NMR with any sense of completeness requires a complete monograph, rather than a single chapter. For this purpose the reader can find a number of excellent texts [9–18]. Our criterion is simple: to lay out the principles needed to understand the task at hand, the use of NMR to track the migrations of parent molecules by the radiofrequency emissions of the nuclei contained within.

4.1.2 Coherence and the spin echo

At the heart of the remarkable power of magnetic resonance lies the idea of coherence [15]. Coherence in classical physics tell us the degree to which waves are correlated in either space or time or in sense of polarisation, waves being characterised by their 'phase', the correspondence with the angular coordinates of a cyclic phenomenon. In quantum mechanics phase is even more significant, all physical properties resulting in an inherent phase that advances with increasing time. That is the principle underlying the Schrödinger equation. When we deal with nuclear spins whose de Broglie waves are very much shorter than any internuclear spacing, the idea of particle-wave interference is unimportant. But there is another sense it which phase and coherence are manifest. The nuclear spin states have an associated quantum phase, which evolves according to the interaction of the nucleus with surrounding fields. And when we are

dealing with countless numbers of nuclei in the vast ensembles of atoms and molecules in macroscopic matter, then the relative phases of the nuclei are just as important to the superposed quantum components contributing to our measurements as are the relative phases of classical waves to the superposition that results when those waves collide. Well-ordered phase relationships across an ensemble of nuclear spin states are known as coherences. Nuclear spin coherences can be long-lived, on the order of many seconds. And using radiofrequency pulses and bursts of applied magnetic field, we may manipulate coherences almost at will, even to the extent that we may move from a process of decoherence, in which nuclei apparently lose their phase registration, to recoherence, where phases are brought back in step once more. That is the principle of the spin echo.

Of all the developments that have assisted NMR measurements of translational dynamics, none is as important as the discovery of the spin echo by Erwin Hahn in 1950 [19]. Indeed, it can be argued that the power of the spin echo underpins all of modern NMR. The formation of the echo, with its inherent time-reversal properties, not only causes lost signals to re-appear, it also has the effect of removing some nuclear spin interactions while retaining others. Hahn pointed out that in the case where the magnetic field was inhomogeneous, the signal obtained by method was sensitive to translations of spin-bearing molecules, providing, for example, a means of measuring random Brownian motion. We will examine these ideas in detail in the following discussion.

In Chapter 3 we laid out the quantum mechanical basis for a description of spins, including an introduction to the way in which density matrices may be used to handle statistical ensembles of nuclei. We introduced the various interactions that nuclei spins experience due to fields, noting the predominant role of the Zeeman interaction, the response of a spin to a surrounding magnetic field. The scope of Chapter 4 is as follows. First we return to the Zeeman interaction, describing the mechanics of the resonance process whereby spin states may be manipulated using radiofrequency fields. Next we detail the signal detection process and the role of Fourier transformations in magnetic resonance spectroscopy. We then return to the details of the nuclear spin Hamiltonian and its implications for the NMR spectrum, as well as the way in which fluctuations of those interactions induce spin relaxation, the re-establishment of the thermal equilibrium ensemble state via T_1 relaxation, and the irreversible loss of phase coherence known as T_2 relaxation. Finally the chapter outlines some of the fundamental radiofrequency pulse sequence components and corresponding spin ensemble responses, which we will meet throughout the book.

4.2 Resonant excitation

So far, amongst the possible terms of the nuclear spin Hamiltonian, we have met just the static Zeeman interaction. Next we will consider the effect of an oscillating magnetic field that may be turned on and off at will, the so-called resonant radiofrequency field. This, we will find, is the device by which we can disturb ρ_0 from equilibrium and hence detect the evolution of the spin ensemble in the various terms of the remaining spin Hamiltonian.

4.2.1 The rotating frame transformation

One of the most powerful tools in the description of magnetic resonance concerns the use of a frame of reference that rotates around the static field B_0. Here we examine some consequences of rotation.

Reference frame transformations for an anticlockwise rotation by ϕ about the z-axis in the case of a ket, a density matrix, or some observable operator A correspond to the passive view and are therefore respectively written $\exp(i\phi I_z)|\Phi\rangle$, $\exp(i\phi I_z)$ $\rho \exp(-i\phi I_z)$, and $\exp(i\phi I_z) A \exp(-i\phi I_z)$[1].

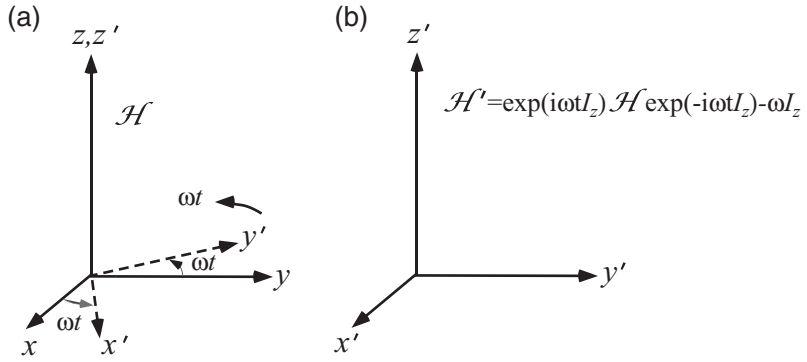

Fig. 4.1 Depiction of primed frame of reference rotating about the unprimed frame z-axis at angular speed ω from the perspective of the (a) unprimed frame and (b) primed frame.

Next, we need to consider the consequences for spin evolution of a time-dependent anticlockwise frame rotation about the z-axis, represented by the operator $\exp(i\omega t I_z)$. This frame rotation is shown in Fig. 4.1. We write the rotated frame ket as $|\Psi'\rangle = \exp(i\omega t I_z)|\Psi\rangle$ and the rotated frame Hamiltonian as $\mathcal{H}_{\text{“rotated”}} = \exp(i\omega t I_z)$ $\mathcal{H} \exp(-i\omega t I_z)$. To understand the evolution we must return to the Schrödinger equation, working in the stationary frame where we can be certain of its applicability. Writing in frequency units (i.e. dropping $\hbar$) we have

$$\begin{aligned} i\frac{\partial}{\partial t} \exp\left(-i\omega t I_z\right) |\Psi'(t)\rangle &= \mathcal{H} \exp\left(-i\omega t I_z\right) |\Psi'(t)\rangle \\ &= \exp\left(-i\omega t I_z\right) \mathcal{H}_{\text{“rotated”}} \exp\left(i\omega t I_z\right) \exp\left(-i\omega t I_z\right) |\Psi'(t)\rangle \end{aligned} \tag{4.1}$$

whence

$$i\frac{\partial}{\partial t}|\Psi'(t)\rangle = \left(\mathcal{H}_{\text{“rotated”}} - \omega I_z\right) |\Psi'(t)\rangle \tag{4.2}$$

Notice that if we are to retain the same form for the Schrödinger equation in the primed frame, then the primed-frame Hamiltonian must be modified by the subtraction of the term ωI_z so that

[1]The latter two ‘sandwich operations’ are easy to understand. Working from right to left, as always in our sequential application or operators, and starting from our rotated frame applicable to the description, $\exp(-i\phi I_z)$ takes us back to the starting (unrotated) frame, the known operator in this starting frame is then applied, following which we return to the rotated frame via $\exp(i\phi I_z)$.

$$\mathcal{H}' = \exp\left(i\omega t I_z\right) \mathcal{H} \exp\left(-i\omega t I_z\right) - \omega I_z \tag{4.3}$$

The idea that additional terms arise in rotating frames of reference is familiar to us in Newtonian mechanics. Retaining Newton's laws in a rotating frame involves introduction of a centrifugal force and a Coriolis force. The additional energy term that arises from requiring Schrödinger's equation to apply in a rotating frame should not surprise us.

Suppose that our Hamiltonian is due to a static magnetic field B_0 along the z-axis so that $\mathcal{H}_{\text{Zeeman}} = -\gamma B_0 I_z$. Then, from eqn 4.3, in the rotating frame

$$\mathcal{H}'_{\text{Zeeman}} = -\gamma \left(B_0 + \omega/\gamma\right) I_z \tag{4.4}$$

The additional term looks exactly like a z-axis field, ω/γ, with sign sensitive to the sign of ω. If the rotation sense is clockwise, that is in the same sense as the precession of the spin phases for positive gyromagnetic ratio γ, then the effective magnetic field long the z-axis is reduced to $B_0 - |\omega|/\gamma$. The reason for the reduction in apparent longitudinal field is easily understood since the apparent precessional rotation of the spin phases about the z-axis is reduced by ω. If we are to preserve the Schrödinger equation then we must interpret the magnetic field as having been reduced accordingly.

4.2.2 The resonant radiofrequency field

Suppose we add to the Zeeman interaction arising from the static field B_0, an interaction due to a field, $2B_1$, oscillating at frequency, ω, along a laboratory-frame transverse axis, which we will take to be x. Then the new Hamiltonian is

$$\mathcal{H}_{\text{lab}} = -\gamma B_0 I_z - 2\gamma B_1 \cos\left(\omega t\right) I_x \tag{4.5}$$

It is helpful to represent the linearly polarised oscillatory field as two counter-rotating circularly polarised components each of amplitude B_1 as shown in Fig. 4.2. Hence we may rewrite eqn 4.5

$$\mathcal{H}_{\text{lab}} = -\gamma B_0 I_z - \gamma B_1 \exp\left(i\omega t I_z\right) I_x \exp\left(-i\omega t I_z\right) - \gamma B_1 \exp\left(-i\omega t I_z\right) I_x \exp\left(i\omega t I_z\right) \tag{4.6}$$

To better understand eqn 4.6 it is helpful to make a coordinate transformation to the frame of reference rotating at frequency ω about the z-axis in the same (clockwise) sense as the spin phases. We find

$$\mathcal{H}_{\text{rot}} = -\gamma \left(B_0 - \omega/\gamma\right) I_z - \gamma B_1 I_x - \gamma B_1 \exp\left(-i2\omega t I_z\right) I_x \exp\left(i2\omega t I_z\right) \tag{4.7}$$

Note that $\mathcal{H}_{\text{rot}}$ should not be confused with $\mathcal{H}_{\text{“rotated”}}$. It is the true effective Hamiltonian in the rotating frame and is the $\mathcal{H}'$ of eqn 4.3.

The final term in eqn 4.7, the so-called counter-rotating component, is fluctuating at 2ω. Suppose we make the B_1 field oscillate at a radiofrequency close to the Larmor precession rate $\omega_0 = \gamma B_0$. If the amplitude of this RF field, B_1, is much smaller than the static field B_0, then $\omega \sim \omega_0 \gg \gamma B_1$ and so the counter-rotating component fluctuates much more rapidly than its size in frequency units. This results in the spins

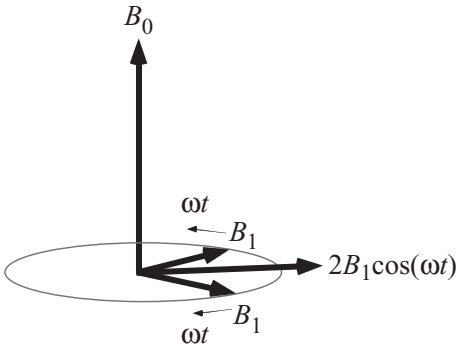

Fig. 4.2 Linearly polarised oscillating magnetic field, $2B_1 \cos(\omega t)$, represented as two counter-rotating circularly polarised fields.

experiencing only the fluctuating field's average value of zero, so that the rotating-frame Hamiltonian simplifies to retain only the co-rotating component and

$$\mathcal{H}_{\text{rot}} = -\gamma \left(B_0 - \omega/\gamma\right) I_z - \gamma B_1 I_x \tag{4.8}$$

Equation 4.8 has a very simple interpretation. At resonance, $\omega = \omega_0$ and the apparent longitudinal field vanishes, thus leaving the effective RF field along the rotating frame x-axis. Earlier, it was shown that the evolution arising from a static magnetic field, is equivalent to a rotation of spin phase about the field axis. As a consequence, the effect of a resonant RF field is to cause the to nutate about the B_1 axis as shown in Fig. 4.3. For example, a pulse of duration t_p, such that $\gamma B_1 t_p = \pi/2$, would reorient the spin magnetisation to the y-axis of the rotating frame. Such a pulse is known as a 90° or $\pi/2$ pulse. Equivalently a 180° pulse would invert the equilibrium magnetisation from I_z to $-I_z$. This disturbance from equilibrium is the NMR phenomenon.

Of course, the I_x operator, which dominates the rotating-frame Hamiltonian at resonance, is just the linear combination of the raising and lowering operators, $\frac{1}{2}\left(I_+ + I_-\right)$. This tells us that, in the case $I = 1/2$, evolution of the system with time corresponds to an inter-conversion of each spin between $\left|\frac{1}{2}\right\rangle$ and $\left|-\frac{1}{2}\right\rangle$, at a rate $\omega_1 = \gamma B_1$.

We can now interpret the resonant re-orientation process for a starting thermal equilibrium density matrix, which, in the laboratory frame, is $\rho^{\text{lab}}(0) \sim I_z$. We begin by transforming our frame of reference from the laboratory to the rotating frame. That requires a passive view rotation of $-\omega_0 t$ about z. In the frame rotating clockwise at ω_0 about the z-axis

$$\rho^{\text{rot}}(0) = \exp\left(-i\omega_0 t I_z\right) \rho^{\text{lab}}(0) \exp\left(i\omega_0 t I_z\right) \sim I_z \tag{4.9}$$

meaning that the starting density matrix is identical in the laboratory and rotating frames. Hence the rotating-frame description of the nutation process is given by an active view rotation by $-\omega_1 t$ about x, namely

$$\begin{aligned} \rho^{\text{rot}}(t) &\sim \exp\left(i\omega_1 t I_x\right) I_z \exp\left(-i\omega_1 t I_x\right) \\ &\sim I_z \cos\left(\omega_1 t\right) + I_y \sin\left(\omega_1 t\right) \end{aligned} \tag{4.10}$$

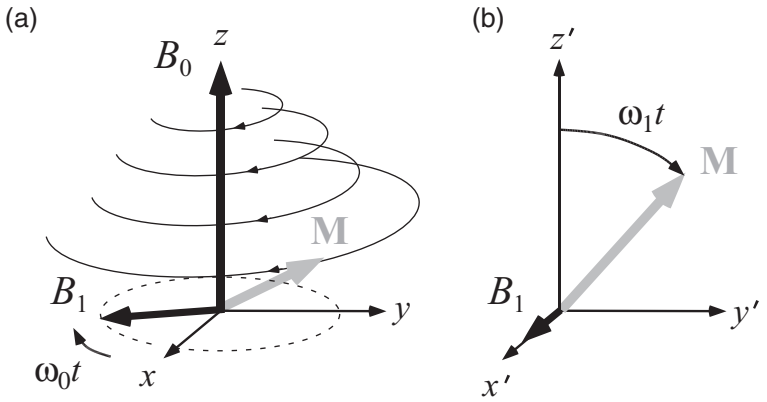

Fig. 4.3 Evolution of nuclear spins in the presence of a resonant RF magnetic field. The ensemble of spins is represented by a magnetisation vector. (a) Evolution in the laboratory frame, in the presence of a longitudinal magnetic field, $\mathbf{B}_0$, and a transverse rotating field, $\mathbf{B}_1$. On resonance the rotation rate ω is identical to $\omega_0 = \gamma B_0$ and the magnetisation vector simultaneously precesses about $\mathbf{B}_0$ at ω_0 and about $\mathbf{B}_1$ at ω_1. (b) as for (a) but in the rotating frame where $\mathbf{B}_1$ is stationary. The effective longitudinal field at resonance is zero and only the precession about $\mathbf{B}_1$ is apparent.

Rewriting the density matrix in the laboratory frame requires that we transform back via $\exp(i\omega_0 t I_z)\rho^{\mathrm{rot}}(0)\exp(-i\omega_0 t I_z)$ to yield

$$\rho^{\mathrm{lab}}(t) \sim I_z \cos(\omega_1 t) + I_y \cos(\omega_0 t)\sin(\omega_1 t) + I_x \sin(\omega_0 t)\sin(\omega_1 t) \tag{4.11}$$

leading to the laboratory-frame observables, $M_\zeta(t) = N\gamma \,\mathrm{Tr}\left(I_\zeta\, \rho^{\mathrm{lab}}(t)\right)$,

$$\begin{aligned} M_x &= M_0 \sin(\omega_0 t)\sin(\omega_1 t) \\ M_y &= M_0 \cos(\omega_0 t)\sin(\omega_1 t) \\ M_z &= M_0 \cos(\omega_1 t) \end{aligned} \tag{4.12}$$

where $M_0 = N\gamma \,\mathrm{Tr}\,(I_z\, \rho_0)$. This combination of precession about the laboratory-frame z-axis and nutation about the rotating frame x-axis is shown in Fig. 4.3.

Note that these passive view transformations, back and forth between the laboratory and rotating frames, always result in implicit local coordinates. Specifically, the x- and y-directions always correspond to the local frame, whether rotating or laboratory-frame coordinates and in future we will drop the prime label for the rotating frame. We now know how to make the transformation between the laboratory and rotating frames. Clearly our description is much easier in the rotating frame and in most of what follows we will so confine our description.

Suppose that the RF field were not precisely on resonance. In that case the rotating-frame effective magnetic field would have a z-component $(B_0 - \omega/\gamma)$ and be inclined out of the transverse plane. This would lead to an oblique precession as shown in Fig. 4.4. In the extreme case where $\gamma B_1 \ll (B_0 - \omega/\gamma)$, the RF field would be entirely ineffective. This understanding leads to two important consequences. Accurate and

simple reorientations of the spin density matrix between the Cartesian axes of the rotating frame requires that γB_1 not only be much larger than the off-resonant field, but also larger than any remaining terms in the spin Hamiltonian. Since the duration of an RF pulse is on the order of the time taken to produce the desired turn angle, via $(\pi/2)(\gamma B_1)^{-1}$, the bandwidth is therefore $\sim \gamma B_1$ and our requirement is equivalent to saying that bandwidth of the RF pulse is larger than all spin Hamiltonian terms other than the Larmor precession in the Zeeman field. This ensures that during application of the RF pulse, the term $\gamma B_1 I_x$ dominates the Hamiltonian and we may neglect the influence of all other terms over the pulse interval t_p. In this case the depiction of resonant re-orientation by a simple active view rotation operator is faithful. Second, when weak RF pulses are used, the on-resonant condition becomes more stringent, and so allows that we might selectively perturb just a part of the NMR spectrum. The subject of selective excitation pulses is covered in Chapter 5.

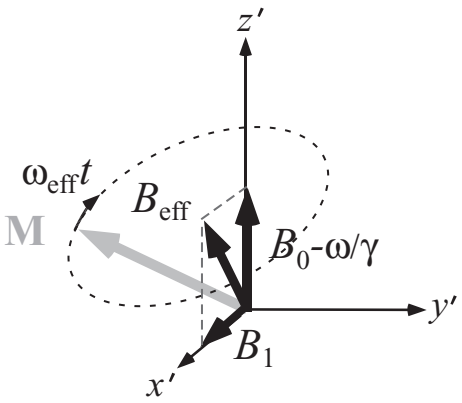

Fig. 4.4 Precession of the nuclear magnetisation vector in the rotating frame when the RF field is off-resonance. The direction of the effective field is determined by the amplitude γB_1 and by the offset frequency $\Delta\omega = \gamma B_0 - \omega$.

It is now easy to visualise the influence of a short burst of resonant RF field, B_1, known in NMR as the RF pulse. If the duration of the pulse is t, the magnetisation will rotate by an angle $\omega_1 t$ about the direction of B_1 in the rotating frame. This is the effect illustrated in Fig. 4.3. At this point in the discussion an obvious question arises. What is the meaning of the direction of B_1 in the laboratory frame where our experiment is performed? Clearly the instantaneous direction will depend on the instant that we start the RF pulse, and that is quite arbitrary. The significance of this direction becomes apparent, however, when a second pulse is applied at some later time. The first pulse establishes an arbitrary reference axis in the rotating frame and, provided that the second pulse oscillates in phase with the first, this axis system will be maintained. Labelling the rotating frame direction of the first pulse as x then the second pulse will also correspond to a field along the x-axis. This immediately suggests that the rotating-frame RF field direction can be oriented at will simply by changing the phase of the pulses. In most NMR experiments these phases are shifted

in multiples of 90°. We denote an RF pulse with duration t as $\theta_{\pm x}$ or $\theta_{\pm y}$, where $\theta = \omega_1 t$ (expressed in degrees) and the subscript indicates the phase according to the chosen direction in the rotating frame.

NMR can be performed with an almost infinite array of pulse train possibilities. The capacity of the experimenter to change both the duration and phase of RF pulses, coupled with the existence of a host of environmentally sensitive terms in the nuclear spin interactions, leads to the essential richness of this branch of spectroscopy.

4.2.3 Quantum view of nutation

Having learned to deal with resonant nutation as an active view rotation of the spin system about the direction of the RF pulse in the rotating frame of reference, it is helpful to look in detail at what happens to the eigen kets, ensemble density matrix, and the expectation values for I_x, I_y, and I_z, at various stages during the evolution process.

Single spin-$\frac{1}{2}$

For simplicity, consider the case of a spin-$\frac{1}{2}$ nucleus in the up state along $\mathbf{B}_0$, before the application of an RF pulse ($-\omega_1 t I_x$ in the rotating frame), with nutation angle $-\omega_1 t_p$. Then the rotating-frame description of the pulse evolution requires an active view rotation operator, $U^{\text{nut}}(t_p) = \exp(i\omega_1 t_p I_x)$, as

$$\begin{aligned} U^{\text{nut}}(t_p)|\tfrac{1}{2}\rangle &= \exp\left(i\omega_1 t_p I_x\right) \begin{bmatrix} 1 \\ 0 \end{bmatrix} \\ &= \begin{bmatrix} \cos\left(\frac{1}{2}\omega_1 t_p\right) & i\sin\left(\frac{1}{2}\omega_1 t_p\right) \\ i\sin\left(\frac{1}{2}\omega_1 t_p\right) & \cos\left(\frac{1}{2}\omega_1 t_p\right) \end{bmatrix} \begin{bmatrix} 1 \\ 0 \end{bmatrix} \\ &= \begin{bmatrix} \cos\left(\frac{1}{2}\omega_1 t_p\right) \\ i\sin\left(\frac{1}{2}\omega_1 t_p\right) \end{bmatrix} \end{aligned} \tag{4.13}$$

Using the angular momentum operators from Table 3.1 it is easy to show the following expectation values after this nutation

$$\begin{aligned} \langle I_z \rangle &= \frac{1}{2}\cos\left(\omega_1 t_p\right) \\ \langle I_y \rangle &= \frac{1}{2}\sin\left(\omega_1 t_p\right) \\ \langle I_x \rangle &= 0 \end{aligned} \tag{4.14}$$

This looks, to all intents and purposes, like the rotation of the spin vector by an angle $-\omega_1 t_p$ about the x-axis in the rotating frame.

However, it is important to realise that throughout the experiment we retain the description of the spin system in terms of its starting I_z eigenstates. What this means is that no matter how simple the description, in terms of the spin being definitely pointing along an axis inclined to z, in the original frame, the RF pulse has produced a superposition state of 'up' and 'down'. Let us take the example of a 90° RF pulse for which $\omega_1 t_p = \pi/2$. The resulting state 'spin pointing along y in the rotating frame', is

in fact the superposition $\frac{1}{\sqrt{2}}|\frac{1}{2}\rangle + \frac{i}{\sqrt{2}}|-\frac{1}{2}\rangle$ in terms of the starting eigenbasis. Figure 4.5 shows how we might depict this.

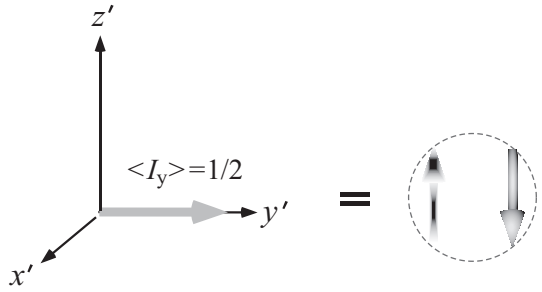

Fig. 4.5 State of spin which starts as $+\frac{1}{2}$ eigenstate of I_z following a 90°_x RF pulse. The expectation value $\langle I_y \rangle = -\frac{1}{2}$ but in terms of the original eigenbasis the final state is a coherent superposition of $+\frac{1}{2}$ and $-\frac{1}{2}$.

And what happens subsequent to the 90° nutation? In the rotating frame, where no Hamiltonian is felt once the RF pulse stops, the spin state remains constant. But in the laboratory frame the Larmor precession continues unabated so that we may write, using the active view operator for a clockwise rotation $-\omega_0 t$ about z, $U^{\text{Larmor}}(t) = \exp(i\omega_0 t I_z)$,

$$\begin{aligned} U^{\text{Larmor}}(t)U^{\text{nut}}(t_p)|\tfrac{1}{2}\rangle &= \begin{bmatrix} \exp(i\omega_0 t/2) & 0 \\ 0 & \exp(-i\omega_0 t/2) \end{bmatrix} \begin{bmatrix} \frac{1}{\sqrt{2}} \\ \frac{i}{\sqrt{2}} \end{bmatrix} \\ &= \frac{1}{\sqrt{2}} \begin{bmatrix} \exp(i\omega_0 t/2) \\ i\exp(-i\omega_0 t/2) \end{bmatrix} \end{aligned} \tag{4.15}$$

This is a coherent superposition state, in which the magnitudes of the amplitudes remain unchanged while their relative phases rotate at a rate ω_0.

Ensemble spin-$\frac{1}{2}$

To handle the case of the ensemble of spins, with the initial state being thermal equilibrium in the Zeeman field, we turn to the density matrix description, and starting with the state

$$\rho(0_-) = \begin{bmatrix} p_\uparrow & 0 \\ 0 & p_\downarrow \end{bmatrix} \tag{4.16}$$

where $p_\uparrow = \overline{|a_{1/2}|^2}$ and $p_\downarrow = \overline{|a_{-1/2}|^2}$. That only the spin excess can contribute to any measurement is made clear by rewriting ρ as

$$\rho(0_-) = \frac{1}{2}\begin{bmatrix} 1 & 0 \\ 0 & 1 \end{bmatrix} + \frac{1}{2}\begin{bmatrix} (p_\uparrow - p_\downarrow) & 0 \\ 0 & -(p_\uparrow - p_\downarrow) \end{bmatrix} \tag{4.17}$$

Now let us apply an ideal 90° RF pulse about the rotating frame x-axis, again using active view operators. The final density matrix is $\rho(0_+)$ given by

$$\begin{aligned}\rho(0_+) &= U^{\text{nut}}(t_p)\,\rho(0_-)\,U^{\text{nut}}(t_p)^{-1} \\ &= \begin{bmatrix}1/\sqrt{2} & i/\sqrt{2}\\ i/\sqrt{2} & 1/\sqrt{2}\end{bmatrix}\begin{bmatrix}p_\uparrow & 0\\ 0 & p_\downarrow\end{bmatrix}\begin{bmatrix}1/\sqrt{2} & -i/\sqrt{2}\\ -i/\sqrt{2} & 1/\sqrt{2}\end{bmatrix} \\ &= \frac{1}{2}\begin{bmatrix}1 & -i(p_\uparrow - p_\downarrow)\\ i(p_\uparrow - p_\downarrow) & 1\end{bmatrix}\end{aligned} \tag{4.18}$$

noting $p_\uparrow + p_\downarrow = 1$. The off-diagonal elements of the density matrix proportional to the spin excess represent states of 1-quantum coherence. Indeed what we have at time 0_+ is a mixed state ensemble in which a population $p_\uparrow$ is a sub-ensemble of kets $|\psi\rangle = \frac{1}{\sqrt{2}}\left|\frac{1}{2}\right\rangle + \frac{i}{\sqrt{2}}\left|-\frac{1}{2}\right\rangle$ and a population $p_\downarrow$ is a sub-ensemble of kets $\frac{i}{\sqrt{2}}\left|\frac{1}{2}\right\rangle + \frac{1}{\sqrt{2}}\left|-\frac{1}{2}\right\rangle$, corresponding to spin states pointing respectively along the rotating frame y and $-y$ axes.[2]

There is no need to calculate the effect of subsequent Larmor precession in the laboratory frame since by now it should be obvious. The spin vectors lying along y and $-y$ simply rotate at ω_0 in the transverse plane. To check this we need only apply the Larmor evolution sandwich $\rho(t) = U^{\text{Larmor}}(t)\,\rho(0_+)\,U^{\text{Larmor}}(t)^{-1}$. More interesting is the case where not every spin experiences the same magnetic field, for example when the Zeeman magnetic field is inhomogeneous. Staying in the rotating frame, we can represent this by considering the precession that arises from an offset frequency $\Delta\omega_0$, namely

$$\begin{aligned}\rho(t) &= \overline{\begin{bmatrix}e^{\frac{i}{2}\Delta\omega_0 t} & 0\\ 0 & e^{-\frac{i}{2}\Delta\omega_0 t}\end{bmatrix}\frac{1}{2}\begin{bmatrix}1 & -i(p_\uparrow - p_\downarrow)\\ i(p_\uparrow - p_\downarrow) & 1\end{bmatrix}\begin{bmatrix}e^{-\frac{i}{2}\Delta\omega_0 t} & 0\\ 0 & e^{\frac{i}{2}\Delta\omega_0 t}\end{bmatrix}} \\ &= \frac{1}{2}\begin{bmatrix}1 & -i(p_\uparrow - p_\downarrow)\overline{\exp(-i\Delta\omega_0 t)}\\ i(p_\uparrow - p_\downarrow)\overline{\exp(i\Delta\omega_0 t)} & 1\end{bmatrix}\end{aligned} \tag{4.19}$$

A first look at relaxation

Suppose that we have a distribution of offsets $f(\Delta\omega_0)$. The terms $\overline{\exp(i\Delta\omega_0 t)}$ represent the integral

$$F(t) = \int_{-\infty}^{\infty} f(\Delta\omega_0)\exp(i\Delta\omega_0 t)\,d\Delta\omega_0 \tag{4.20}$$

where $F(t)$ is the Fourier transform of $f(\Delta\omega_0)$. For a symmetric distribution of $\Delta\omega_0$ about the mean Larmor frequency, that is about zero in the rotating frame, $\overline{\exp(i\Delta\omega_0 t)}$ represents a decay from unity, a progressive loss of phase coherence in the spin ensemble due to the distribution of field offsets and a consequent continuous decay of transverse magnetisation. This describes what is known as the T_2^* relaxation process. With time-reversal, something that is possible using the spin echo, this inhomogeneous broadening decay may be reversed.

However, other processes contribute to a decay that is inherently stochastic in nature and hence irreversible. Look at the density matrix off-diagonal terms of the form $\overline{|a_\uparrow||a_\downarrow|e^{i(\phi_\uparrow - \phi_\downarrow)}}$, arising from quantum superposition states $|\Psi\rangle = |a_\uparrow|e^{i\phi_\uparrow}\,|\uparrow\rangle + |a_\downarrow|e^{i\phi_\downarrow}\,|\downarrow\rangle$. These contribute the single-quantum coherence that is manifest as

[2] To convert one to the other apply the spin=1/2 rotation matrix $R_z(\pi)$.

transverse magnetisation. Spin–spin relaxation processes involve energy-conserving 'flip-flop' terms in which the phases $\phi_\uparrow$ and $\phi_\downarrow$ fluctuate, thus causing $|a_\uparrow||a_\downarrow|e^{i(\phi_\uparrow - \phi_\downarrow)}$ to decay. At the same time, energy-absorbing spin–lattice processes involves changes in the magnitudes $|a_\uparrow|$ and $|a_\downarrow|$ as the spins regain thermal equilibrium, a state in which, for any spin, either $|a_\uparrow|$ or $|a_\downarrow|$ is zero. Both spin–lattice and spin–spin processes cause the decay of the transverse magnetisation. Only spin–lattice processes can contribute to the restoration of thermal equilibrium and the growth of $\langle I_z \rangle$. For this reason the transverse relaxation rate T_2^{-1} always exceeds the longitudinal rate T_1^{-1}.

4.2.4 Classical descriptions of resonant reorientation

Classical precession

Precession and nutation are very familiar phenomena in classical physics, a simple example being provided by the case of a spinning wheel whose axle is suspended at a pivot point by a string, as shown in Fig. 4.6. The gravitational force acting through the centre of mass provides a torque, τ, whose direction is normal to the direction of the wheel's angular momentum, thus resulting in an azimuthal precession about the vertical axis. The magnitude of the torque is $mgd\sin\theta$, where d is the distance from the centre of mass to the pivot and θ is the polar angle to the vertical made by the axle, and hence the angular momentum vector. Of course Newton's second law requires that the rate of change of angular momentum is equal to that torque, as

$$\Delta \mathbf{L} = \tau \Delta t \tag{4.21}$$

Figure 4.6 shows that the change in azimuthal orientation of the angular momentum in time Δt is $\Delta\phi = \Delta L / L\sin\theta$, and so the precession frequency is

$$\begin{aligned} \omega_0 &= \frac{\Delta\phi}{\Delta t} = \frac{mgd\sin\theta\Delta t}{L\sin\theta\Delta t} \\ &= \frac{mgd}{L} \end{aligned} \tag{4.22}$$

The spinning wheel example is very similar to the case of a magnetic dipole moment μ with co-linear angular momentum, placed in a vertical magnetic field B_0, as shown in Fig. 4.7. The only difference is that the torque is now $\mu B_0 \sin\theta$. For exact analogy with the wheel geometry, we depict a dipole with negative magnetogyric ratio, i.e. with the angular momentum vector oppositely directed to the dipole moment. Following the same reasoning as for the wheel we have

$$\begin{aligned} \omega_0 &= \frac{\Delta\phi}{\Delta t} = \frac{\mu B_0 \sin\theta\Delta t}{L\sin\theta\Delta t} \\ &= \frac{\mu B_0}{L} \\ &= \gamma B_0 \end{aligned} \tag{4.23}$$

Note that in both cases, the precession frequency, ω_0, is independent of polar angle θ.

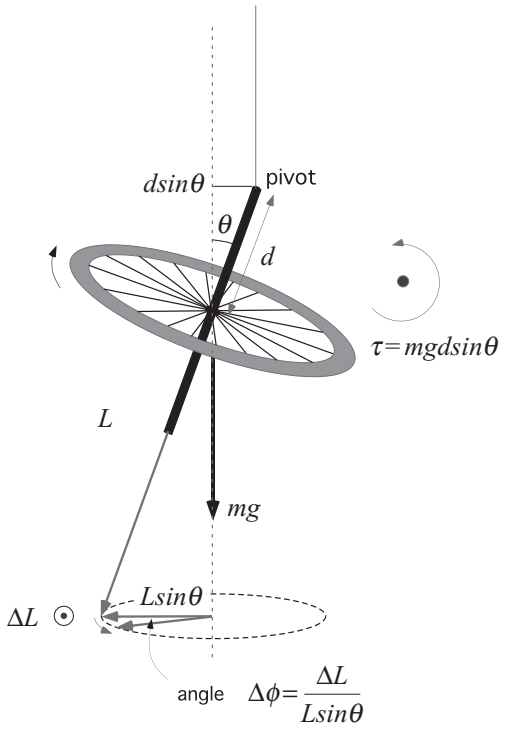

Fig. 4.6 Precession of a spinning mechanical wheel with angular momentum L, while suspended from a pivot on a string. The tension in the string exerts a torque $\tau = mg\sin\theta$ about the wheel centre. This torque, which is normal to the plane of the diagram, causes a rate of change of angular momentum, also normal to the plane, of $\Delta L/\Delta t = \tau$. This results in the angular momentum vector **L** precessing as shown in the lower circle, at a rate independent of θ.

Classical resonant nutation

We have seen that for the precession of a magnetic dipole with angular momentum, the introduction of a transverse magnetic field co-rotating at the Larmor frequency γB_0 causes resonant re-orientation. Is there an analogy for resonant re-orientation for the wheel? Indeed there is, as is shown in Fig. 4.8. Here we introduce another torque, τ_1, normal to both the angular momentum vector and the torque provided by gravity. The mechanism for achieving this is to apply a transverse force, F_1, to the axle which follows the precessional motion. To do so the force must rotate along with the precession, an effect which could result if we were to pull horizontally on a string attached to the end of the axle (at a distance $2d$ from the pivot), at the same time moving our hand in a circular path so that we stayed in step with the circular motion. Now the direction of the torque is such as to cause a change in polar inclination, θ, of the angular momentum L as $\Delta\theta = \Delta L'/L$. The magnitude of the torque is $\tau_1 = F_1 2d$, leading to a nutation frequency

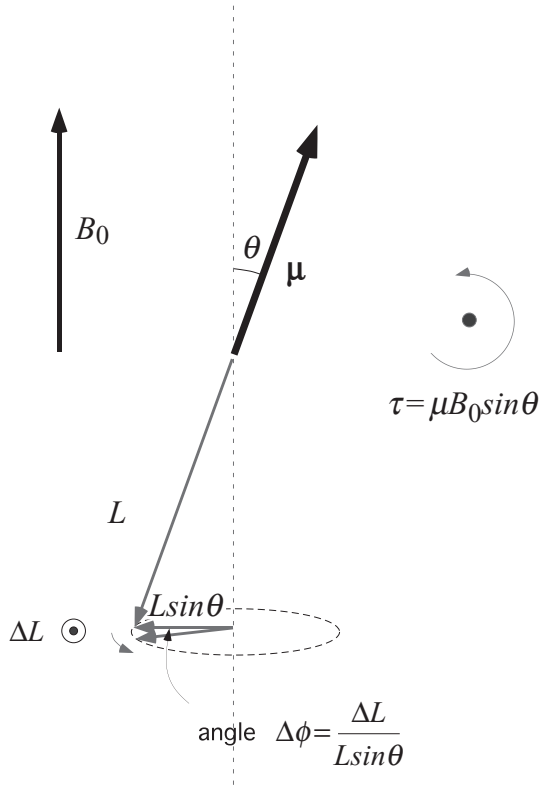

Fig. 4.7 Classical dipole with angular momentum immersed in a magnetic field that exerts a torque $\mu B_0 \sin\theta$, normal to the plane of the diagram, and hence a rate of change of angular momentum, also normal to the plane, of $\Delta L/\Delta t = \tau$. This results in the angular momentum vector **L** precessing, as shown in the lower circle, at a rate independent of θ.

$$\begin{aligned} \omega_1 &= \frac{\Delta\theta}{\Delta t} \\ &= \frac{F_1 2d}{L} \end{aligned} \tag{4.24}$$

The nutation process is quite independent of the precession around the polar axis which continues unabated at frequency ω_0. It results in a continuous polar reorientation of the angular momentum vector at a nutation frequency ω_1 which is independent of polar angle.

4.2.5 Semi-classical description

In the case of independent spin-$\frac{1}{2}$ nuclei, the motion of the ensemble of spins may always be described in terms of the precession of the spin magnetisation vector **M**. In such a model the macroscopic angular momentum vector is simply $\mathbf{M}/\gamma$. By equating the torque to the rate of change of angular momentum we obtain

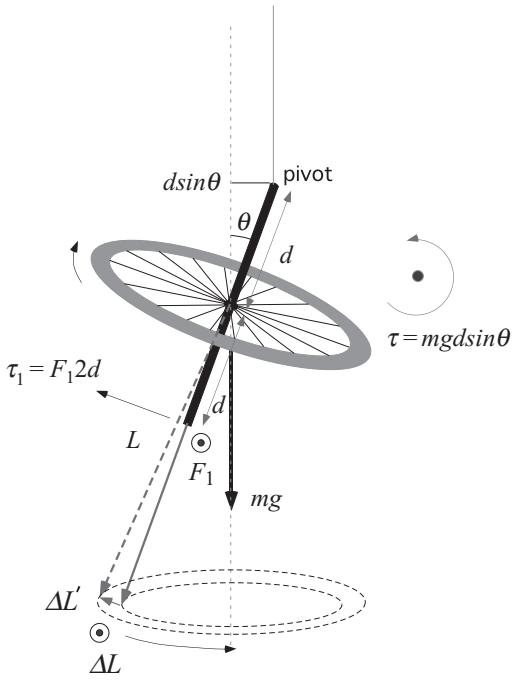

Fig. 4.8 As for Fig. 4.6, but with an additional resonant nutational torque τ_1 applied normal to the precessional torque τ and circulating in reference to the precession at exactly the Larmor frequency.

$$\frac{d\mathbf{M}}{dt} = \gamma \mathbf{M} \times \mathbf{B} \tag{4.25}$$

The solution to eqn 4.25 when $\mathbf{B}$ is a magnetic field of amplitude B_0 corresponds to a precession of the magnetisation about the field at rate $\omega_0 = \gamma B_0$, the Larmor frequency. The resonance phenomenon results on application of a transverse magnetic field oscillating at ω_0. To obtain the expression for the spin evolution we need retain only the circularly polarised component of the oscillating transverse field that is rotating in the same sense as the spin precession, namely

$$\mathbf{B}_1(t) = B_1 \cos(\omega_1 t)\,\mathbf{i} - B_1 \sin(\omega_1 t)\,\mathbf{j} \tag{4.26}$$

where $\mathbf{i}$, $\mathbf{j}$ and $\mathbf{k}$ are unit vectors along the x-, y- and z-axes, respectively. Then, under the same starting condition, $\mathbf{M}(0) = M_0\mathbf{k}$, eqns 4.25 and 4.26 return the result derived from quantum mechanics, eqns 4.12.

4.2.6 Relaxation and the Bloch equations

The effect of a resonant RF pulse is to disturb the spin system from its thermal equilibrium state. In due course, that equilibrium will be restored by a process known as spin–lattice relaxation. As the name implies, the process involves an exchange of

energy between the spin system and the surrounding thermal reservoir, known as the 'lattice', with which it is in equilibrium. The equilibrium is characterised by a state of polarisation with magnetisation M_0 directed along the longitudinal magnetic field, B_0. The restoration of this equilibrium is therefore alternatively named longitudinal relaxation. The phenomenological description of this process is given by the equation

$$\frac{dM_z}{dt} = -\frac{M_z - M_0}{T_1} \tag{4.27}$$

with solution

$$M_z(t) = M_z(0) + M_0(1 - \exp(-t/T_1)) \tag{4.28}$$

T_1 is known as the spin–lattice or longitudinal relaxation time. At room temperature it is typically in the range 0.1 to 10 seconds for protons in dielectric materials.

At first sight it may appear that the time constant T_1 will also describe the lifetime of transverse magnetisation resulting from the application of an RF pulse. In fact transverse relaxation, which is characterised by the time constant T_2, is the process whereby nuclear spins come to thermal equilibrium among themselves. It is therefore known also as spin–spin relaxation. While indirect energy exchange via the lattice may play a role, additional direct processes are also responsible. This leads to the result $T_2 < T_1$. As indicated in the earlier quantum mechanical description, transverse magnetisation corresponds to a state of phase coherence between the nuclear spin states. This means that transverse relaxation, unlike longitudinal relaxation, is sensitive to interaction terms that cause the nuclear spins to dephase. As we shall see later in Section 4.5, this may lead to T_2 relaxation being exceedingly rapid in comparison with T_1, where the interaction between the nuclear spins fluctuates very slowly, as in the case of solids or rigid macromolecules. T_2 values are usually in the range 10 ms to 10 s.

The phenomenological description for transverse relaxation is written

$$\frac{dM_{x,y}}{dt} = -\frac{M_{x,y}}{T_2} \tag{4.29}$$

with solution

$$M_{x,y}(t) = M_{x,y}(0)\exp(-t/T_2) \tag{4.30}$$

It should be emphasised that the exponential description applies in the case where the interaction terms responsible for transverse relaxation are weak. This is the regime of Bloembergen, Purcell, and Pound (BPP) theory [20], an approach that works well for spins residing in liquid-state molecules. However, for solids and macromolecules undergoing very slow motions, the decay is more complicated than that represented by eqn 4.30. For most NMR translational motion measurements we are confined to observe slowly relaxing spins for which the phenomenological approach is entirely appropriate.

Combining eqns 4.25, 4.27, and 4.29 in the rotating frame yields a set of relationships known as the Bloch equations [21–23]

$$\begin{aligned}\frac{dM_x}{dt} &= \gamma M_y \left(B_0 - \omega/\gamma\right) - \frac{M_x}{T_2} \\ \frac{dM_y}{dt} &= \gamma B_1 - \gamma M_x \left(B_0 - \omega/\gamma\right) - \frac{M_y}{T_2} \\ \frac{dM_z}{dt} &= -\gamma M_y B_1 - \frac{M_z - M_0}{T_1}\end{aligned} \tag{4.31}$$

These will provide a valuable reference in describing many phenomena important in NMR.

4.3 Signal detection

4.3.1 Free precession and Faraday detection

Resonant nutation of the spins disturbs the spins from equilibrium, but what constitutes the signal in NMR? To understand this point it is helpful to imagine a nutation in which the magnetisation is reoriented to leave a component in the transverse (x-y) plane of the rotating frame, a simple example being the case of a 90°_x pulse that causes the magnetisation to lie along the rotating frame y-axis. Following the application of this RF field the spins now experience only their natural spin Hamiltonian and are said to be in 'free-precession'. Because of the dominant Zeeman Hamiltonian, in the laboratory frame the transverse magnetisation appears to rotate at the Larmor frequency ω_0, though other weaker terms in the spin Hamiltonian may produce more subtle spectral variations.

That Larmor precession of non-equilibrium macroscopic nuclear magnetisation in the laboratory frame provides the means for signal detection. An antenna coil (for example a solenoid with its axis orthogonal to the z-axis as in Fig. 4.9) can detect such free-precession via Faraday induction. The output of that coil is an oscillating voltage. We will not be concerned here with the details of the absolute signal amplitude, which will depend on the dimensions or the RF antenna coil, and its electrical properties such as numbers of turns and resistance. However, with Faraday induction, one important factor which emerges is that the signal strength will be proportional to the Larmor precession frequency, γB_0. Combining this effect with the available magnetisation given by eqn 3.89, it is clear that the total sensitivity of the NMR signal will be proportional to $\gamma^3 B_0^2$. This places a premium on high magnetic field strength and large γ.

There are other methods of detecting the nuclear magnetisation, which are sensitive to magnetic field rather than the time rate of change of magnetic field, examples being the squid magnetometer [24, 25] or atomic magnetometer [26, 27]. For these the relevant sensitivity parameter is $\gamma^2 B_0$. These methods have special advantages for very low field ($< \mu T$) NMR. Also important for enhancing sensitivity by significantly enhancing nuclear magnetisation above the thermal equilibrium value are the so-called hyperpolarisation methods, such as dynamic nuclear polarisation [28, 29] and spin exchange [30–32]. The latter method has particular importance in the study of translational motion in gases and will be discussed further in Chapter 6.

With its gyromagnetic ratio the largest of any stable nucleus, its high isotopic abundance, its ubiquity in the hydrogen atoms of biological tissue, organic molecules, and synthetic and natural materials, the spin-$\frac{1}{2}$ proton is the predominant choice for

NMR applications using thermal polarisation and Faraday detection. Notwithstanding that emphasis, other stable nuclei such as ^{2}H,^{13}C,^{15}N, ^{31}P, and ^{129}Xe present significant specific advantages as we shall see later.

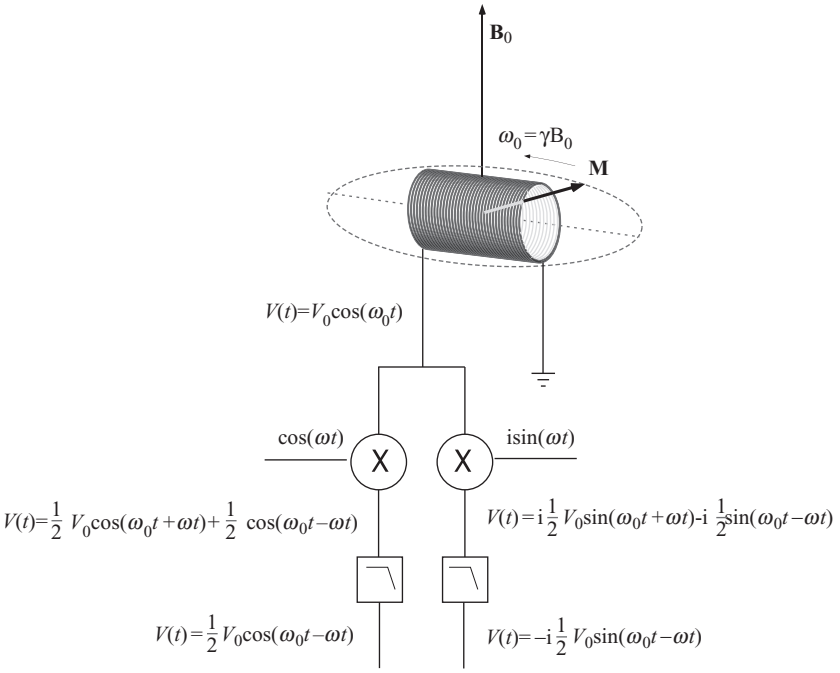

Fig. 4.9 Faraday detection of emf resulting from magnetisation vector **M** precessing at $\omega_0 = \gamma B_0$ in a solenoid coil. Also shown is the heterodyne detection scheme, whereby the complex difference signal $\frac{1}{2}V_0 \exp(-i\,(\omega_0 - \omega)\,t)$ is obtained by a combination of independent mixers and low-pass filters assigned respectively to real and imaginary channels.

Neglecting relaxation for the moment, let us write down an expression for the evolution of laboratory-frame density matrix for the free precession that follows application of an infinitesimally short 90°_{x} RF pulse to the thermal equilibrium ensemble $\rho_0 \sim I_z$. Using the same approach used to generate eqn 4.11, the subsequent time-dependence at time t after the pulse is switched off can be written

$$\rho^{\mathrm{lab}}(t) \sim I_y \cos(\omega_0 t) + I_x \sin(\omega_0 t) \tag{4.32}$$

This density matrix, which represents transverse magnetisation in clockwise rotation about the z-axis, has two orthogonal components of magnetisation that oscillate in quadrature phase at the Larmor frequency. If we were to observe this precession not in the laboratory frame but in a frame rotating clockwise at ω, the result would be

$$\rho^{\mathrm{rot}}(t) \sim I_y \cos((\omega_0 - \omega)\,t) + I_x \sin((\omega_0 - \omega)\,t) \tag{4.33}$$

Now imagine that we were able to make a measurement that could be represented by a complex signal operator $N\gamma\,[I_x + iI_y]$. Of course measurements are always real

numbers, and so the assignment of real and imaginary parts to the signal means that we must detect in two independent channels. But allowing this, such a measurement on the rotating frame density matrix of eqn 4.33 would yield

$$\mathrm{Tr}\left(\left[I_x + iI_y\right]\rho^{\mathrm{rot}}(t)\right) \sim i\,\mathrm{Tr}\left(I_y^2\right)\cos\left(\left(\omega_0 - \omega\right)t\right) + \mathrm{Tr}\left(I_x^2\right)\sin\left(\left(\omega_0 - \omega\right)t\right) \qquad (4.34)$$

Using eqns 3.89 and 3.90 we may then write

$$N\gamma\,\mathrm{Tr}\left(\left[I_x + iI_y\right]\rho^{\mathrm{rot}}(t)\right) = iM_0\exp\left(-i\left(\omega_0 - \omega\right)t\right) \qquad (4.35)$$

The coefficient i tells us that at $t = 0$, when $\rho^{\mathrm{rot}} \sim I_y$, the signal is at a maximum in the quadrature channel. We will see that just such a rotating frame measurement is possible in practice using RF heterodyne detection.

Radiofrequency receivers work by mixing the signal voltage with a the output from a reference RF oscillator, a process known as heterodyning. This method of detection is inherently phase-sensitive. This means that by separately mixing the signal with two heterodyne references, each 90° out of phase, we obtain separate in-phase and quadrature-phase output signals, which are then ascribed to real and imaginary parts of a complex number. Of course, the actual Faraday detection of Larmor precession in a single coil[3] corresponds to a voltage oscillation of the form $V_0\cos\left(\omega_0 t\right)$. Heterodyning with two quadrature channels, assigned respectively to real and imaginary parts, is equivalent to the multiplication

$$V_0\cos\left(\omega_0 t\right)\exp\left(i\omega t\right) = \frac{1}{2}V_0\left[\exp\left(-i\left(\omega_0 - \omega\right)t\right) + \exp\left(i\left(\omega_0 + \omega\right)t\right)\right] \qquad (4.36)$$

The receiver filters reject the sum frequency term and return only the difference $\frac{1}{2}V_0\exp(-i\left(\omega_0 - \omega\right)t)$. This is exactly proportional to the rotating-frame signal generated by the operator $N\gamma\left[I_x + iI_y\right]$. The fact that the negative frequency difference, $(\omega_0 - \omega)$, is measured is irrelevant, merely reflecting the clockwise nature of the spin precession. The important point is that we really are able to measure $[I_x + iI_y]$ in a frame of reference rotating at the heterodyne mixing frequency. Thus we place ourselves naturally in the rotating frame. We not only use a rotating-frame depiction of the RF excitation process but use it equally in the case of detection. Henceforth, the rotating frame will provide the natural perspective from which to discuss magnetic resonance phenomena.

Note that for simple precession in a magnetic field, where the mixing reference is oscillating at the Larmor frequency ω_0, we obtain dc quadrature output signals. At any other mixing frequency ω, the signal will oscillate at the offset frequency $\Delta\omega = \omega_0 - \omega$. The absolute sign attributed to that difference is an arbitrary choice to be made, but the ability to detect both real and imaginary parts of the signal lies at the heart of our ability to distinguish opposite signs of that offset frequency, to have access to both positive and negative domains of $\Delta\omega$. In practice, the absolute phase of the heterodyne receiver will not be identical to that of the precessing magnetisation. For

[3]Some RF antennas employ two orthogonal coils, which independently provide the cosine and sine components of the induced emf. This method can in principle be used to determine the absolute sign of the Larmor precession, unlike heterodyning a single component signal from a single coil.

that reason the signal contains an arbitrary phase factor, $\exp(i\phi)$. This factor can easily be removed in the signal processing as we shall show in the next section.

As a final consideration, let us return to the idea of the multiple quantum coherence discussed in Chapter 3, asking the question, what is the order of coherence p, which is observed in the NMR Faraday detection process? To understand this question we need to return to the definition of our observable as $\mathrm{Tr}\left([I_x + iI_y]\,\rho^{\mathrm{rot}}(t)\right) = \mathrm{Tr}\left(I_+\rho^{\mathrm{rot}}(t)\right)$, where in the case that we wish to distinguish multiple spins, we replace I_+ by $\sum_{i=1}^{K} I_{i+}$. A non-zero signal is only possible when $\rho^{\mathrm{rot}}(t) \sim I_-$, so clearly the detected coherence in NMR is $p = -1$.

4.3.2 Fourier transformation and the spectrum

The measurement of a complex time-domain signal, $S(t)$, lends itself to simple interpretation using the Fourier transformations

$$\begin{aligned} F\{S(t)\} &= s(\omega) \\ &= \int_{-\infty}^{\infty} S(t)\exp\left(i\omega t\right) dt \\ F^{-1}\{s(\omega)\} &= S(t) \\ &= \frac{1}{2\pi}\int_{-\infty}^{\infty} s(f)\exp\left(-i\omega t\right) d\omega \end{aligned} \tag{4.37}$$

or

$$\begin{aligned} F\{S(t)\} &= s(f) \\ &= \int_{-\infty}^{\infty} S(t)\exp\left(i2\pi f t\right) dt \\ F^{-1}\{s(f)\} &= S(t) \\ &= \int_{-\infty}^{\infty} s(f)\exp\left(-i2\pi f t\right) df \end{aligned} \tag{4.38}$$

The use of cyclic frequency $f = \omega/2\pi$ allows for a more symmetric form for the Fourier integral pair and we shall sometimes follow such a description in this book.

Suppose we consider the action of Fourier transformation on a signal corresponding to an oscillation at fixed offset frequency and with relaxation included, i.e.

$$\begin{aligned} S(t) &= S_0\exp\left(i\phi\right)\exp\left(i\Delta\omega t\right)\exp\left(-t/T_2\right) \qquad t \geq 0 \\ &= 0 \qquad t < 0 \end{aligned} \tag{4.39}$$

where S_0 is the signal immediately following the pulse, a number that is simply proportional to M_0. The primary NMR signal is measured in the time domain as an oscillating, decaying electromotive force (emf) induced by the magnetisation in free precession. It is therefore known as the free induction decay (FID). By Fourier transformation the same signal may be represented in the frequency domain. This process is shown in Fig. 4.10 for the case $\phi = 0$. The result in the real part of the domain is

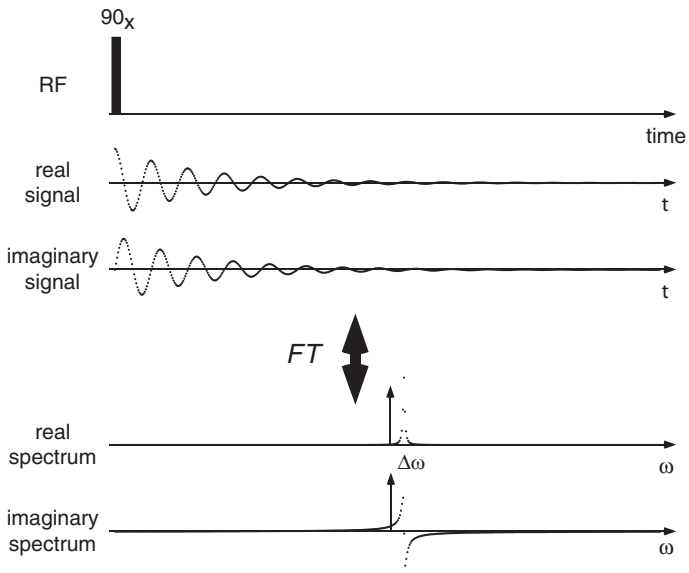

Fig. 4.10 Free induction decay (FID) following a single 90° RF pulse. The real and imaginary parts of the signal correspond to the in-phase and quadrature receiver outputs. The signal is depicted with receiver phase $\phi = 0$ and, on complex Fourier transformation, gives real absorption and imaginary dispersion spectra at the offset frequency $\Delta\omega = \omega_0 - \omega$.

a Lorentzian lineshape of cyclic frequency offset $\Delta\omega/2\pi$ and full-width-half-maximum (FWHM) $1/\pi T_2$, the so-called absorption spectrum,

$$s_{\text{abs}}(\omega) = \frac{T_2}{1 + (\omega - \Delta\omega)^2 T_2^2} \tag{4.40}$$

The imaginary lineshape is known as the dispersion spectrum and for this function the width is somewhat greater.

$$s_{\text{disp}}(\omega) = \frac{(\omega - \Delta\omega)\, T_2^2}{1 + (\omega - \Delta\omega)^2 T_2^2} \tag{4.41}$$

It is an elementary exercise in calculus to show that the real and imaginary parts of $F(S(t))$ are given by

$$\begin{aligned} \text{Re}\left\{F\left\{S(t)\right\}\right\} &= \cos\phi \frac{T_2}{1 + (\omega - \Delta\omega)^2 T_2^2} + \sin\phi \frac{(\omega - \Delta\omega)\, T_2^2}{1 + (\omega - \Delta\omega)^2 T_2^2} \\ \text{Im}\left\{F\left\{S(t)\right\}\right\} &= \sin\phi \frac{T_2}{1 + (\omega - \Delta\omega)^2 T_2^2} - \cos\phi \frac{(\omega - \Delta\omega)\, T_2^2}{1 + (\omega - \Delta\omega)^2 T_2^2} \end{aligned} \tag{4.42}$$

Note that the imaginary dispersion spectrum exists in the case $\phi = 0$, only because the signal is acquired for positive time only. It is hard to imagine what sampling at 'negative time' could possibly mean in the context of the simple experiment being discussed

here, so the existence of the dispersion spectrum seems quite natural. However, where the dephasing of the magnetisation does not result from an irreversible T_2 process, but instead from some coherent interaction, it is possible to produce rephasing as well as dephasing effects. We will return to this point, and the concept of negative time acquisition, in the discussion of spin echoes in Section 4.6.2.

The area under the absorption spectrum is precisely the height of the FID at $t = 0$. The advantage of using the peak integral rather than the FID height in order to determine the NMR signal amplitude is twofold. Of course, integration in the frequency domain allows individual spectral components to be analysed. But, in addition, such integration over a defined frequency width provides a bandpass filtering of the signal, the only noise contribution arising from that lying within the defined spectral limits. Hence, even if only a single spectral component exists, it is highly advantageous to use the area under the spectral peak to determine signal amplitude. To carry out this integration it is necessary to first ensure that the real part of the spectrum is in pure absorption mode. That requires either setting the receiver phase so that $\phi = 0$ or post-processing the data, the latter being the more obviously convenient approach. Where $\phi \neq 0$ the real and imaginary parts of the transformed signal contain admixtures of absorption and dispersion parts and the spectrum may be restored to the 'correct phase' by simply multiplying by $\exp(-i\phi)$. This is equivalent to the operation

$$\begin{aligned} \mathrm{Re}\left\{F\left\{S(t,0)\right\}\right\} &= \cos\phi\ \mathrm{Re}\left\{F\left\{S(t,\phi)\right\}\right\} + \sin\phi\ \mathrm{Im}\left\{F\left\{S(t,\phi)\right\}\right\} \\ \mathrm{Im}\left\{F\left\{S(t,0)\right\}\right\} &= \cos\phi\ \mathrm{Im}\left\{F\left\{S(t,\phi)\right\}\right\} - \sin\phi\ \mathrm{Re}\left\{F\left\{S(t,\phi)\right\}\right\} \end{aligned} \tag{4.43}$$

Phasing the spectrum is an important operation in NMR spectroscopy and can be performed either manually or automatically in the computer by inspecting the real transform and adjusting ϕ until the result is a perfect absorption spectrum in the real part (maximum spectral integral) or a perfect dispersion spectrum in the imaginary part (zero spectral integral).

4.3.3 Digital Fourier transformation

In practice, NMR signals are digitised for subsequent processing and are represented by a finite set of N time-domain points sampled at dwell-time interval T. When data are digitised in this manner then the detection bandwidth is the inverse of the sampling interval, namely $1/T$, and the separation of points in the frequency domain is $1/NT$, with values ranging between $-\frac{1}{2}N\,(1/NT)$ and $\left(\frac{1}{2}N - 1\right)(1/NT)$. The digital Fourier transformation is given by

$$s(n/NT) = \sum_{-N/2}^{N/2-1} S(mT)\exp\left(-i2\pi mn/N\right) \tag{4.44}$$

the conjugate transformation being given by

$$S(mT) = \sum_{-N/2}^{N/2-1} s(n/NT)\exp\left(i2\pi mn/N\right) \tag{4.45}$$

For an FID signal represented by $S(mT)$, where m ranges from 0 to $N - 1$, the application of eqn 4.44 involves a shift transformation $m' = m - N/2$ and hence a

sign alternation between adjacent points in the frequency domain, an effect easily corrected in the computer. In fact, as we shall see later, it is possible to acquire signals at negative time using spin echoes. A further consequence of the finite sampling range means in effect that the data is multiplied by a hat function given by

$$\begin{aligned} H(t) &= 1 \qquad 0 \leq t \leq NT \\ &= 0 \qquad NT < t \end{aligned} \tag{4.46}$$

which means that the frequency-domain spectrum is convoluted with the digital Fourier transform of $H(t)$, namely,

$$F\{H(t)\} = \frac{NT \sin(2\pi f NT)}{2\pi f NT} + i\frac{NT(1-\cos(2\pi f NT))}{2\pi f NT} \tag{4.47}$$

where $f = k(1/NT)$ and k is an integer ranging from $-\frac{1}{2}N$ to $\left(\frac{1}{2}N - 1\right)$. It is immediately clear that this apparent convolution introduces no real broadening, since $F\{H(t)\}$ is unity for $k = 0$ and zero elsewhere.

4.4 Intrinsic spin interactions

In Chapter 3 we met the spin Hamiltonian involving the Zeeman interaction, the chemical shift, the internuclear spin–spin scalar coupling, the electric quadrupole interaction, and the internuclear dipolar interaction. Here we reprise the spin Hamiltonian in the context of a dominant zeroth-order Zeeman interaction in which, for most cases, only secular parts of the remaining terms play a role as first-order perturbations. We will then outline some simple NMR experiments where the additional effect of RF pulses allows us to manipulate the evolution pathways of spin coherence such that desired terms in the spin Hamiltonian may be observed through the final detected magnetisation.

4.4.1 Resolution in NMR

The visibility of fine details

The Zeeman interaction arising from the static magnetic field, B_0, dominates the energy of the nuclear spins. It is a feature of NMR that many other much weaker interaction terms can still be observed, a consequence of the remarkable coherence times that spin ensembles exhibit. For example, because the T_2 times for nuclear spins in liquids may be of order seconds, the fundamental linewidth $1/\pi T_2$ may be eight or nine orders of magnitude smaller than the Larmor frequency. This means that very fine features in the Hamiltonian may be detected. The situation is not so favourable in solids, where the strong dipolar interactions between the spins serve to broaden the linewidth considerably, so destroying the transverse magnetisation coherence a few tens of microseconds after its formation.

The influence of interactions superposed on the applied longitudinal Zeeman field are of considerable importance in NMR and provide some extraordinary insights regarding molecular chemical structure, molecular rotational dynamics, and intramolecular dynamics, as well as molecular proximity, secondary structure, and organisation. However, in focusing on NMR measurements of translational dynamics, we will

be interested in these various interactions to the extent that they enable molecular identification or enhance (or possibly limit) the timescales over which motion may be observed. For this reason we provide only a limited overview, leaving the reader to seek a more complete discussion of spin interactions specific to molecular chemistry in the many excellent texts on NMR spectroscopy. There is, however, one member of the wide class of possible spin interactions that is of particular relevance to translational motion measurement, namely the degree to which the magnetic field has spatial dependence, whether through imperfection in the polarising magnet, through magnetic inhomogeneity arising from local sample structure, or through deliberate application by the experimenter of additional inhomogeneous magnetic fields.

Magnetic field inhomogeneity

The manufacturers of NMR magnets go to great lengths to provide a homogeneous magnetic field in the region of the sample space, incorporating first-, second-, and higher-order shim coils for fine correction. However, it is inevitable that some variation in B_0 across the sample will occur, although typically this leads to a broadening of no more than a few hertz in the proton NMR spectrum of a homogeneous sample of favourable geometry, for example a sample water contained in a long cylinder coaxial with the magnetic field. However, in many real samples where there is material inhomogeneity, for example where liquid is interspersed within a porous solid matrix of different diamagnetic susceptibility, local inhomogeneities in magnetic field will exist. The fractional variation in magnetic field throughout the sample will be on the order of the fractional diamagnetic susceptibility differences, typically a few ppm. In a superconducting magnet, such a spread can represent several kilohertz of extra linewidth.

The additional broadening caused by field inhomogeneity arises from a spread in the frequency spectrum, the spins experiencing a distribution of Larmor precession frequencies that results in a spreading of spin phases as time progresses. Following an RF excitation pulse, such spreading causes a decay of the FID more rapid than that due to T_2 effects alone. The resultant time constant is often labelled T_2^*, but it is important to appreciate that coherence loss due to relaxation is inherently random and irreversible whereas that caused by field imperfection is ordered and, given an appropriate pulse sequence, can be 'undone'. This leads to the important distinction between inhomogeneous and homogeneous broadening of the NMR spectral line. In practice, coherence loss that can be refocused by an appropriate pulse sequence is said to arise from inhomogeneous broadening. This broadening is typically caused by local differences in Hamiltonian between spin packets. Homogeneous broadening, by contrast, is common to each spin packet and is essentially irreversible. It arises from random motion of the spins. Note that the localised sub-ensemble of spins in an inhomogeneous magnetic field is often termed an 'isochromat' of the spin system, in other words a sub-ensemble of spins labelled by a single Larmor frequency.

The pulse sequence that provides the facility to distinguish reversible and reversible coherence loss is the spin echo, discovered by Erwin Hahn [19]. The echo principle underlies most of the methods for translational motion measurement discussed in this book. As we shall see later, by pulsed application of suitable magnetic fields, tailored to give a spatially dependent Larmor frequency, it is possible to use the echo to measure translational motion with great precision.

4.4.2 Chemical shift

First discovered in 1950 [33, 34], the chemical shift which arises from the diamagnetic shielding arising from the electrons that surround atomic nuclei in atoms and molecules, imparts to the NMR spectrum information about chemical structure. We focus here on the secular part of the chemical shift. For spin i

$$\mathcal{H}_{\mathrm{CS}_0} = -\delta_i \omega_0 I_{iz} - \frac{1}{2}\left(3\cos^2\beta - 1\right)\left(\delta_{zz} - \delta_i\right)\omega_0 I_{iz} \tag{4.48}$$

where δ_i is the isotropic chemical shift equal to $\mathrm{Tr}\left(\underline{\delta}\right)$ and β is the polar angle between the polarising field direction and the principal axis system of the shift tensor. The additional term is known as the anisotropic chemical shift and transforms under rotation as a second rank tensor, hence the role of the Legendre polynomial $P_2\left(\cos\beta\right) = \frac{1}{2}\left(3\cos^2\beta - 1\right)$. It leads to a broadened spectrum as shown in Fig. 4.11. In the liquid state, where molecules tumble rapidly, this term averages to zero, leaving only the isotropic part of the chemical shift. Chemical shifts depend strongly on the atomic number and are of order a few parts per million in ^{1}H, but several hundred parts per million in ^{13}C or up to thousands in ^{129}Xe.

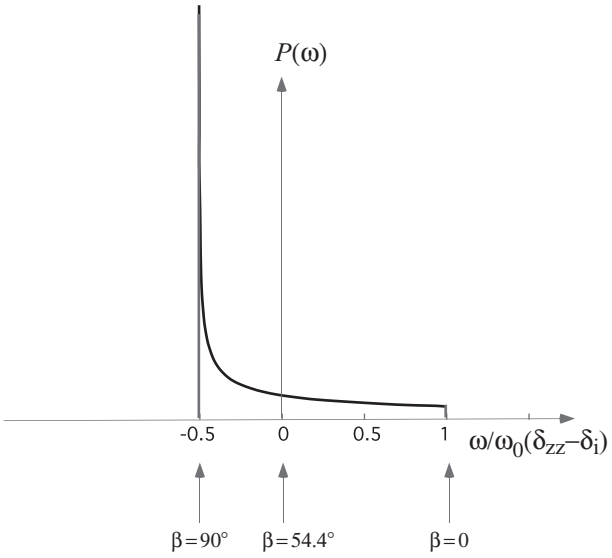

Fig. 4.11 Anisotropic chemical shift spectrum resulting from a random (isotropic) distribution of orientations ($P(\beta) = 1/4\pi$). The singularity for polar angle $\beta = 90^\circ$ arises because of increasing solid angle near the equator.

4.4.3 Scalar coupling

The scalar spin–spin coupling, $\mathcal{H}_{\mathrm{scalar}} = 2\pi J\,\mathbf{I}_i \cdot \mathbf{I}_j$, is an indirect interaction between nuclei, which arises via the mediation of electrons in the molecular orbital. The nuclear

spin causes a slight electron polarisation, which, because of electron delocalisation, is transmitted to neighbouring nuclei. $\mathcal{H}_{\text{scalar}}$ provides the finest structural detail in the liquid-state nuclear spin Hamiltonian It is typically between 1 and 50 Hz for protons. The spin–spin interaction, acting in conjunction with the chemical shift, imparts a characteristic signature to the high-resolution spectrum. Because the spin–spin interaction requires a molecular orbital, it acts only through the medium of covalent bonds. For this reason the scalar coupling is always intramolecular. The indirect nature of $\mathcal{H}_{\text{scalar}}$ leads to its rotational invariance. Note that we here simplify the notation used in Chapter 3 to write $i = 1$, $j = 2$, $J = J_{ij}$ and to express $\mathcal{H}$ in angular frequency units, the equivalent angular frequency energy associated with the scalar coupling prefactor being $2\pi J\hbar = Jh$.

When considering the role of the scalar coupling operator for a two-spin system it is helpful to write the combined chemical shift and scalar coupling Hamiltonian as

$$\begin{aligned}\mathcal{H} &= -\Delta\omega_1 I_{1z} - \Delta\omega_2 I_{2z} + 2\pi J\mathbf{I}_1 \cdot \mathbf{I}_2 \\ &= -\Delta\omega\,(I_{1z} + I_{2z}) - \tfrac{1}{2}\delta\,(I_{1z} - I_{2z}) + 2\pi J\mathbf{I}_1 \cdot \mathbf{I}_2\end{aligned} \tag{4.49}$$

where $\Delta\omega_1 = \delta_1\omega_0$, $\Delta\omega_2 = \delta_2\omega_0$ and we have centred the resonance frequency by setting $\frac{1}{2}(\Delta\omega_1 + \Delta\omega_2) = \Delta\omega$, the average offset frequency in the rotating frame, and simplified notation by $\delta = (\Delta\omega_1 - \Delta\omega_2)$. The operator $\mathbf{I}_1 \cdot \mathbf{I}_2$ commutes with $I_{1z} + I_{2z}$ but not with $I_{1z} - I_{2z}$. Hence the chemical shift, δ, plays a crucial role in the visibility of the scalar coupling interaction.

A convenient representation for two spins involves a simple product of kets $|m_1, m_2\rangle = |m_1\rangle|m_2\rangle$, where the column vectors are formed by simple outer products. However, in this representation the spin operator $\mathbf{I}_1 \cdot \mathbf{I}_2$ certainly contains off-diagonal components, $I_{1x}I_{2x}$ and $I_{1y}I_{2y}$, as well as the diagonal term $I_{1z}I_{2z}$. In practice, this off-diagonal part of the Hamiltonian only mixes product states $\left|\frac{1}{2}, -\frac{1}{2}\right\rangle$ and $\left|-\frac{1}{2}, \frac{1}{2}\right\rangle$ while $\left|\frac{1}{2}, \frac{1}{2}\right\rangle$ and $\left|-\frac{1}{2}, -\frac{1}{2}\right\rangle$ remain eigenstates. The states $|\psi_1\rangle = \left|-\frac{1}{2}, -\frac{1}{2}\right\rangle$ and $|\psi_4\rangle = \left|\frac{1}{2}, \frac{1}{2}\right\rangle$ are separated by $2\Delta\omega$, while states $|\psi_2\rangle$ and $|\psi_3\rangle$ involve superpositions of the product states, with admixture coefficients $\cos\frac{1}{2}\phi$ and $\sin\frac{1}{2}\phi$, where $\phi = \tan^{-1}(Jh/\delta)$. The set of eigenstates and their associated energy levels are are shown in Fig. 4.12. To obtain the spectra, one calculates the single-spin transition probabilities associated with the raising or lowering operators $J_{1\pm} + J_{2\pm}$. These allow for transition $E_4 - E_3$ and $E_3 - E_1$, with respective intensities proportional to $\left(\cos\frac{1}{2}\phi - \sin\frac{1}{2}\phi\right)^2$ and for $E_4 - E_2$ and $E_2 - E_1$, with respective intensities proportional to $\left(\cos\frac{1}{2}\phi + \sin\frac{1}{2}\phi\right)^2$.

In the limit $Jh \ll \delta$, where $\frac{1}{2}\phi \to 0$, we may write the scalar coupling interaction in its secular form as $\mathcal{H}_{\text{scalar}_0} = 2\pi J\, I_{1z}I_{2z}$. Here the Hamiltonian is diagonal in the $|m_1, m_2\rangle$ product representation and plays the role for spin 1 of an additional magnetic field proportional to the $m_2 = \pm\frac{1}{2}$ eigenvalue of I_{2z}, thus splitting the two chemically shifted resonance lines of the 1 and 2 spins by Jh angular frequency units. This weak coupling case is shown in the uppermost spectrum of Fig. 4.12, where the intensities of all four lines are seen to be equal.

For nuclei with identical resonant frequencies, $Jh \gg \delta$ and $\frac{1}{2}\phi \to 45°$. Here $\mathbf{I}_1 \cdot \mathbf{I}_2$ is invisible. In that case, known as the AA coupled spin system, $\cos\frac{1}{2}\phi = \sin\frac{1}{2}\phi = \frac{1}{\sqrt{2}}$ and the triplet $|\psi_1\rangle$, $|\psi_3\rangle$, $|\psi_4\rangle$ and singlet $|\psi_2\rangle$ are, respectively, eigenstates of $2\pi J\,\mathbf{I}_1 \cdot \mathbf{I}_2$,

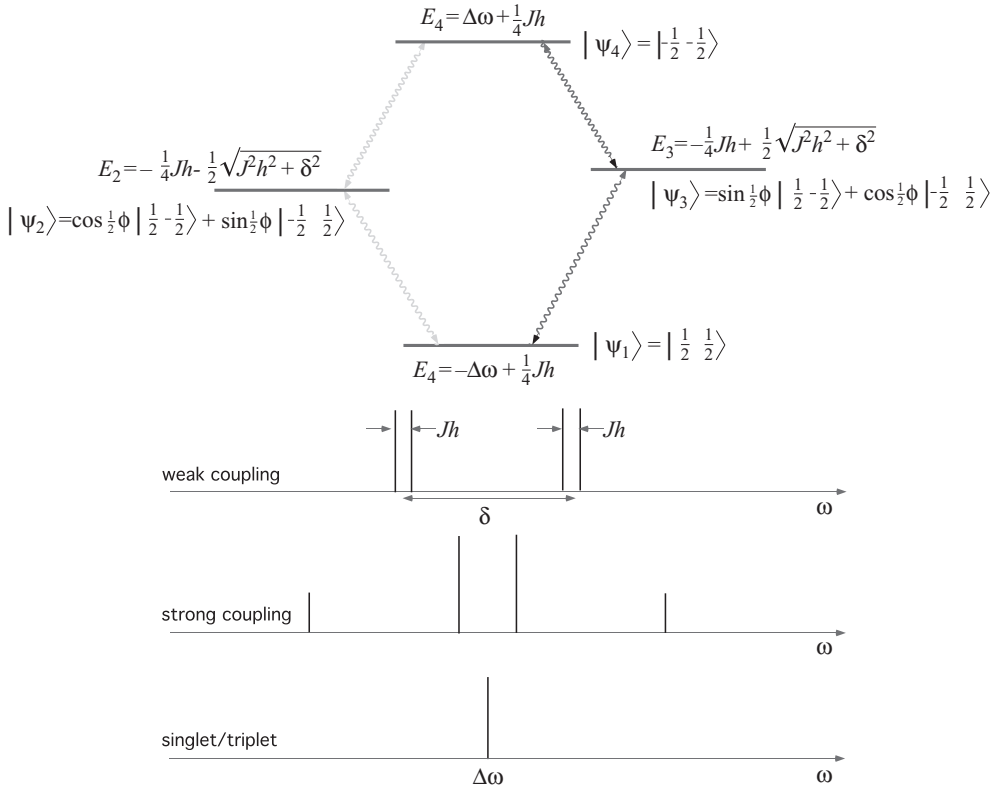

Fig. 4.12 Energy levels for a system of two spin-$\frac{1}{2}$ nuclei coupled by the scalar interaction, $2\pi J\mathbf{I}_1\cdot\mathbf{I}_2$.

with energy eigenvalues of $\pi Jh\left[I(I+1)-\frac{3}{2}\right]$,[4] where for the triplet, $I=1$, and for the singlet, $I=0$. These are total angular momentum states formed by the coupling of angular momentum vectors $\mathbf{I}_1+\mathbf{I}_2$, to form a total angular momentum vector $\mathbf{I}$. Clearly the total angular momentum states form a diagonal eigenbasis for $\mathbf{I_1}\cdot\mathbf{I_2}$, while the product states are an eigenbasis for $\gamma B_{01}I_{1z}+\gamma B_{02}I_{2z}$. Only transitions between the Zeeman separated triplet state levels are observable[5] and these are all identically shifted so that no effect of the scalar coupling is seen.

For the intermediate strong coupling case $Jh\sim\delta$, known as the AB spin system, neither the product nor total angular momentum representations provide an eigenbasis and the general superposition of product states shown in Fig. 4.12 applies. Here the single-spin transition probabilities for E_4-E_3 and E_3-E_1 are unequal to those for E_4-E_2 and E_2-E_1, as seen in the central spectrum.

[4]This is simple to show from $\mathbf{I}^2=(\mathbf{I}_1+\mathbf{I}_2)^2=\mathbf{I}_1^2+\mathbf{I}_2^2+2\mathbf{I}_1\cdot\mathbf{I}_2$, noting $\mathbf{I}_1^2=I_1\,(I_1+1)=\frac{3}{4}$

[5]The reason being that the NMR transition involves an $I_{i\pm}+I_{j\pm}$ operator, which commutes with $\mathbf{I}_i\cdot\mathbf{I}_j$.

The simple weak coupling interpretation has the resonance frequency of spin i split into a doublet because of the coupling to a single nucleus elsewhere in the molecule, the strength of this splitting reducing with increasing bond distance. Similarly, a nearby group of two nuclei with identical chemical shift and scalar couplings will have possible spin states $\left|\frac{1}{2},\frac{1}{2}\right\rangle$, $\left|-\frac{1}{2},\frac{1}{2}\right\rangle$, $\left|\frac{1}{2},-\frac{1}{2}\right\rangle$, and $\left|-\frac{1}{2},-\frac{1}{2}\right\rangle$, leading to a triple peak of intensity ratio 1:2:1. In a similar binomial fashion, coupling to three identical nuclei leads to a quadruplet with intensity ratio 1:3:3:1. By this means the multiplicity of coupled nuclei of common chemical shift may be determined. By means of chemical shift and scalar couplings, it is possible to identify the local chemical character of the molecular orbital surrounding that nucleus, as well as the intramolecular connectivity to nuclei at common chemical sites. The discovery of the chemical shift and the spin–spin coupling in the 1950s has revolutionised modern chemistry.

4.4.4 Quadrupole coupling

For nuclei with $I > 1/2$, the single-spin Hamiltonian contains a term representing the interaction of the nuclear quadrupole moment with the electric field gradient associated with the surrounding molecular orbital. Quadrupole interactions are of considerable significance in solid state NMR of inorganic materials, given that the periodic table contains a large number of stable $I > 1/2$ nuclei. In the present context, where we are concerned with the fluidic state, deuterium ($I = 1$) NMR provides a means of obtaining information about molecular orientation in anisotropic soft matter or liquid crystalline states. Note that symmetry considerations dictate that the quadrupole moment of a spin-$\frac{1}{2}$ nucleus is identically zero.

Again we write down only the secular part of the quadrupole interaction in the zeroth order $\{|m\rangle\}$ basis of the dominant Zeeman interaction. Using (X, Y, Z) for the principal axis frame of the electric field gradient and retaining (x, y, z) for the laboratory frame, in which the B_0 field is along z, the rotation to take (X, Y, Z) to (x, y, z) comprises polar angle θ and azimuthal angle ϕ. Then the secular component of $\mathcal{H}_{\mathrm{Q}}$ is [9]

$$\mathcal{H}_{\mathrm{Q}_0} = \frac{3eV_{ZZ}Q}{4I(2I-1)}\frac{1}{2}\left(3\cos^2\theta - 1 + \eta\cos 2\phi\,\sin^2\theta\right)\left(3I_z^2 - \mathbf{I}^2\right) \tag{4.50}$$

with Q being the nuclear quadrupole moment of spin-I, V_{ZZ} the principal axis diagonal element of the electric field gradient tensor, $V_{\alpha\beta} = \partial^2 V/\partial\alpha\partial\beta$, and η the asymmetry parameter $(V_{XX} - V_{YY})/V_{ZZ}$. In many molecules, the local electronic orbital is inherently axially symmetric so that $\eta = 0$ and

$$\mathcal{H}^0_{\mathrm{Q}_0} = \frac{3eV_{ZZ}Q}{4I(2I-1)}\frac{1}{2}\left(3\cos^2\theta - 1\right)\left(3I_z^2 - \mathbf{I}^2\right) \tag{4.51}$$

$\frac{1}{2}\left(3\cos^2\theta - 1\right)$ being the second rank Legendre polynomial $P_2(\cos\theta)$.

The effect of the spin operator $\left(3I_z^2 - \mathbf{I}^2\right)$ is to shift the energies of the $2I + 1$ Zeeman levels so that the transition frequencies are no longer equal. This results in spectrum of $2I$ different resonances, equally spaced around the Larmor frequency and

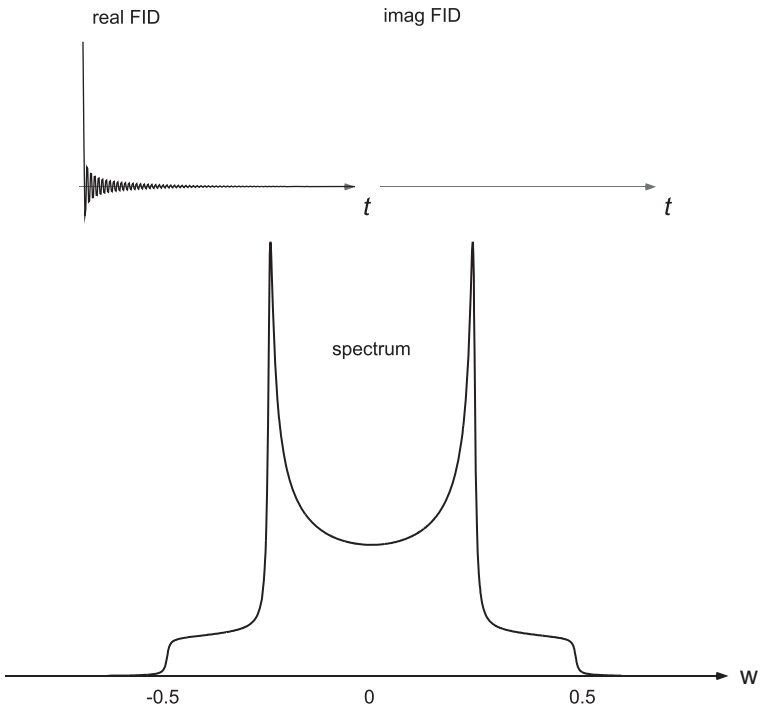

Fig. 4.13 Quadrupolar spectrum for $I = 1$ resulting from a random (isotropic) distribution of orientations ($P(\cos\theta, \phi) = 1/4\pi$). By contrast with Fig. 4.11, the singularities for polar angle $\theta = 90°$ have been smoothed by inclusion of some relaxation in the associated FID. Note that symmetry of the spectrum implies a pure cosine FID (zero imaginary). The frequency scale is in units $3eV_{ZZ}Q/4I(2I-1)$.

separated by $2\omega_{\mathrm{Q}} = 6\frac{3eV_{zz}Q}{4I(2I-1)}P_2(\cos\theta))$[6] For example, in spin-1, the single resonance line of the Larmor spectrum would be split in two for a particular value of ω_{Q}. In a nematic liquid crystal with director aligned at a fixed direction to the magnetic field, the NMR spectrum for the deuterium nucleus, with $I = 1$, would be a doublet with a unique quadrupole splitting. In a polydomain nematic or in the solid state, the distribution of director angles α would ensure a 'powder broadened line', as shown in Fig. 4.13.

Quadrupole interaction frequencies for deuterons in organic molecules in the solid state are on the order of 100 kHz. However, in material environments where molecules may tumble, the interaction is significantly reduced. Indeed, in simple isotropic liquids, molecular tumbling causes θ and hence $\mathcal{H}_{\mathrm{Q}_0}$ to fluctuate. Provided that this motion is more rapid than the quadrupolar interaction strength, a condition, which is true for all but the most viscous liquids, the quadrupolar Hamiltonian is averaged to zero.

[6]The splitting is set here to $2\omega_{\mathrm{Q}}$ for convenience. It allows us to use ω_{Q} as the precession frequency of transverse magnetisation under the influence of the quadrupole interaction, so that for $I = 1$ the spectrum consists of two lines, at $\pm\omega_{\mathrm{Q}}$.

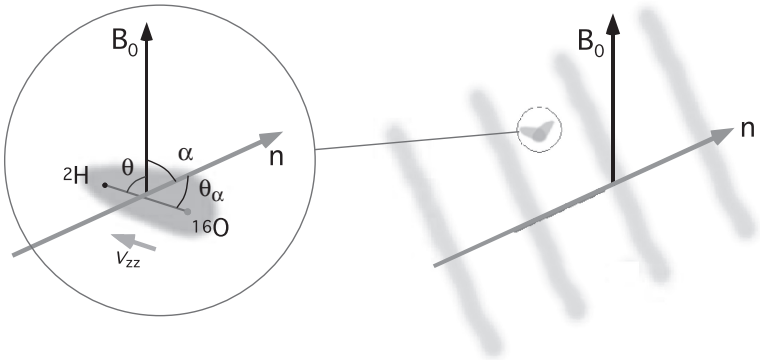

Fig. 4.14 Motional averaging of quadrupole interaction due to water molecule tumbling in a lyotropic lamellar phase with director **n**. The principal axis of the deuterium quadrupole interaction makes angle $\theta(t)$ with the magnetic field and angle $\theta_\alpha(t)$ with respect to the director. Rapid fluctuations of $\theta_\alpha(t)$ leave the effective quadrupole interaction scaled by $\overline{P_2(\cos\theta_\alpha(t))}P_2(\cos\alpha)$.

In anisotropic liquids, the motional averaging is incomplete. An example would be a liquid crystal for which there exists a local nematic director inclined at angle α to the magnetic field B_0, as shown in Fig. 4.14. If this director is fixed in space or fluctuating only slowly by comparison with the quadrupolar frequency, then the tumbling motion leads to a projection of the averaged quadrupole interaction along the director, with a second angular transformation to the laboratory Zeeman frame. The orientation (θ, ϕ) of the electric field gradient (bond) axis with respect to B_0 can be decomposed into $(\theta_\alpha, \phi_\alpha)$, describing the bond axis with respect to the director, and the polar angle α by which the director is inclined to the magnetic field. Allowing for averaging of the azimuthal angle ϕ_α[7] the spherical harmonic addition theorem may be used to factorise as [36]

$$\overline{P_2(\cos\theta)} = \overline{P_2(\cos\theta_\alpha)}P_2(\cos\alpha) \tag{4.52}$$

$\overline{P_2(\cos\theta_\alpha)}$ thus defines a motionally averaged local order parameter that scales down the effective size of quadrupole interaction strength. The angular dependence of that scaled interaction now follows the local director axis.

Next we look at another source of line broadening in the solid state, one which is inherently more complex than the quadrupole interaction and which plays an important role for all nuclear spins.

4.4.5 Internuclear dipolar interactions

The last term in the spin Hamiltonian arises from through-space dipolar interactions between nuclei. It is of immense importance in magnetic resonance because of the ubiquity of these interactions in all matter, and is seen in all nuclei of non-zero spin angular momentum. In the case of protons, for which the nuclear dipole moment is

[7]This is tantamount to a requirement of axial symmetry of the material with respect to the nematic director. Where the sample is biaxial, the asymmetry effects are observable [35].

largest, these interactions may be on the order of 100 kHz, comparable with quadrupole interaction strengths in spin-1 and higher spin nuclei. Again, dipolar interactions are but a first-order perturbation in the presence of a Zeeman field of hundreds of megahertz. When calculating the spin energy levels and hence the NMR spectrum, we may, to a good approximation, retain just the secular part of the dipolar interaction between like spins, i and j, and write

$$\mathcal{H}_{\mathrm{D}}^{0} = \frac{\mu_0 \gamma^2 \hbar}{4\pi} \sum_{i<j} \frac{1}{r_{ij}^3} \tfrac{1}{2} \left(1 - 3\cos^2\theta_{ij}\right) \left[3I_{iz}I_{jz} - \mathbf{I}_i \cdot \mathbf{I}_j\right] \tag{4.53}$$

where $\mathbf{r}_{ij}$ is the inter-nuclear vector that makes a polar angle θ_{ij} with the magnetic field direction. Note again the role of the Legendre polynomial $P_2(\cos\theta_{ij})$ in determining the dipolar interaction strength. As with the chemical shift anisotropy and the quadrupole interaction, the dipolar interaction transforms under rotation as a second rank tensor. The complexity of $\mathcal{H}_{\mathrm{D}}^{0}$ arises for a number of reasons. First, there is the bilinear nature of the spin operator, similar to the spin–spin scalar coupling but with both $I_{iz}I_{jz}$ and $\mathbf{I}_i \cdot \mathbf{I}_j$ components. As with the weak scalar coupling case, the $I_{iz}I_{jz}$ term leads to a splitting of the resonance, a simple doublet in the case of spin-$\frac{1}{2}$. But in nearly all materials there is a multiplicity of i to j dipolar interactions contributing in the sum and, for each i spin in the sum, numerous j term splittings of differing width. This spread arises because of the various internuclear separations and θ_{ij} orientations associated with proximate intermolecular and intramolecular spins. The net result is an approximately Gaussian spectrum associated with a Gaussian signal decay of the form

$$S(t) = S(0) \exp\left(-\frac{1}{2} M_2 t^2\right) \tag{4.54}$$

where M_2 is the second moment of the linewidth given by

$$M_2 = -\operatorname{Tr}\left(\left[\mathcal{H}_{\mathrm{D}}^{0}, I_x\right]^2\right) / \operatorname{Tr}\left(I_x^2\right) \tag{4.55}$$

In most rigid solids the decay of this Gaussian for proton NMR will be on the order of microseconds, consistent with the dipolar linewidth on the order of of 100 kHz.[8] Note that these solid-state dipolar interactions are static and represent a form of inhomogeneous broadening. In principle, and given the right pulse sequence, the associated decay can be reversed and the linewidth narrowed. An example of a pulse sequence that does this will be discussed in Section 4.6.2.

The effect of either dipolar or quadrupolar interactions is dramatically different in the case of liquids. Here molecular tumbling leads to rapid fluctuations in θ_{ij} and provided that these are fast compared with the dipolar linewidth in frequency units, and isotropic in character, then $P_2(\cos\theta_{ij})$ and hence H_D^0 is averaged to zero, this narrowing the NMR linewidth. However, the off-diagonal (non-secular) terms in $\mathcal{H}_{\mathrm{D}}$ of $\mathcal{H}_{\mathrm{Q}}$ are thereby caused to fluctuate, inducing transitions between nuclear energy levels and thus contributing to both T_1 and T_2 relaxation. Provided field inhomogeneity is made sufficiently small then it is the decay associated with T_2 relaxation that sets the

[8] For other nuclei it will be scaled (down) by the respective gyromagnetic ratio factors.

spectral linewidth in the liquid state, typically on the order of 1 Hz and thus narrow enough to reveal fine details of remaining terms in the nuclear spin Hamiltonian. That decay, being exponential, leads to a Lorentzian lineshape of finite width. By contrast with the solid state, the decay of the liquid-state signal arises from stochastic fluctuations and leads to irreversible decay and hence homogeneous broadening of the spectral line.

4.5 Fluctuations, spin relaxation, and motional averaging

The multiplicity of interactions experienced by nuclear spins each result in deterministic quantum phase evolution. But where those interactions result from multiple sources, as in the case of the dipolar interaction whose sum may involve the multiple possibilities of intra- and intermolecular internuclear vectors, a distribution of phase shifts arises. That distribution represents a loss of phase coherence, with consequent decay of the FID or, more generally, loss of the non-equilibrium spin ensemble coherence. In that sense, such dephasing lies at the heart of spin–spin (T_2) relaxation. However, T_2 is a rather slippery concept. In principle, given the right pulse sequence, deterministic phase shifts may be reversed, a phenomenon observed by Hahn in his discovery of the spin echo. To the extent that phase-spreading is not recoverable, we might say that 'true' T_2 decay remains; that which was observed in the simple FID being an 'effective' T_2. These distinctions will be clearer once we embark on a description of specific pulse sequences in the next section.

The factor that mitigates against such recovery of spin phase will be stochastic fluctuations in the spin interactions. Fluctuations may arise from lattice vibrations, from molecular translational and rotational diffusion, or from internal vibrations and segmental motions of molecules. All of these cause those spin interactions sensitive to orientation and/or internuclear spacing to vary with a complex dynamical spectrum. Predominant are the internuclear dipolar interaction and, in the case of $I > 1/2$, the nuclear quadrupole interaction. Of course, if the motion is isotropic and rapid enough, then dipolar and quadrupolar interactions will be averaged to zero. Rapid enough in this context means, in the Heisenberg uncertainty sense, by comparison with the size of the dipolar and quadrupolar interactions (typically 100 kHz). In such a sense we may define an 'NMR liquid', namely one for which T_2 decay is slow because the molecular tumbling is sufficiently fast.[9] Herein lies a subtle idea. In the absence of motion, a distribution of spin interactions leads to rapid T_2 decay but one which is pulse sequence dependent. Fluctuations will render spin phase shifts irreversible and so increase the irreversible part of T_2 while at the same time reducing the effective size of the spin interactions as the degree of stochastic excursion increases. The ultimate limit of 'extreme motional averaging' is one in which there is only one T_2, albeit long and robustly pulse sequence independent. This is almost invariably the case for liquids comprising small molecules at room temperature, where isotropic tumbling is associated with rotational correlation times on the order of picoseconds.

However, fluctuations, while having the potential to diminish the spin dephasing associated with a distribution of spin interactions present in the solid state, also have

[9]Nothing quite so baffles the general physics community as the idea of motional averaging and its consequence of slow NMR signal decays arising from fast motion.

the capacity to induce transitions between spin states. Thus they lie at the heart of T_1 relaxation, the process of return to thermal equilibrium associated with the re-establishment of a Boltzmann distribution of spin state populations. For this reason T_1 will be generally very long in a solid, while T_2 is short. At the other extreme, simple liquids are characterised by T_2 and T_1 both long, identically equal in the 'motion-narrowed limit'. Understanding this transition from solid to liquid in the relaxation sense is important for two reasons. First, in materials where spin translational motion is permitted, for example complex fluids or soft-condensed matter, a hierarchy of dynamics may exist in which both slow and fast motions are present. For biological tissue, polymeric materials, liquid crystals, fluid-imbibed porous media, and colloids, there may be a sense in which both solid *and* liquid descriptors may apply. But, most importantly, as we shall later discover, T_1 and T_2 relaxation provide a fundamental limiting timescale for the measurement of translational motion. For these reasons it is helpful to expand a little on the fundamental processes involved. But we shall not delve deeply. Relaxation is an immensely interesting and complex topic, worthy of many chapters of discussion. Indeed, relaxation may in its own right be used as a probe of translational dynamics, although doing so requires a modelling process to interpret the way in which spin interactions translate the effects of translational motion to the relaxation time. This aspect of magnetic resonance is well treated in a number of other volumes [9, 37–40]

In spin-$\frac{1}{2}$ nuclei, the dominant interaction causing spin relaxation arises from the dipolar Hamiltonian, whereas in higher spin systems quadrupolar interactions are significant. Because of the pre-eminent role of the proton in NMR, our discussion will concentrate on the effect of $\mathcal{H}_{\mathrm{D}}$.

4.5.1 Spin–lattice relaxation

Spin–lattice relaxation is quite naturally described in the laboratory frame, where the difference in energy levels is dominated by the longitudinal Zeeman field and the dipolar interaction can be regarded as weak by comparison. This permits the use of time-dependent perturbation theory [9, 10, 41]. By a simple argument, Hebel and Slichter [42] showed that the spin–lattice relaxation rate could be written

$$\frac{1}{T_1} = \frac{1}{2}\frac{\sum_{nm} W_{nm}\left(E_n - E_m\right)^2}{\sum_n E_n^2} \tag{4.56}$$

where the transition rate between the two states, n and m, is given by perturbation theory as

$$W_{nm} = \frac{1}{\hbar^2}\int_0^\infty \exp\left[i\left(E_n - E_m\right)(\tau)/\hbar\right]\,\overline{\langle n|\,\hbar\mathcal{H}_{\mathrm{D}}(0)\,|m\rangle\,\langle m|\,\hbar\mathcal{H}_{\mathrm{D}}(\tau)\,|n\rangle}\,d\tau + c.c. \tag{4.57}$$

Evaluating eqn 4.57 requires decomposition of $\mathcal{H}_{\mathrm{D}}(t)$ into spatial and spin operators. The matrix elements of spin operators imply specific selection rules for n and m, and so determine which energy differences are relevant. Unsurprisingly, given the bilinear nature of the dipolar (or quadrupolar) Hamiltonian, the relevant separations of $n = m \pm q$, where q is 1 or 2. The respective spatial operator parts of $\mathcal{H}_{\mathrm{D}}(0)$ and $\mathcal{H}_{\mathrm{D}}(\tau)$

appear in correlation functions $G^q(\tau)$, which are Fourier transformed by the integral in eqn 4.57 to produce spectral density functions $J^{(q)}(\omega)$. Clearly the relevant frequencies are ω_0 and $2\omega_0$. Following some algebraic manipulation, one finds [9]

$$\frac{1}{T_1} = \left(\frac{\mu_0}{4\pi}\right)^2 \gamma^4 \hbar^2 \frac{3}{2} I(I+1) \left[J^{(1)}(\omega_0) + J^{(2)}(2\omega_0)\right] \tag{4.58}$$

4.5.2 Spin-spin relaxation

The case of transverse relaxation is not amenable to such an approach, since here we are dealing with a process that is naturally described in the rotating-frame, where the transverse magnetisation is stationary. In this frame of reference there is no large zeroth order Hamiltonian that will dominate the dipolar interaction. Instead the behaviour of the magnetisation is best handled using the density operator formalism. Following eqn 3.53, the density matrix in the rotating frame, $\rho^*(t)$, obeys

$$i\frac{d\rho^*(t)}{dt} = [\mathcal{H}_{\mathrm{D}}^*(t), \rho^*(t)] \tag{4.59}$$

where $\mathcal{H}_{\mathrm{D}}^*$ is the transformed dipolar Hamiltonian, $\exp(i\omega_0 t I_z) H_D(t) \exp(-i\omega_0 t I_z)$. Once the evolution of $\rho^*(t)$ is calculated, all relevant spin properties, such as the decay of the transverse magnetisation, can be determined. The problem with an equation such as 4.59 is that it cannot easily be integrated. To first order, however [9],

$$\frac{d\rho^*(t)}{dt} = -i[H_D^*(t), \rho^*(0)] - \int_0^t [H_D^*(t), [H_D^*(t'), \rho^*(0)]]dt' \tag{4.60}$$

Taking the ensemble average, noting that $\overline{H_D^*(t)} = 0$, replacing $t' = t - \tau$, and extending the integration limit to ∞ , one obtains [9] the vital result from which the decay of M_y (ie $Tr[\rho^* I_y]$) can be calculated, namely,

$$\frac{d\rho^*(t)}{dt} = -\int_0^\infty \overline{[H_D^*(t), H_D^*(t-\tau), \rho^*(0)]]}d\tau \tag{4.61}$$

This linear differential equation leads to exponential relaxation, a key property of Bloembergen, Purcell and Pound (BPP) theory [20]. Equation 4.61 contains oscillatory phase factors due to the transformation of H_D to the rotating frame and so, like eqn 4.57, can be shown to to comprise the Fourier spectra of dipolar correlation functions, $G^q(\tau)$. The various matrix element evaluations in the calculation of dM_y/dt lead to

$$\frac{1}{T_2} = \left(\frac{\mu_0}{4\pi}\right)^2 \gamma^4 \hbar^2 \frac{3}{2} I(I+1)[\frac{1}{4}J^{(0)}(0) + \frac{5}{2}J^{(1)}(\omega_0) + \frac{1}{4}J^{(2)}(2\omega_0)] \tag{4.62}$$

The assumptions involved in the various steps leading to eqn 4.62 are delicate, but the key assumption underpinning BPP theory is $\overline{\langle H_D^2 \rangle}^2 \tau_c^2 \ll 1$ (or $M_2 \tau_c^2 \ll 1$. Thus the relevant timescale for fast motion in the BPP sense is the 'precession period in

the dipolar field'. This is simply the inverse of the dipolar linewidth in the absence of motion, $M_2^{1/2}$. The regime of motion in which $M_2\tau_c^2 \ll 1$ is termed 'motionally narrowed'.

One other relaxation time can be calculated using the spectral density approach. This is the rotating-frame relaxation time, $T_{1\rho}$, which describes the rate at which transverse magnetisation decays in the presence of an RF field, B_1. Provided the rotating frame Zeeman energy of the spins in the RF field exceeds the residual dipolar interaction (i.e. the NMR linewidth) the magnetisation is said to be 'spin-locked' and the perturbative treatment of relaxation, which applies in the case of the T_1 process along the B_0 Zeeman field in the laboratory frame, also applies for the $T_{1\rho}$ process along the B_1 Zeeman field in the rotating frame [41]. The result is derived from an expression akin to eqn 4.57, but where m and n refer to eigenstates along I_y and $H_D(t)$ is now $H_D*(t)$, the dipolar interaction in the rotating frame. The relevant matrix elements in eqn 4.57 cause selection rules $n-m=0,\pm1,\pm2$, and their evaluation yields

$$\frac{1}{T_{1\rho}} = \left(\frac{\mu_0}{4\pi}\right)^2 \gamma^4\hbar^2\frac{3}{2}I(I+1)[\frac{1}{4}J^{(0)}(2\omega_1) + \frac{5}{2}J^{(1)}(\omega_0) + \frac{1}{4}J^{(2)}(2\omega_0)] \tag{4.63}$$

As expected, the expression for $T_{1\rho}$ equals that for T_2 in the limit as $\omega_1 \to 0$ although in practice the spin locking condition breaks down as the RF field amplitude is decreased.

In order to appreciate the physical significance of eqns 4.58 and 4.62, it is helpful to evaluate them for a simple isotropic rotational diffusion model, an excellent representation of the fluctuations in dipolar interactions that occur in most liquids. Here the $J^{(q)}$ are given by [9]

$$\begin{aligned} J^{(0)}(w) &= \frac{24}{15r_{ij}^6}\frac{\tau_c}{1+\omega^2\tau_c^2} \\ J^{(1)}(w) &= \frac{4}{15r_{ij}^6}\frac{\tau_c}{1+\omega^2\tau_c^2} \\ J^{(2)}(w) &= \frac{16}{15r_{ij}^6}\frac{\tau_c}{1+\omega^2\tau_c^2} \end{aligned} \tag{4.64}$$

where τ_c is the rotational correlation time (for reorientation of the rank 2 spatial tensor). The result of substituting these spectral density functions in the expression for T_1 and T_2 is shown in Fig. 4.15. The most obvious feature is the existence of two distinct motional regimes separated by a minimum in T_1 when the correlation time is of order the Larmor period. The regime corresponding to $\tau_c^{-1} \gg \omega_0$ is characterised by identity of T_1 and T_2 and, in accordance with the reduction in the homogeneous linewidth, $1/\pi T_2$, as T_2 increases, is termed 'extreme narrowed'. Such a regime applies typically for small molecules in the liquid state (such as water at room temperature), where correlation times are of order 10^{-12} s to 10^{-14} s.

The divergence of T_1 and T_2 below the T_1 minimum is characteristic of highly viscous liquids, concentrated flexible polymers, and semi-rigid polymers, where rotational tumbling of the inter-nuclear vector r_{ij} is slowed or restricted. Molecular motion in which $M_2^{1/2} \ll \tau_c^{-1} \ll \omega_0$ is identified by $T_2 \ll T_1$.

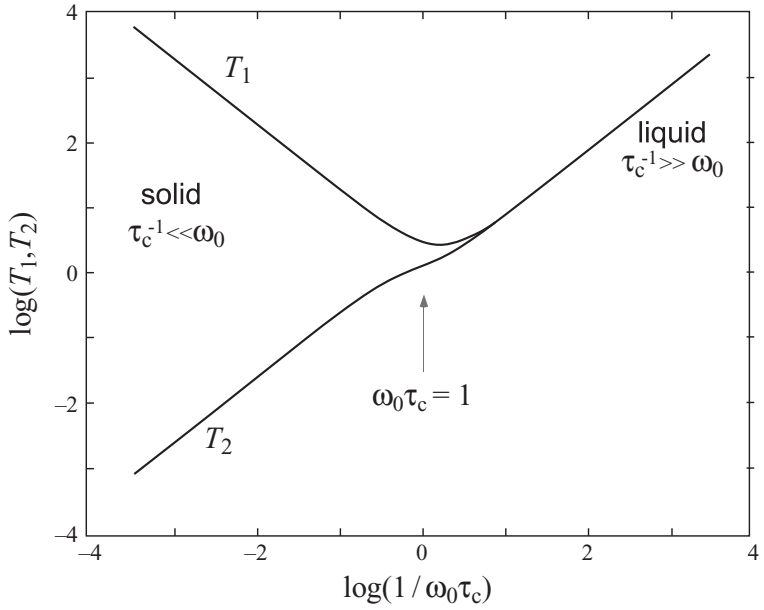

Fig. 4.15 T_1 and T_2 relaxation as a function of correlation time τ_c at fixed Larmor frequency, ω_0.

All three expressions, eqns 4.64, correspond to a dipolar interaction between a pair of like spins. Where a spin experiences a dipolar interaction with more than one other spin, these expressions can be scaled up proportionately. Similarly, if the interaction arises between spins in different molecules in relative translational motion some effective value for $\overline{1/r_{ij}^6}$ is required. Furthermore, the expressions can be simply modified for dipolar interactions between unlike spins (such as ^{13}C and ^{1}H) or to allow for different types of perturbative interactions such as the quadrupole interaction. Such formulae are covered in detail elsewhere [9, 10]. In all such analyses the motional features apparent in Fig. 4.15 remain the same.

4.5.3 Motional averaging

When the reorientation of the dipolar interaction slows sufficiently that $M_2\tau_c^2 \gtrsim 1$, the line-narrowing assumption inherent in the BPP theory breaks down. However, the perturbation theory approach that yields the spin–lattice relaxation behaviour is still quite good, since $\gamma B_0 \gg M_2^{-1/2}$. Consequently the T_1 formula, eqn 4.56, is applicable in the slow motion limit. In the case of solids, it is clear that T_1 will be long (usually many seconds) and in insulators will arise from the spectrum of lattice vibrations.

For T_2 in solids and semi-solids, a different approach is required. A nice treatment, due to Anderson and Weiss [43], represents the fluctuating dipolar fields as a a time-dependent Larmor frequency, $\Delta\omega(t)$, which varies randomly such that the time-averaged and ensemble-averaged mean square values are the same, namely, $\overline{\Delta\omega^2}$. Note that $\Delta\omega(t)$ is measured in the rotating frame. It represents the offset from the

average longitudinal field precession frequency, ω_0. The normalised free induction decay, $G(t) = S(t)/S(0)$, is therefore,

$$G(t) = \overline{\exp(i \int_0^t \Delta\omega(t')dt')} \tag{4.65}$$

There are a great many problems in physics where such an average of phase factors are required to be calculated, but in magnetic resonance eqn 4.65 is ubiquitous. We entered this discussion from a consideration of fluctuating dipolar interactions. But any randomly varying local field, any fluctuating term in the spin Hamiltonian, will require us to address the matter of phase factors with exponents $i \int_0^t \Delta\omega(t')dt'$. The Anderson–Weiss method is therefore of major significance in dealing with a wide class of magnetic resonance problems for which the effect of time-varying interactions is to be calculated.

Two assumptions make the problem tractable. The first is that the distribution of $\Delta\omega(t)$ is Gaussian, in which case the distribution of $X(t) = \int_0^t \Delta\omega(t')dt'$ is also Gaussian[10] with probability distribution

$$P(X) = [2\pi\overline{X^2}]^{-1/2} \exp(-\frac{1}{2}X^2/\overline{X^2}). \tag{4.66}$$

This leads to the result

$$\begin{aligned} \overline{\exp(i \int_0^t \Delta\omega(t')dt')} &= \int P(X) \exp(iX)dX \\ &= \exp(-\frac{1}{2}\overline{X^2}) \end{aligned} \tag{4.67}$$

The second assumption is that the local field fluctuation is described in the usual manner by a correlation function[11]

$$\overline{\Delta\omega(t)\Delta\omega(t-\tau)} = \overline{\Delta\omega^2}g(\tau) \tag{4.68}$$

This allows one to calculate $\overline{X^2}$ as $2\overline{\Delta\omega^2} \int_0^t (t-\tau)g(\tau)d\tau$ so that

$$G(t) = \exp(-\overline{\Delta\omega^2} \int_0^t (t-\tau)g(\tau)d\tau) \tag{4.69}$$

This Anderson–Weiss expression is an extremely useful result, applicable in a wide range of dynamical situations. For example we shall use this result in Chapter 6 to deal with spin relaxation in microscopically inhomogeneous media. But one of the most important insights provided is an understanding of slow and fast motion limits.

[10]This follows from the Central Limit Theorem which states that the averaged sum of a sufficiently large number of identically distributed independent random variables each with finite mean and variance will be approximately normally distributed.

[11]Note that for dipolar interactions, $g(\tau)$ is a sort of 'normalised, q-averaged' $G^q(t)$.

In the slow motion limit, $\overline{\Delta\omega^2}\tau_c^2 \gg 1$, $g(\tau)$ in eqn 4.69 is approximately unity and so as $t \to 0$

$$G(t) = \exp(-\frac{1}{2}\overline{\Delta\omega^2}t^2) \tag{4.70}$$

Strictly speaking such a Gaussian decay is due to inhomogeneous broadening and cannot strictly be termed 'relaxation', since the signal may be recovered by using appropriate pulse sequences as discussed in Section 4.6.2. Nonetheless it tells us that that signal decay is rapid when the motion is slow. In the fast motion limit $\overline{\Delta\omega^2}\tau_c^2 \ll 1$, $g(\tau)$ decays rapidly in eqn 4.69 and the integral approximates $t\int_0^\infty g(\tau)d\tau$, leading to a FID given by $\exp(-\overline{\Delta\omega^2}\tau_c t)$. Such an exponential decay corresponds to a transverse relaxation rate $1/T_2 = \overline{\Delta\omega^2}\tau_c$. Note that the shorter τ_c, the longer the relaxation time T_2. Fast motion leads to slow relaxation decay. This contrary aspect of motional averaging is often counterintuitive to those who do not live in the world of magnetic resonance.

Before leaving the Anderson–Weiss model we note that it reproduces two familiar results in the slow and fast motion limits of the dipolar interaction. We start with slow motion. Noting $\overline{\Delta\omega^2} = M_2$, eqn 4.69 is precisely the solid-state Gaussian decay behaviour of eqn 4.54. For the fast motion limit, an exponential decay is found and, using the definition of the second moment in eqn 4.55,

$$\begin{aligned}\frac{1}{T_2} &= M_2\tau_c \\ &= \left(\frac{\mu_0}{4\pi}\right)^2 \gamma^4\hbar^2\frac{3}{2}I(I+1)\frac{1}{r_{ij}^6}\tau_c.\end{aligned} \tag{4.71}$$

Hence the T_2 relaxation rate is equivalent to the dominant zero-frequency term of the BPP theory (eqn 4.62), namely

$$\frac{1}{T_2} \approx \left(\frac{\mu_0}{4\pi}\right)^2 \gamma^4\hbar^2\frac{3}{2}I(I+1)\left[\frac{1}{4}J^{(0)}(0)\right] \tag{4.72}$$

What happened to the remaining terms? In short, they are absent because, like those that determine the T_1 relaxation rate, they arise from resonant transitions that are unrepresented in the Anderson–Weiss model. But for fluctuations slower than the Larmor frequency ($\omega_0\tau_c \gg 1$), but still fast enough to result in motional narrowing ($M_2^{1/2}\tau_c \ll 1$), the Anderson–Weiss model works extremely well.

4.6 Pulse sequences

4.6.1 Basic spin manipulation

Among the enormous number of pulse sequences that are used in modern NMR are four that have their origins in the early beginnings of the subject but the usefulness of which is enduring. These are the inversion recovery sequence, the simple Hahn echo [19], the Carr–Purcell echo train [44, 45], and the stimulated echo [46]. Each concerns the manipulation of the spin system under the influence of the Zeeman

Hamiltonian and the T_1 and T_2 relaxation processes. Each can be understood using a simple vector description of the nuclear magnetisation. For more sophisticated pulses sequences, and especially when Hamiltonian terms bilinear in the spin operator play a role, the vector picture lets us down. We simply cannot understand such phenomena without recourse to quantum mechanics. That doesn't make for difficulty. On the contrary, a simple and effective quantum description of spin evolution and resulting NMR signals can be found by using the density matrix expressed in terms of spin operators.

In the sense that NMR fundamentally concerns quantum coherence, the idea of 'coherence transfer' is central to any understanding of evolution under the influence of the spin Hamiltonian. Here the precession diagrams introduced in Chapter 3 are particularly helpful. We start with the basics of precession under static magnetic fields and resonant RF fields as shown in Fig. 4.16. The cases illustrated correspond to the rotating frame of reference, with transverse magnetisation precessing under a Zeeman offset and, for the interchange of I_z with I_x and I_y, under a resonant RF pulse.

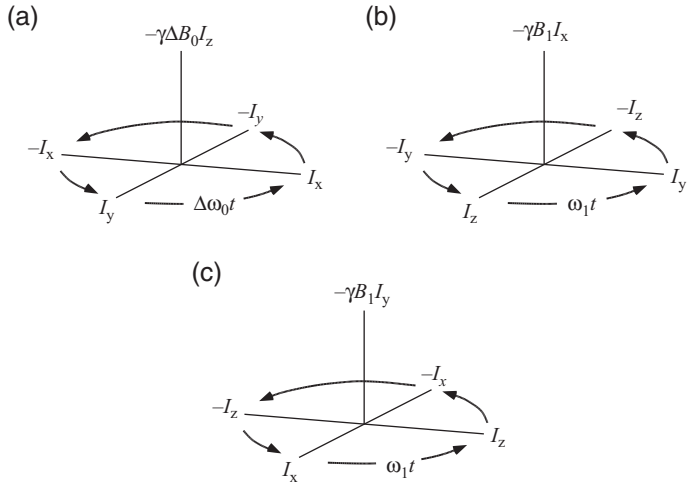

Fig. 4.16 Rotating-frame precession diagrams for states of the density matrix in the presence of a Zeeman interaction: (a) evolution of I_y under the off-resonant Zeeman interaction, $-\Delta\omega_0 I_z$; (b) I_z, under the influence of the RF field $-\omega_1 I_x$; and (c) I_x under $-\omega_1 I_y$.

Later in this section we visit the more sophisticated sequences involving coherence transfer amongst the 'non-vectorial' components of Liouville space. But even for the simplest sequence involving Zeeman terms alone, the density matrix approach will often give us the quickest route to understanding. In consequence, we will present such a description in parallel with our simple vector diagrams.

Usually, each application of a particular pulse sequence to the NMR spin system is not performed in single shot but in rapid succession, the resulting signal from each experiment being successively added. It is this aspect of NMR methodology that we consider first.

Signal averaging

Because of the low sensitivity of NMR, it is customary to co-add signals from N successive experiments in order to enhance the signal-to-noise ratio. Successive addition has the effect that the signals add coherently while the noise adds in random phase. Because the noise power is additive, the root mean-squared (rms) noise amplitude is proportional to $N^{1/2}$. As a result the signal-to-noise ratio improves as $N/N^{1/2}$ or $N^{1/2}$. There is, however, a limitation to the rate at which successive additions can be performed. To retain full signal strength the nuclear spin system must be allowed to recover its z-axis magnetisation between experiments, and this recovery requires a time delay of several T_1-relaxation times. This recovery imposes a limit to the number of co-additions that are possible in a given time duration.

Of course it is possible to repeat excitation pulses more rapidly than the time taken for full recovery, in which case the spins establish an equilibrium longitudinal magnetisation before each excitation pulse that is less than the thermal equilibrium value. This effect is known as partial saturation [47]. The time over which the longitudinal magnetisation recovers before the next excitation pulse is the simply the pulse repetition time. Given a repetition time T_R and longitudinal relaxation time T_1, the equilibrium magnetisation immediately before the RF pulse for a repetitive single θ_x pulse experiment is

$$M_z = M_0 \frac{\exp(-T_R/T_1)}{1 - \cos\theta \exp(-T_R/T_1)} \tag{4.73}$$

The method by which this result is obtained is instructive since it is generally applicable to more complicated pulse sequences. The dynamic equilibrium is established by equating the z-magnetisation just before the RF pulse, $M_z(0_-)$ to the z-magnetisation, $M_z(T_R)$, that remains from the preceding sequence, following relaxation. In the derivation of eqn 4.73, a simplifying assumption is made, namely that the role of transverse magnetisation can be neglected because of irreversible decay after each excitation and signal acquisition. Using the symbol $M_z(0_+)$ to represent the z-magnetisation immediately following the RF pulse, we can write [14]

$$M_z(0_+) = M_z(0_-)\cos\theta \tag{4.74}$$

and

$$M_z(T_R) = M_z(0_+)\exp(-T_R/T_1) + M_0(1 - \exp(-T_R/T_1)) \tag{4.75}$$

Equating $M_z(T_R)$ and $M_z(0_-)$, eqn 4.73 follows directly.

The initial amplitude of the transverse magnetisation just after the θ pulse is

$$M_y = M_0 \frac{\exp(-T_R/T_1}{1 - \cos\theta \exp(-T_R/T_1)} \sin\theta \tag{4.76}$$

The maximum partial saturation signal amplitude is therefore not obtained for $\theta = 90°$, except where T_R/T_1 is large. An optimum condition can be found by adjusting the nuclear turn angle θ to a value known as the Ernst angle, θ_E , for which

$$\cos\theta_E = \exp(-T_R/T_1) \tag{4.77}$$

For T_R/T_1 of around three, the relaxation between pulses is fairly complete and the optimum turn angle close to 90°. The signal-to-noise advantage in a repetitive pulse

experiment, in which T_R is chosen to be much shorter than this and in which θ is set to θ_E, is around $\sqrt{2}$.

It should, however, be noted that use of the Ernst angle requires care. Incomplete transverse relaxation between successive experiments can lead to unexpected signals appearing in multiple pulse sequences [14, 48]. Pulsed magnetic field gradient experiments, however, are not necessarily subject to this effect because the gradient pulses used during acquisition of the signal cause a destruction of magnetisation coherence. This feature facilitates the use of rapidly repeated low turn-angle pulse experiments.

Whatever the repetition delay and nuclear turn-angle employed, the T_1 relaxation time provides a fundamental limit to the available signal-to-noise ratio.

Phase cycling

Because the phase of the signal depends on the RF pulse phase, it becomes possible to distinguish the NMR FID signal from any background interference by RF phase alternation. For example, incrementing the RF phase by 180° will lead to signal inversion. Thus a successive phase alternation in 180° steps linked to successive addition and subtraction of the incoming signal from the data sum will lead to coherent superposition of the FID while the background interference is nulled. The process of addition and subtraction can be thought of as an alternation of the receiver phase so that the phase cycle can be written (0°,0°)-(180°,180°), where the RF transmitter and receiver phases are given in brackets. This particular cycle is called coherent noise cancellation.

The (0°,0°)-(180°,180°) sequence represents the simplest possible form of phase cycling. Other more sophisticated schemes enable the spectroscopist to correct for phase and amplitude anomalies in quadrature detection [49], transverse magnetisation interference due to rapid pulse repetition [50], and echo artifacts due to pulse amplitude errors. Among these phase and amplitude errors in quadrature detection are the primary cause of artifacts in NMR imaging and they can be nicely corrected in the 4-pulse CYCLOPS sequence of Hoult and Richards [49], a sequence which is so useful that it is generally incorporated as a subcycle of all other phase cycles.

When the amplitudes of the quadrature signal channels are unmatched or the relative phases are not precisely 90° apart, the complex Fourier transformation results in foldback artifacts. By successively swapping the channels used to acquire the real and imaginary signals, equivalent to a 90° transmitter and receiver phase-shift, the error is compensated to first order as shown in Fig. 4.17. The CYCLOPS sequence also incorporates the usual 0°/180° alternation of coherent noise cancellation, giving a four-pulse cycle (0°,0°)-(90°,90°)-(180°,180°)-(270°,270°).

Generally, phase cycling procedures are performed via the data acquisition software. Most modern NMR spectrometers select the phase of the RF transmitter by digital means so that the RF pulse phase can be simply manipulated through the software, usually in steps of 90°, although smaller steps are also available for some experiments involving multiple quantum filters. Similarly it is possible to 'adjust the receiver phase' in 90° steps. In practice, this is usually performed not in the phase sensitive detector, but after digitisation, by means of a software 'trick'. Whereas a shift of 180° corresponds to negation of both the incoming real and imaginary signals, a shift of 90° corresponds to negation of the incoming real followed by an interchange

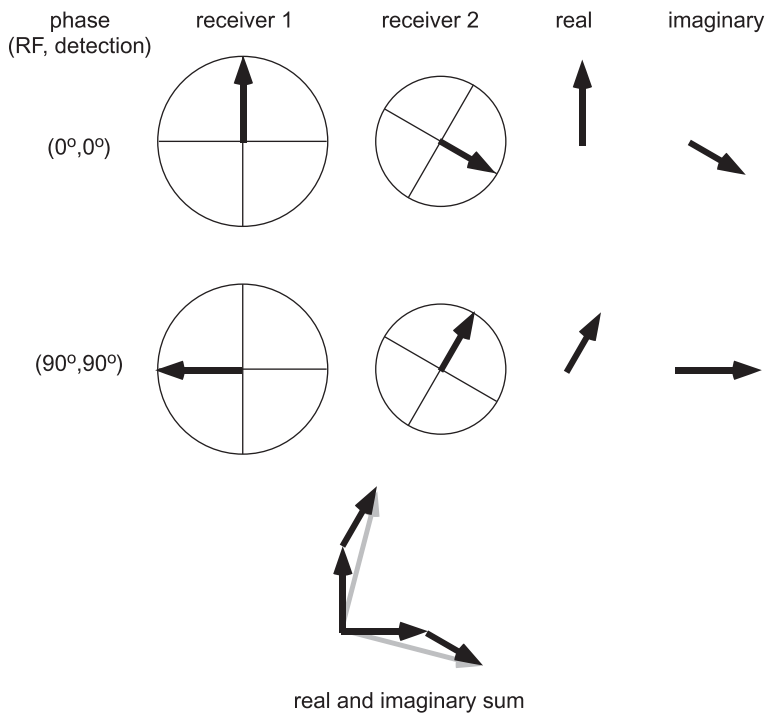

Fig. 4.17 The CYCLOPS method of phase cycling. The two receivers are shown as having different gains and phase setting not precisely in quadrature. By alternating both the transmitter and receiver phase between 0° and 90°, the real and imaginary signals are routed through both receivers and the summed resultants have matched amplitudes and quadrature phases to first order.

of the real and imaginary signals. It is of course this interchange that is so essential to the success of the CYCLOPS cycle.

Inversion recovery

Inversion recovery [51] is used for the measurement of T_1-relaxation times, as well as for the selective suppression of unwanted spin signals. The RF pulse sequence and resulting magnetisation trajectories are shown in Fig. 4.18. The first 180° RF pulse inverts the magnetisation vector, so subjecting the system to the most severe disturbance from equilibrium. Spin–lattice relaxation proceeds for a time t, following which a 90°_x pulse is used to inspect the remaining longitudinal magnetisation. The signal amplitude is described by

$$M_y(t) = M_0(1 - 2\exp(-t/T_1)) \tag{4.78}$$

A noteworthy feature of this method is the crossover from a negative signal (proportional to $-M_0$) at $t = 0$ to a positive signal (proportional to M_0) as $t \to \infty$. This crossover through zero magnetisation occurs at $t = 0.6931T_1$ and can be exploited to good effect. First it is clear that a measurement of time for the crossover null can yield T_1 in a single measurement. Second, the method may be used to remove the

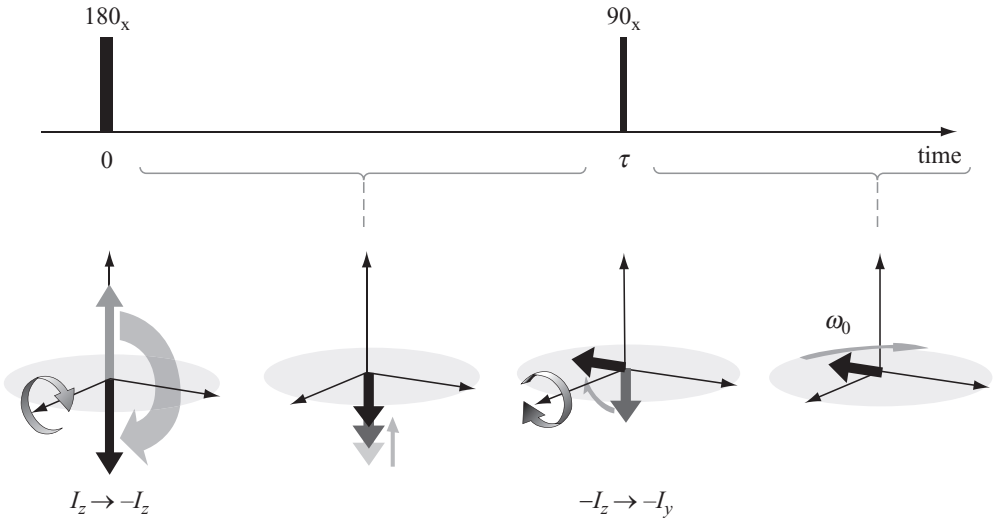

Fig. 4.18 Inversion recovery pulse sequence and magnetisation trajectories. At each RF pulse the grey arrow represents the magnetisation prior to the pulse, while the black vector represents the magnetisation after the pulse. Also shown is the evolution of the density matrix under the action of the pulse sequence.

contribution from a spin with specific T_1-value by applying a pulse at a time interval $0.6931T_1$ before the experimental pulse sequence. Such signal suppression is particularly important in biological experiments where water suppression is desired. While the inversion recovery method of signal suppression is simple, it can lead to distortions in the NMR spectrum. Other more sophisticated and effective methods for selective signal suppression include binomial pulse sequences [52] and SUBMERGE [53].

4.6.2 Echoes

Spin echo

Magnetic field inhomogeneity causes nuclear spins to precess at differing Larmor frequencies according to their location in the sample, an effect which forms the basis of the NMR imaging method. Even in conventional NMR experiments, where no magnetic field gradient is deliberately applied, the inhomogeneity of the polarising magnet will result in a field spread across the sample of ΔB_0. This spread causes a dephasing of transverse magnetisation following a 90°_x RF pulse. Transverse magnetisation phase coherence therefore lasts only for a time of order $(\gamma \Delta B_0)^{-1}$, a transience which apparently constrains the length of time over which this magnetisation can be manipulated or detected. Many years ago Erwin Hahn [19] discovered that this loss of phase coherence was inherently reversible. Application of a second 180° RF pulse after a time delay τ will cause refocusing at 2τ, as shown in Fig. 4.19, and the resulting phase coincidence is known as a spin echo, with the phase of the 180° pulse determining the sign of the echo signal.

At this point it is useful to introduce the idea of precession using the density matrix picture. Equation 3.53 describes the evolution of the density matrix in terms of operators involving the Hamiltonian. We will not solve these equations explicitly in the case of the spin echo but we will describe the successive evolution stages. To help visualise this process we can use rotating frame 'precession diagrams', like those shown in Fig. 4.16. Here the Hamiltonian term is in each case a Zeeman interaction, in (a) caused by an offset, ΔB_0, in magnetic field, applied along the z-axis, and giving a Hamiltonian $\Delta\omega_0 I_z$; in (b) caused by an RF pulse θ_x; and in (c) caused by an RF pulse θ_y.

In thermal equilibrium the spin system density matrix has a state of longitudinal polarisation so that the density matrix is proportional to I_z. The first RF pulse, applied along the x-axis in the rotating frame, corresponds to a Hamiltonian $\gamma B_1 I_x$, which causes a cyclic precession of I_z to I_y and back to I_z at a rate γB_1, a process which is illustrated in Fig. 4.16. 90° rotation is achieved by terminating the pulses at a time when ρ has evolved into I_y. Following the RF pulse, the new density matrix is now subject to the local Zeeman field offset.[12] This next stage in the evolution, the precession due to the Hamiltonian, $\Delta B_0 I_z$, is shown in Fig. 4.16. The evolution diagram for the second RF pulse can be easily worked out by cyclically permuting the vectors of Fig. 4.16. A 180°_y pulse inverts the I_x terms in the density matrix, but leaves the I_y terms unchanged. If the time of initial evolution in the field offset ΔB_0 was τ, the final evolution for an equal time τ in the same field offset ΔB_0 will therefore cause a perfect restoration of the I_y density matrix state that existed immediately after the first RF pulse, a process which is also shown in Fig. 4.19. It is important to note that the phase of the 180° inversion pulse is relevant. A 180°_x pulse, for example, results in an echo of negative sign.

We can follow the evolution of the density matrix polarisation state by using a succession of arrows to represent the time progression, where the Hamiltonian term under which ρ evolves is written above the arrow. For example, the evolution progression for the Hahn echo would have the following appearance:

$$\begin{aligned} & I_z \\ & \xrightarrow{-(\pi/2)I_x} \quad I_y \\ & \xrightarrow{-\Delta\omega_0\tau I_z} \quad I_y\cos\phi + I_x\sin\phi \\ & \xrightarrow{-(\pi)I_y} \quad I_y\cos\phi - I_x\sin\phi \\ & \xrightarrow{-\Delta\omega_0\tau' I_z} \quad I_y\cos\phi\cos\phi' + I_x\cos\phi\sin\phi' - I_x\sin\phi\cos\phi' + I_y\sin\phi\sin\phi' \end{aligned} \tag{4.79}$$

where ϕ and ϕ' are the precessional phase shifts, $\Delta\omega_0\tau$ and $\Delta\omega_0\tau'$, τ and τ' being evolution times in the dephasing and rephasing intervals of the echo sequence. Note that magnetic field inhomogeneity leads to a distribution of offsets, $\Delta\omega_0$, and hence a dephasing of the transverse magnetisation. However, the effect on the density matrix

[12] Of course, this field was also present during the RF pulse but we are able to neglect its effect by ensuring that the RF field strength is very much greater than ΔB_0.

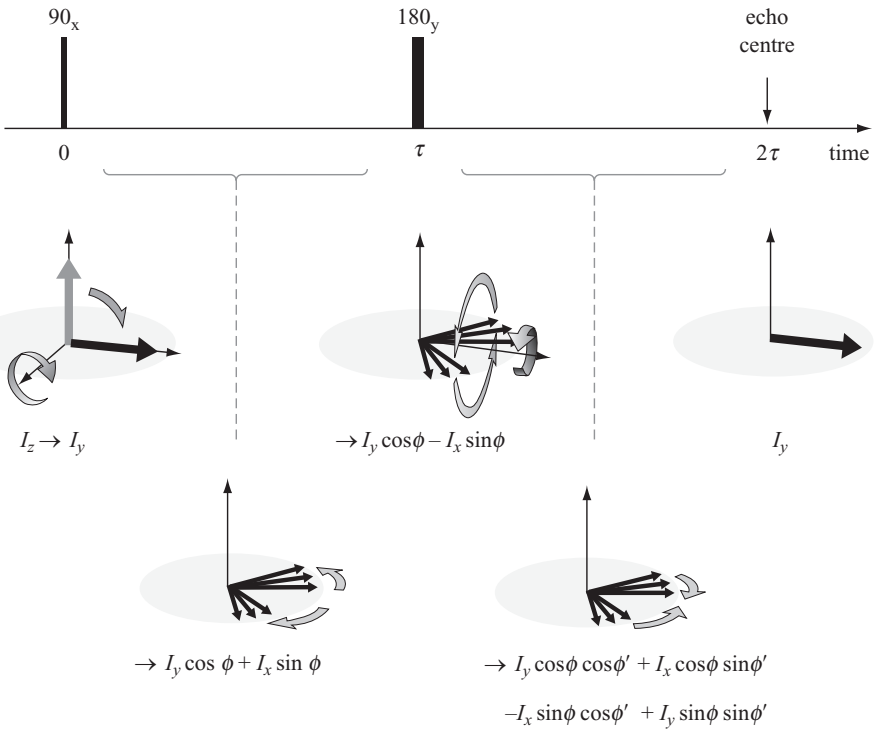

Fig. 4.19 Spin-echo pulse sequence showing the evolution of magnetisation and the density matrix. Note that the 180°_x pulse inverts the phase of each spin isochromat (i.e. $\phi \rightarrow -\phi$) so that perfect refocusing occurs at time $t = 2\tau$ where $\phi = \phi'$. The diagram shows a sample of three isochromats.

of the 180° RF pulse $(-(\pi)I_y)$ is to make it appear as though the time interval τ (and hence the phase evolution ϕ) were reversed in sign. This 'time-reversal' property lies at the heart of all echo methods.

Consider the case where the intervals τ and τ' are equal so that $\phi = \phi'$. Then the final state of the density matrix is

$$\overline{I_y \cos^2\phi + I_x \cos\phi \sin\phi - I_x \sin\phi \cos\phi + I_y \sin^2\phi} = I_y \tag{4.80}$$

The 180°_y RF pulse (denoted $-(\pi)I_y$) causes the phases to be inverted (ie angle $\Delta\omega_0\tau$ becomes $-\Delta\omega_0\tau$) so that the effect of the next evolution period τ' is to restore the the polarisation to I_y at the time $\tau' = \tau$. Of course, I_y is an observable under the transverse magnetisation detection operator $I_x + iI_y$. In other words

$$\begin{aligned} Tr([I_x + iI_y][I_y]) &= iTr(I_y^2) \\ &= i\frac{1}{3}(2I+1)I(I+1) \end{aligned} \tag{4.81}$$

We may use eqn 3.88 to relate the expectation value, $\langle I_x + iI_y \rangle$, of our detection operator to the initial expectation value of longitudinal angular momentum, $\langle I_z \rangle_0 = Tr(I_z \rho_0)$, namely

$$\langle I_x + iI_y \rangle = i\langle I_z \rangle_0 \tag{4.82}$$

Note again that all observables are in fact real numbers. The use of the complex numbers here is simply a device that we choose to utilise in order to independently manage the in-phase and quadrature channels. What eqn 4.82 states is that our signal derives from the full $\langle I_z \rangle_0$ angular momentum of the initial thermal equilibrium state and that it is detected in the quadrature channel, in other words, along I_y in the rotating frame.

Suppose the second RF pulse were 90°_x, identical to the first.[13] The density matrix treatment makes the analysis simple.

$$\begin{aligned} & I_z \\ & \xrightarrow{-(\pi/2)I_x} \quad I_y \\ & \xrightarrow{-\Delta\omega_0\tau I_z} \quad I_y\cos\phi + I_x\sin\phi \\ & \xrightarrow{-(\pi/2)I_x} \quad -I_z\cos\phi + I_x\sin\phi \\ & \xrightarrow{-\Delta\omega_0\tau' I_z} \quad -I_z\cos\phi + I_x\sin\phi\cos\phi' - I_y\sin\phi\sin\phi' \end{aligned} \tag{4.83}$$

The echo appears where the intervals τ and τ' are equal, so that $\phi = \phi'$ and the final state of the density matrix is

$$\overline{-I_z\cos\phi + I_x\sin\phi\cos\phi - I_y\sin^2\phi} \tag{4.84}$$

Noting $Tr(I_zI_x) = Tr(I_yI_z) = Tr(I_yI_x) = 0$, the detection operator gives

$$\begin{aligned} Tr([I_x + iI_y]\rho) &= Tr([I_x + iI_y]\overline{[-I_z\cos\phi + I_x\sin\phi\cos\phi - I_y\sin^2\phi]}) \\ &= Tr(I_x^2)\overline{\sin\phi\cos\phi} - iTr(I_y^2)\overline{\sin^2\phi} \\ &= -\frac{1}{2}iTr(I_y^2) \end{aligned} \tag{4.85}$$

The overbar represents the averaging needed to account for the distribution of offsets resulting from the magnetic field inhomogeneity. For a uniform distribution of precessional phase shifts, $\phi = \Delta\omega_0\tau$, this average gives $\overline{\sin\phi\cos\phi} = 0$ and $\overline{\sin^2\phi} = 1/2$ and hence leads to an echo signal $-\frac{1}{2}iTr(I_y^2)$, exactly -1/2 of that found for the echo obtained using the 180°_y refocusing pulse.

In spin systems experiencing only Zeeman Hamiltonians, the spin-echo sequence refocuses all dephasing due to inhomogeneous broadening, chemical shift, and heteronuclear scalar spin–spin interactions. Because the 180° RF pulse inverts all spins and so leaves the interaction term $\pi J 2\mathbf{I_1}\cdot\mathbf{I_2}$ invariant, homonuclear scalar spin–spin interactions are not refocused and therefore remain to modulate the echo. Over and above this modulation, residual attenuation of the echo is due to spin–spin relaxation

[13] Historically, this was the first echo experiment performed by Hahn.

alone and, in principle, a plot of echo amplitudes $M_y(2\tau)$ obtained from differing τ values can be used to yield T_2 according to

$$M_y(2\tau) = M_0 \exp(-2\tau/T_2) \tag{4.86}$$

Earlier we saw that sampling of the decaying NMR signal at positive times only leads to the existence of a dispersion signal in the imaginary domain following Fourier transformation. Figure 4.20 suggests a mechanism by which 'negative' time may be sampled. If we take the centre of the echo as our time origin and begin sampling the signal at this point, the resulting spectrum is the same as that shown earlier for the single-pulse experiment, with the exception that T_2 relaxation will have attenuated the signal at $t = 0$ and hence reduced the area under the absorption peak by the same factor. [14] Furthermore the dispersion spectrum will still exist.

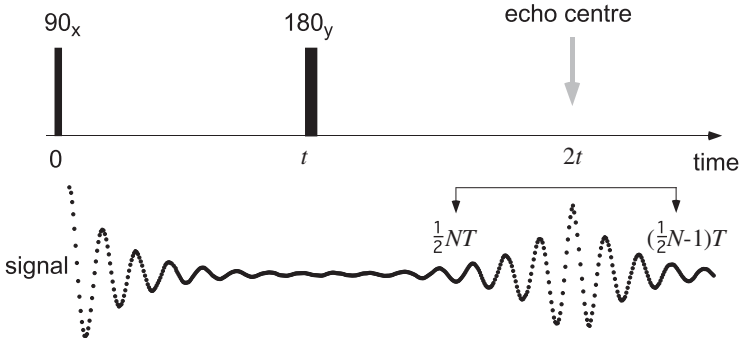

Fig. 4.20 Echo signal in a simple spin echo (real part only shown). Note that the echo centre represents a local time origin. Because of echo symmetry, sampling of the full echo leads to a spectrum without dispersion.

Suppose, however, that we were to sample the entire echo, dividing our sampling time period equally before and after the echo, with $t = 0$ at the echo centre. In this case the digitised time values run between $-\frac{1}{2}NT$ and $(\frac{1}{2}N - 1)T$, and, as before, the Fourier-domain points run between $-\frac{1}{2}N(1/NT)$ and $(\frac{1}{2}N - 1)(1/NT)$. Neglecting T_2 effects and presuming a signal phase $\phi = 0$, it is clear that the in-phase and quadrature signals are, respectively, symmetric and antisymmetric, leading to an entirely real spectrum. If $\phi \neq 0$ then the spectrum is multiplied by $\exp(i\phi)$ and will contain both real and imaginary parts, although the real spectrum can be recovered by the usual 'phasing' process. There is, however, a crucial difference between this situation the case of $t > 0$ sampling. When full echo sampling is used the resulting modulus spectrum for $\phi \neq 0$ exactly reproduces the real spectrum for $\phi = 0$, a restoration process which is impossible in the case of data sampled only at positive times because of the existence of the dispersion component in the spectrum.

[14] For the purpose of the present argument we will neglect the role of bilinear spin interactions such as homonuclear couplings, which are non-refocusable via the Hahn echo and remain to modulate the echo envelope.

CPMG

The phase coherence recovered in the nuclear spin echo is subsequently lost for $t > 2\tau$. Successive recoveries are, however, possible if a train of additional 180° RF pulses is used, as suggested by Carr and Purcell in 1954 [44]. The choice of phase with which these pulses are applied is important if the cumulative effects of small turn-angle errors is to be avoided. In the Meiboom–Gill modification [45] to the Carr–Purcell train, the use of quadrature 180°_y pulses provides the appropriate compensation. The envelope of the echoes in a Carr–Purcell–Meiboom–Gill (CPMG) sequence is determined by T_2 decay alone, and so it is possible to determine T_2 in a single experiment. The method is illustrated in Fig. 4.21.

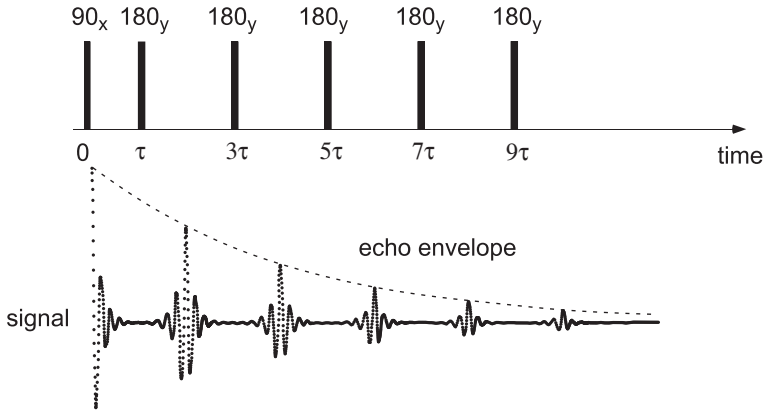

Fig. 4.21 CPMG pulse sequence exhibiting multiple spin echoes at times $2n\tau$, modulated by a T_2 relaxation envelope.

The production of multiple echoes in the CPMG pulse sequence suggests an obvious application in signal averaging. Co-addition of echoes within a train leads to signal-to-noise enhancement [54] in addition to that obtained by addition of the independent experiments separated by the T_1 recovery period, T_R.

Stimulated echo

In many materials, especially those with molecules undergoing motion that is slow compared with the period of the nuclear Larmor precession, the transverse relaxation time T_2 is considerably shorter than T_1. The fact that the 'lifetime of spin polarisation' exceeds the 'lifetime of first-order spin coherence' can be turned to advantage where one wishes to 'store' coherence over a long time interval. Suppose that the transverse magnetisation existing at some point of time, τ, is required to be stored for later recall. An example might be where one wishes to use this magnetisation at a later time to see how far the molecules containing the NMR nuclei have moved. The method used is shown in Fig. 4.22, where a single 90°_x pulse applied after a time t has the effect of rotating the y-component of magnetisation into longitudinal polarisation along the z-axis, a state in which only T_1 relaxation will occur. Of course any x-magnetisation will be unaffected, so that only half the transverse magnetisation can be stored in this

way. Recall is made at some later stage using another 90°_x pulse. As shown, this leads to an echo at time τ after the last RF pulse. This stimulated echo [19] is of particular importance where the translational motions of molecules are being measured using pulsed field gradient spin-echo methods.

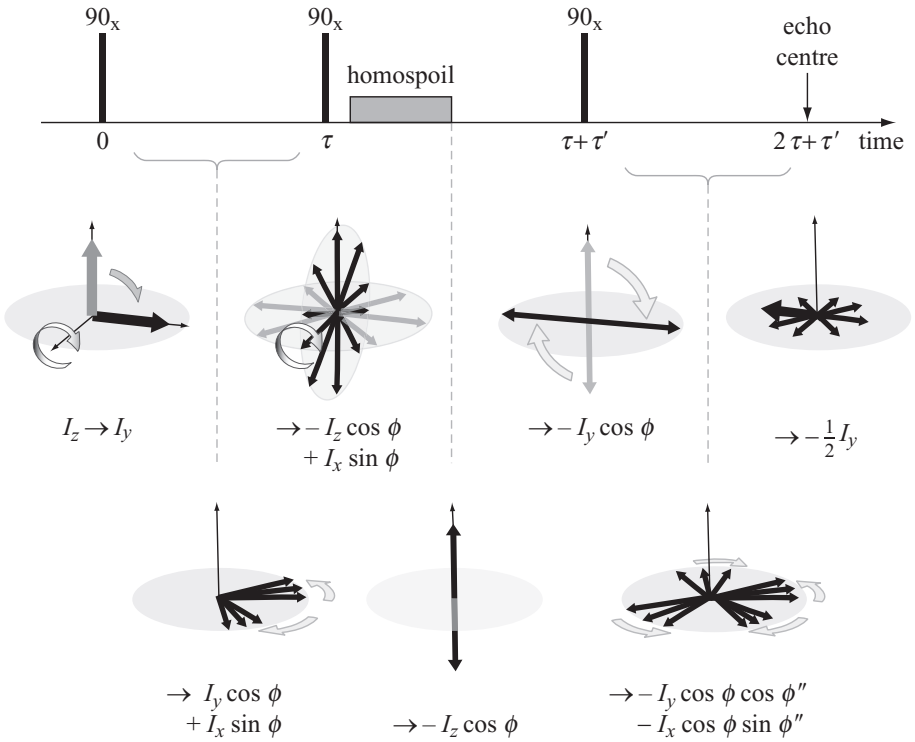

Fig. 4.22 stimulated-echo pulse sequence incorporating a 'homospoil' gradient pulse during the 'z-storage' period τ'. The final density matrix is obtained from an ensemble average over the isochromats $-I_y\overline{\cos\phi\cos\phi''} - I_x\overline{\cos\phi\sin\phi''}$. At $\tau'' = \tau$, $\phi'' = \phi$ and $\overline{\cos^2\phi} = \frac{1}{2}\overline{(1+\cos(2\phi))} = 1/2$, while $\overline{\cos\phi\sin\phi} = \frac{1}{2}\overline{\sin(2\phi)} = 0$. Note that the final echo state represents a vector $-\frac{1}{2}I_y$ along with an ensemble spread of $-\frac{1}{2}\left(I_y\cos(2\phi) + I_x\sin(2\phi)\right)$, a set of isochromats distributed in the transverse plane whose net contribution is zero.

Let us analyse the stimulated echo using the same density matrix method employed earlier. The pulse sequence chosen consists of three 90°_x RF pulses separated by time intervals τ, τ', and τ''. Then

$$
\begin{aligned}
& I_z \\
& \xrightarrow{-(\pi/2)I_x} \quad I_y \\
& \xrightarrow{-\Delta\omega_0\tau I_z} \quad I_y\cos\phi + I_x\sin\phi \\
& \xrightarrow{-(\pi/2)I_x} \quad -I_z\cos\phi + I_x\sin\phi
\end{aligned}
$$

$$\begin{aligned}
&\xrightarrow{-\Delta\omega_0\tau' I_z} && -I_z\cos\phi + I_x\sin\phi\cos\phi' - I_y\sin\phi\sin\phi' \\
&\xrightarrow{-(\pi/2)I_x} && -I_y\cos\phi + I_x\sin\phi\cos\phi' + I_z\sin\phi\sin\phi' \\
&\xrightarrow{-\Delta\omega_0\tau'' I_z} && -I_y\cos\phi\cos\phi'' - I_x\cos\phi\sin\phi'' + I_x\sin\phi\cos\phi'\cos\phi'' \\
& && -I_y\sin\phi\cos\phi'\sin\phi'' + I_z\sin\phi\sin\phi'
\end{aligned} \tag{4.87}$$

The detection operator $I_x + iI_y$ gives

$$\begin{aligned}
Tr(I_x + iI_y\rho) = Tr(I_x^2)[-\overline{\cos\phi\sin\phi''} + \overline{\sin\phi\cos\phi'\cos\phi''}] \\
+iTr(I_y^2)[\overline{\cos\phi\cos\phi''} - \overline{\sin\phi\cos\phi'\sin\phi''}]
\end{aligned} \tag{4.88}$$

and yields echoes $-\frac{1}{2}iTr(I_y^2)$ at $\tau'' = \tau$, $-\frac{1}{2}iTr(I_y^2)$ at $\tau'' = \tau - \tau'$, and $\frac{1}{2}iTr(I_y^2)$ at $\tau'' = \tau' - \tau$. The first of these is the desired stimulated echo. But the stimulated-echo RF pulse sequence also generates two additional spin echoes. These are, respectively, the echo of the initial pulse FID caused by the second pulse and the echo of that echo caused by the third pulse. Special care is needed to avoid interference between the stimulated echo and the two spin echoes. One effective approach is the use of a homogeneity-spoiling (homospoil) magnetic field gradient pulse applied during the 'z-storage' period between the second and third RF pulses, as shown in Fig. 4.22. This has the effect of destroying the unwanted transverse magnetisation without influencing the magnetisation that has been stored along the z-axis.

Density matrix precessions for coupled spins under $I_{1z}I_{2z}$

Let us revisit the spin–spin (scalar coupling) interaction of eqn 4.49. In the weak coupling case, $Jh \ll \delta$ ($\frac{1}{2}\phi \to 0$), we may write the scalar coupling interaction in its secular form as $H_{scalar_0} = 2\pi J I_{1z}I_{2z}$. Just as the Hamiltonian operator may be written, for coupled spins, in the product basis so may the density matrix, meaning that an operator such as I_{1z} is implicitly an outer product of I_{1z} and the identity for the second spin. Also, since we are dealing with a two-spin problem, we must be careful to always express our density matrix in terms of both spins, so that the starting thermal equilibrium state is $\sim (I_{1z} + I_{2z})$, the θ RF pulse in the rotating frame is the rotation operator $\exp(i\theta(I_{1x} + I_{2x}))$, and the density matrix after a 90°_x pulse is $\sim (I_{1y} + I_{2y})$. Subsequent evolution under the influence of the Zeeman terms, the RF pulses, and the secular part of the scalar coupling, $I_{1z}I_{2z}$, are shown in Fig. 4.23.

As a simple exercise, let us follow the evolution of the density matrix under the influence of the scalar coupling and under the RF pulses of a spin echo. Note that we will need to allow for the effect of both the chemical shift terms present in eqn 4.49. In other words, we allow each spin to have different Larmor frequencies $\delta_1\omega_0$ and $\delta_2\omega_0$. Note that because the Zeeman and scalar coupling terms commute in this weak coupling case, we are entitled to apply each evolution sequentially. The evolution progression for the Hahn echo, up to and including the effect of the 180°_y pulse, would have the following appearance:

$$
\begin{aligned}
&I_{1z} + I_{2z} \\
&\xrightarrow{-(\pi/2)(I_{1x}+I_{2x})} && I_{1y} + I_{2y} \\
&\xrightarrow{-\delta_1\omega_0\tau I_{1z}+\delta_2\omega_0\tau I_{2z}} && I_{1y}\cos\phi_1 + I_{2y}\cos\phi_2 + I_{1x}\sin\phi_1 + I_{2x}\sin\phi_2 \\
&\xrightarrow{-2\pi J I_{1z} I_{2z}} && I_{1y}\cos\phi_1 cos(\pi J\tau) - 2I_{1x}I_{2z}\cos\phi_1\sin(\pi J\tau) \\
& && +I_{1x}\sin\phi_1 cos(\pi J\tau) + 2I_{1y}I_{2z}\sin\phi_1\sin(\pi J\tau) \\
& && +I_{2y}\cos\phi_2 cos(\pi J\tau) - 2I_{1z}I_{2x}\cos\phi_2\sin(\pi J\tau) \\
& && +I_{2x}\sin\phi_2 cos(\pi J\tau) + 2I_{1z}I_{2y}\sin\phi_2\sin(\pi J\tau) \\
&\xrightarrow{-(\pi)(I_{1y}+I_{2y})} && I_{1y}\cos\phi_1 cos(\pi J\tau) - 2I_{1x}I_{2z}\cos\phi_1\sin(\pi J\tau) \\
& && -I_{1x}\sin\phi_1 cos(\pi J\tau) - 2I_{1y}I_{2z}\sin\phi_1\sin(\pi J\tau) \\
& && +I_{2y}\cos\phi_2 cos(\pi J\tau) - 2I_{1z}I_{2x}\cos\phi_2\sin(\pi J\tau) \\
& && -I_{2x}\sin\phi_2 cos(\pi J\tau) - 2I_{1z}I_{2y}\sin\phi_2\sin(\pi J\tau)
\end{aligned}
\tag{4.89}
$$

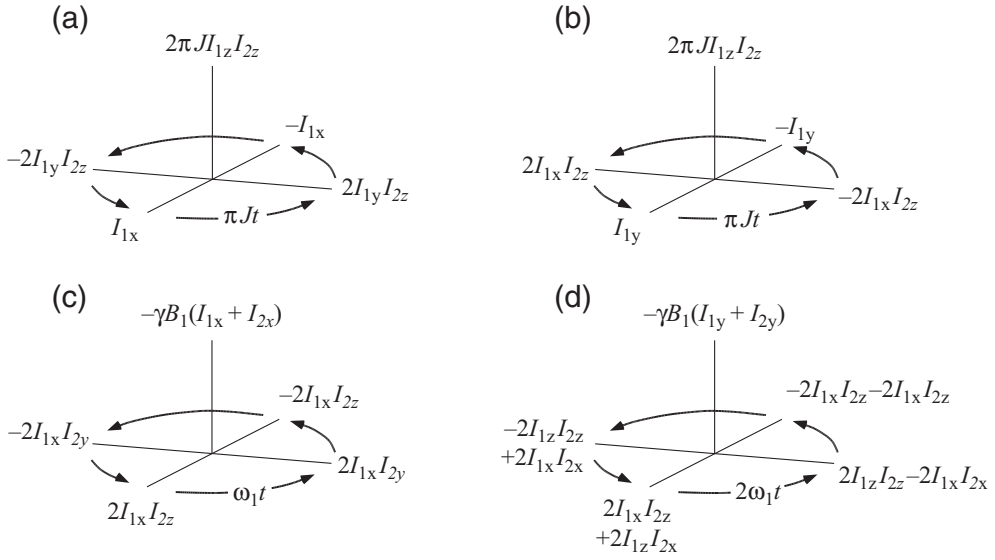

Fig. 4.23 Precession diagrams for states of a scalar coupled spin-$\frac{1}{2}$ pair. The bilinear interaction $2\pi J I_{1z} I_{2z}$ causes the magnetisation states to evolve into two-spin coherences. Note that the RF pulse consists of a sum of spin 1 and spin 2 operators if it is applied non-selectively (i.e. with broad bandwidth). (a) and (b) show evolution of I_x and I_y under the bilinear interaction into states comprising single-quantum coherence of spin 1 in antiphase with spin 2. (c) and (d) show evolution of these antiphase states under the influence of a broadband RF pulse. Note that the precession rate in (d) is $2\omega_1$, meaning that a 45° RF pulse causes a precession of the total spin density matrix state, $(2I_{1x}I_{2z} + 2I_{1z}I_{2x})$, into $(2I_{1z}I_{2z} - 2I_{1x}I_{2x})$. $2I_{1x}I_{2x}$ is an equal admixture of double and single-quantum coherence.

At this point we can see that the evolutions of the 1 and 2 spins are the same, apart from their different Larmor frequencies. Hence we may focus our attention on the 1 spin. The chemical shift evolution in the equal period τ after the 180°_y pulse leads to additional $\cos\phi_1$ and $\sin\phi_1$ modulation. The echo arises from the sum $\cos^2\phi_1 + \sin^2\phi_1 = 1$. Allowing for the scalar coupling evolution as well, these $\cos^2\phi_1$ and $\sin^2\phi_1$ contributions come from each of the four 1-spin terms, respectively, as $I_{1y}\cos^2\phi_1 cos^2(\pi J\tau)$, $-I_{1y}\cos^2\phi_1 sin^2(\pi J\tau)$, $I_{1y}\sin^2\phi_1 cos^2(\pi J\tau)$, and $-I_{1y}\sin^2\phi_1 sin^2(\pi J\tau)$. Thus the full density matrix at the point of the echo is $(I_{1y} + I_{2y})\cos(2\pi J\tau)$.

The modulation of the echo occurs because the 180°_y pulse has the effect of flipping both the 1 and 2 spins, leaving the scalar coupling Hamiltonian term, $2\pi J I_{1z} I_{2z}$, unchanged. The effect of the modulation by $\cos(2\pi J\tau)$ will be apparent in the successive echo amplitudes of a CPMG train. Fourier transformation will lead to a spectrum split into a doublet separated by J in cyclic frequency. Indeed, the very first observation of J-coupling was made using just such an echo train to remove field inhomogeneity effects, while leaving the spin–spin coupling revealed [55, 56].

The solid echo

Echoes arise when it is possible to devise a pulse sequence in which, at some point, undesired prior evolutions of the density matrix are made to undergo a time reversal so that subsequent evolution results in a perfect cancellation or 'refocusing'. In the case of the spin echo and stimulated echo, the evolutions that we seek to refocus are those due to a spread of Zeeman interactions, arising, for example, from inhomogeneous magnetic fields. In this section we demonstrate another echo phenomenon where the undesired evolution arises from a spread of internuclear dipolar interactions. These will typically occur in a solid where each nucleus experiences, with its many neighbours, static dipolar interactions characterised by a distribution of internuclear vectors of varying orientation and length. The dipolar interaction (eqn 4.53) involves a bilinear spin operator, $\omega_{ij}[3I_{iz}I_{jz} - \mathbf{I_1}\cdot\mathbf{I_2}]$, where ω_{ij} is a 'dipolar precession frequency', which we use to characterise the strength of the interaction for the particular spin pair, i and j. For the purpose of this exercise we may neglect the term, $\mathbf{I_i}\cdot\mathbf{I_j}$, which commutes with the initial density matrix term $I_{iy} + I_{jy}$, and with the term $I_{ix}I_{jz} + I_{iz}I_{jx}$, which evolves from $I_{iy} + I_{jy}$ under the influence of $I_{iz}I_{jz}$.

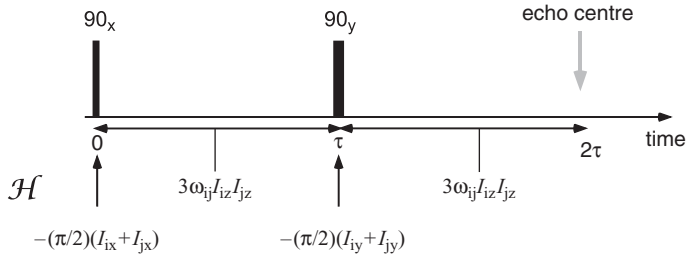

Fig. 4.24 Solid echo pulse sequence showing the active Hamiltonian terms at different times during the sequence.

Of course, for each nucleus i there will exist a distribution of ω_{ij}, arising from the various internuclear separations and θ_{ij} orientations associated with the various j spins, resulting in a coherence dephasing. That in turn leads to decaying signal, sometimes called the 'Bloch decay', as represented by eqn 4.54. It is that dephasing that the solid echo seeks to reverse.

Let us consider the echo formation from the standpoint of the product operator formalism, using the precession diagrams shown in Fig. 4.23. The dipolar interaction causes precession of the initial I_{iy} state of the density matrix into $I_{ix}I_{jz}$, and hence a dephasing of I_{iy} into an admixture $-I_{iy}\cos(\omega_{ij}\tau) + 2I_{ix}I_{iz}\sin(\omega_{ij}\tau)$. Note that ω_{ij} will be of order $M_2^{1/2}$. The time-reversal process will therefore require an RF pulse that will convert $I_{ix}I_{iz}$ to $-I_{ix}I_{iz}$, in effect inverting the phase. This is achieved by a 90°_y RF pulse in the following sequence in which, following our previous practice, we use ϕ to represent the phase acquired. In the case of the dipolar interaction, the phase angle after time τ is $\phi = \frac{3}{2}\omega_{ij}\tau$. Hence

$$
\begin{aligned}
&I_{iz} + I_{jz} \\
&\qquad \xrightarrow{-(\pi/2)(I_{ix}+I_{jx})} \quad I_{iy} + I_{jy} \\
&\qquad \xrightarrow{3\omega_{ij}I_{iz}I_{jz}} \quad (I_{iy} + I_{jy})\cos\phi - (2I_{ix}I_{jz} + 2I_{iz}I_{jx})\sin\phi \\
&\qquad \xrightarrow{-(\pi/2)(I_{iy}+I_{jy})} \quad (I_{iy} + I_{jy})\cos(\phi) + (2I_{ix}I_{jz} + 2I_{iz}I_{jx})\sin(\phi) \\
&\qquad \xrightarrow{3\omega_{ij}I_{iz}I_{jz}} \quad (I_{iy} + I_{jy})\cos\phi\cos\phi' \\
&\qquad\qquad\qquad -(2I_{ix}I_{jz} + 2I_{iz}I_{jx})\cos\phi\sin\phi' \\
&\qquad\qquad\qquad +(2I_{ix}I_{jz} + 2I_{iz}I_{jx})\sin\phi\cos\phi' \\
&\qquad\qquad\qquad +(I_{iy} + I_{jy})\sin\phi\sin\phi'
\end{aligned}
\tag{4.90}
$$

The echo appears where the intervals τ and τ' are equal, so that $\phi = \phi'$ and the final state of the density matrix is $I_{iy} + I_{jy}$, exactly the magnetisation following the initial 90°_x pulse. Note that the detection operator in this multispin problem is now $[(I_{ix} + I_{jx} + i(I_{iy} + I_{jy})]$.

It is a simple, though tedious, extension to combine dephasing due to inhomogeneous magnetic fields and the distribution of (secular) dipolar interactions. Provided that the local magnetic field experienced by two spins, i and j, coupled by the dipolar interaction is the same, then the Zeeman operator involves $I_{iz} + I_{jz}$. This operator commutes with the full dipolar Hamiltonian so that the respective dephasings may be treated independently. The requirement of similar Zeeman interactions for i and j is satisfied for inhomogeneous magnetic fields because spins coupled by the dipolar interaction are within a few nanometers of each other and hence experience practically identical local fields.[15]

Because the 90°_y echo pulse is only capable of refocusing half the Zeeman dephasing, the echo turns out to be only half as big. However, by subtracting the signal of a $90^\circ_x - \tau - 90^\circ_x - \tau$ from that of the $90^\circ_x - \tau - 90^\circ_y - \tau$ sequence, both Zeeman and secular dipolar dephasings may be fully refocused.

[15] Of course a very different situation applies for intramolecular scalar couplings, where the chemical shift can make proximate spins experience different local fields.

The solid echo sequence equally works for high spin nuclei experiencing a distribution of quadrupolar interactions ($\sim I_z^2$), although the algebra is slightly more complicated. For example, for deuterium in the solid state the respective quadrupolar interactions may vary from nucleus to nucleus as a result of variations in the orientation of the electric field gradient, as would be the case in a powder or polydomain liquid crystal. Note that when dealing with the spin-1 deuteron in the solid state we can generally neglect dipolar interactions because the deuteron gyromagnetic ratio is so much smaller than that for the spin-$\frac{1}{2}$ proton.

4.6.3 Multiple pulse line-narrowing

In the liquid state, the rapid fluctuation of the dipolar interaction caused by molecular tumbling results in an average Hamiltonian in which the dipolar interaction is effectively zero. In order to produce this averaging it is necessary that the fluctuation rate, τ_c, be greater than the dipolar linewidth, $M_2^{1/2}$. In 1966 Ostroff and Waugh [57] and Mansfield and Ware [58] discovered that by application of a suitable train of RF pulses, the effective dipolar spin Hamiltonian could be made to fluctuate in a controlled way, thus leading to dipolar line-narrowing, sometimes referred to as 'decoupling'. The ability to slow the decay of the transverse magnetisation and hence to 'narrow the line' arises from the fact that, in the solid state, the dephasing of the FID is caused by static interactions that constitute an inhomogeneous broadening. Given the right pulse sequence these phase shifts can always be reversed, the solid echo being a simple example of such an approach.

A thorough description of multiple pulse line-narrowing is given in the book by Mehring [12], and the reader wishing to understand this subject in depth will find this text particularly helpful. Here we briefly review the essentials. The key element in the method is to introduce a periodic time-dependence in the dipolar Hamiltonian, and then to strobe the signal acquisition synchronously with the period of this Hamiltonian. Time-dependence is caused by a sequence of RF pulses, since these rotate the spin orientations and hence the vectors $\mathbf{I}_i$ and $\mathbf{I}_j$ in eqn 4.53. Of course, these pulses not only affect the Hamiltonian but also cause a sudden transformation in the density matrix as well. We can think of this by saying that in the rotating frame the total evolution operator is a product, $U_{RF}(t)U_D(t)$, where $U_{RF}(t)$ is the evolution operator representing the cumulative effect of the RF pulses and $U_D(t)$ is the evolution operator for the 'toggled' dipolar interaction. In order to separate the evolutions in this way, the appropriate time-dependent form for the dipolar Hamiltonian turns out to be

$$\mathcal{H}_D^*(t) = U_{RF}^{-1}(t)\mathcal{H}_D U_{RF}(t) \tag{4.91}$$

A key point to note is that, in comparison with density matrix evolution, the order of the U operators is reversed.

Before finding $U_D(t)$, we consider the role of $U_{RF}(t)$ in the product $U_{RF}(t)U_D(t)$. The longer-term influence of U_{RF} can be removed by making the RF pulse sequence cyclic, such that its associated evolution operator, $U_{RF}(t)$, is unity where t is a multiple of the cycle time, t_c. Provided the signal is sampled stroboscopically at multiples of this period, the net effect on the density matrix is due only to the evolution caused by $U_D(t)$. The manner in which this fluctuation is introduced must have the symmetry

necessary to cancel the dipole–dipole interaction and so make $U_D(t)$ equal to the identity operator.

Average Hamiltonian

Each time an RF pulse is applied the Hamiltonian suddenly changes with the time dependence given by eqn 4.91. If we imagine that the RF pulses are infinitesimally narrow then $\mathcal{H}_D^*(t)$ becomes 'piecewise constant' such that

$$\mathcal{H}_D^*(t) = \mathcal{H}_{D_k}^* \tag{4.92}$$

for $(\tau_1 + \tau_2 + ... + \tau_{k-1}) < t < (\tau_1 + \tau_2 + ... + \tau_k)$. To understand how the evolution of the density matrix occurs, we return to the Liouville equation 3.53. The relevant evolution operator is

$$U_D(t) = \exp(-i\mathcal{H}_{D_n}^*\tau_n)....\exp(-i\mathcal{H}_{D_1}^*\tau_1) \tag{4.93}$$

where

$$t = \sum_{k=1}^{n} \tau_n \tag{4.94}$$

Of course the order of these successive evolution operators is crucial. Because a product of unitary transformations is itself unitary, the product in eqn 4.93 can be written as a single operator

$$U(t) = \exp(-i\overline{\mathcal{H}}_D(t)t) \tag{4.95}$$

$\overline{\mathcal{H}}_D(t)$ is the average Hamiltonian [59]. In the case of the dipolar interaction, we attempt to make this zero. $\overline{\mathcal{H}}_D(t)$ is not simply the time average of the various $\mathcal{H}_{D_k}^*$, although such an average is one of the leading terms. It can be shown that $\overline{\mathcal{H}}_D(t)$ comprises a sum of terms, $\overline{\mathcal{H}}_D^{(0)} + \overline{\mathcal{H}}_D^{(1)} + \overline{\mathcal{H}}_D^{(2)}) + ...$, where, for example,

$$\begin{aligned}
\overline{\mathcal{H}}_D^{(0)} &= \frac{1}{t}\{\mathcal{H}_{D_1}^*\tau_1 + \mathcal{H}_{D_2}^*\tau_2 + ... + \mathcal{H}_{D_n}^*\tau_n\} \\
\overline{\mathcal{H}}_D^{(1)} &= -\frac{i}{t}\{[\mathcal{H}_{D_2}^*\tau_2, \mathcal{H}_{D_1}^*\tau_1] + [\mathcal{H}_{D_3}^*\tau_3, \mathcal{H}_{D_1}^*\tau_1] + [\mathcal{H}_{D_3}^*\tau_3, \mathcal{H}_{D_2}^*\tau_2] + ...\}
\end{aligned} \tag{4.96}$$

The ideal RF pulse sequence is one that renders all terms $\overline{\mathcal{H}}_D^{(k)}$ zero. Removal of the zeroth-order term is relatively straightforward, and can be achieved with a cycle of four pulses. Provided this cycle is symmetric in the sense $\mathcal{H}_D^*(t) = \mathcal{H}_D^*(t_c - t)$, then all odd-order terms also vanish. Removal of higher, even-order terms can, in principle, be achieved by including more pulses in the cycle, but often the cumulative effect of RF pulse imperfections leads to additional decay of the transverse magnetisation.

WHH-4 and MREV-8 sequences

One of the first line-narrowing sequences proposed was the WHH cycle [60] shown in Fig. 4.25. The dipolar Hamiltonian[16] starts in the form given by eqn 4.53. The trick

[16]We mean here the secular part, denoted $\mathcal{H}_D^0$ in eqn 4.53.

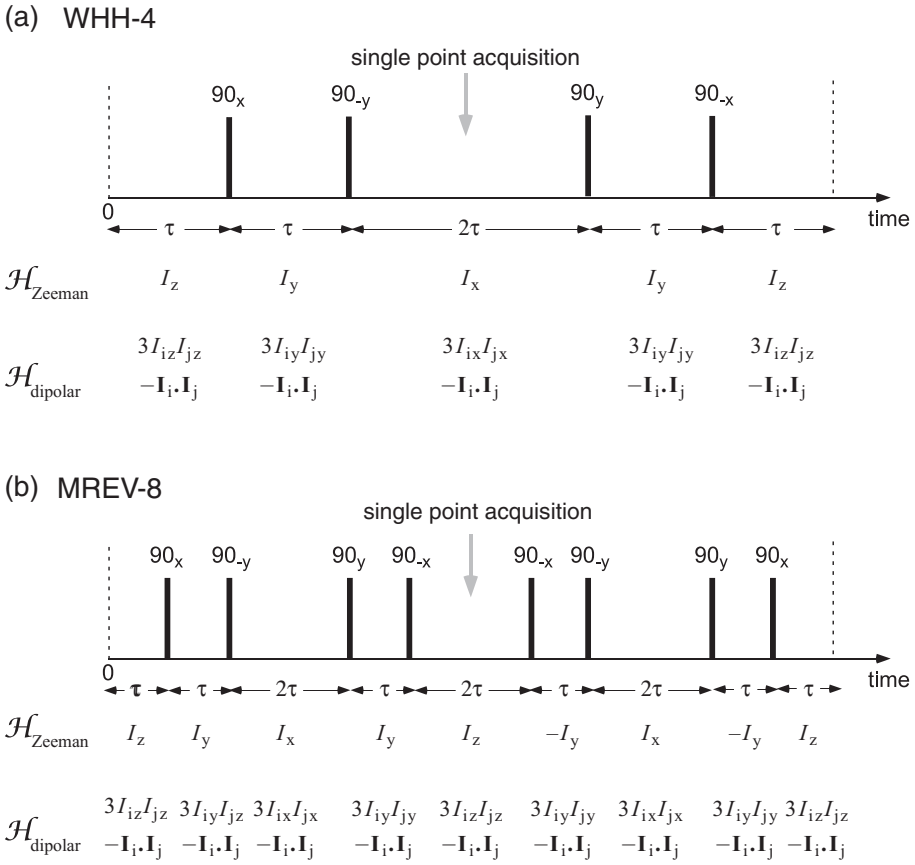

Fig. 4.25 Pulse sequences for (a) WHH-4 and (b) MREV-8 dipolar line-narrowing. The states of the Zeeman and dipolar Hamiltonians are shown below each respective precession frequency. The averaged $\mathcal{H}_{dipolar}$ is zero in both sequences, while the averaged Zeeman Hamiltonian is $\frac{1}{3}\Delta\omega_0(I_x + I_y + I_z) = \frac{1}{\sqrt{3}}\Delta\omega_0 I'_z$ for WHH-4 and $\frac{1}{3}\Delta\omega_0(I_x + I_y) = \frac{\sqrt{2}}{3}\Delta\omega_0 I''_z$ for MREV-8.

involved in this cycle is to cause the $I_{iz}I_{jz}$ terms in $\mathcal{H}_D$ to progressively change to $I_{iy}I_{jy}$ then $I_{ix}I_{jx}$ then $I_{iy}I_{jy}$, returning to $I_{iz}I_{jz}$ at the end of the cycle. Of course the term $\mathbf{I}_i \cdot \mathbf{I}_j$ is invariant under the rotations caused by the pulses.

The zeroth-order average Hamiltonian term, $\overline{\mathcal{H}}_D^{(0)}$, will vanish according to eqn 4.96 if the respective times spent in these states is τ, τ, 2τ, τ, and τ. Note that because of the evolution matrix order reversal represented by eqn 4.91, the effect of the RF pulses on the angular momentum operators I_{iz}, etc, must also be calculated in reverse order. For the WHH sequence the RF pulses are antisymmetric such that pulse 4 is the inverse of pulse 1 and pulse 3 is the inverse of pulse 3. The piecewise constant $\mathcal{H}^*_{D_k}$ terms are therefore

$$\begin{aligned}
\mathcal{H}^*_{D_1} &= \mathcal{H}_D \\
\mathcal{H}^*_{D_2} &= U^{-1}_{RF}(1)\mathcal{H}_D U_{RF}(1) \\
\mathcal{H}^*_{D_3} &= U^{-1}_{RF}(1)U^{-1}_{RF}(2)\mathcal{H}_D U_{RF}(2)U_{RF}(1) \\
\mathcal{H}^*_{D_4} &= U^{-1}_{RF}(1)U^{-1}_{RF}(2)U^{-1}_{RF}(3)\mathcal{H}_D U_{RF}(3)U_{RF}(2)U_{RF}(1) \\
&= U^{-1}_{RF}(1)\mathcal{H}_D U_{RF}(1) \\
\mathcal{H}^*_{D_5} &= U^{-1}_{RF}(1)U^{-1}_{RF}(2)U^{-1}_{RF}(3)U^{-1}_{RF}(4)\mathcal{H}_D U_{RF}(4)U_{RF}(3)U_{RF}(2)U_{RF}(1) \\
&= \mathcal{H}_D
\end{aligned} \tag{4.97}$$

So far we have considered the Hamiltonian in the rotating frame to be dominated by the secular part of the dipolar interaction. If this is largely removed by multiple pulse line-narrowing then the weaker chemical shift terms can be revealed. Of course these terms will also be affected by the RF pulse train, but because the symmetry of the Zeeman and dipolar interactions differ, the average Hamiltonian is not necessarily zero. Writing the total (isotropic and anisotropic) chemical shift Hamiltonian, $\mathcal{H}_{CS}$, of eqn 4.48 as $\delta_{CS}I_z$ and including the effect of any resonant offset term, $\Delta\omega_0 I_z$, the total rotating-frame Zeeman Hamiltonian is

$$\mathcal{H}_Z = (\delta_{CS}I_z + \Delta\omega_0 I_z) \tag{4.98}$$

It is a simple exercise to show that $\overline{\mathcal{H}}^{(0)}_Z$ is $\frac{1}{3}(\delta_{CS} + \Delta\omega_0)(I_x + I_y + I_z)$, which results in a precession about a tilted axis I'_z in the rotating frame, with effective frequency $\frac{1}{\sqrt{3}}(\delta_{CS} + \Delta\omega_0)$. The chemical shift and resonance offset do not vanish under the WHH-4 sequence but are reduced by a factor of $\frac{1}{\sqrt{3}}$. Normally, in solid state samples, the chemical shift is 'buried' in the much larger dipolar linewidth. Where information about $\mathcal{H}_{CS}$ is sought in these systems, retention of the isotropic and anisotropic chemical shift, albeit somewhat attenuated, is a valuable feature of multiple pulse line-narrowing experiments.

The WHH-4 cycle does not remove $\overline{\mathcal{H}}^{(2)}_D$. Furthermore, it suffers from the effects of RF pulse imperfections. An noticeable improvement results from using an eight-pulse cycle such as the MREV-8 method proposed independently by Mansfield [61, 62] and by Rhim, Elleman, and Vaughan [63]. Although MREV-8 also does not remove $\overline{\mathcal{H}}^{(2)}_D$, it has the added advantage of being less adversely affected by the effects of finite RF pulse width, RF inhomogeneity, and pulse-phase deviations. This particular sequence is shown in Fig. 4.25. In the MREV-8 cycle, the chemical shift and resonance offsets are scaled by $\frac{\sqrt{2}}{3}$ in comparison with the $\frac{1}{\sqrt{3}}$ factor in WHH-4.

Note that a simple 'pulse and collect' experiment would involve the line-narrowing sequence being preceded by a preparation (excitation) RF pulse, but the WHH-4 or MREV-* train can be inserted in a variety of more complex pulse sequences, where removal of dipolar interactions is required.

4.6.4 Multiquantum pathways

In Chapter 3, the concept of multiple-quantum coherence was introduced. The importance of such coherences in the measurement of spin translational motion arises for

several reasons. First, the rate of Larmor precession in an applied magnetic field is determined by the coherence order p, so that by utilising higher-order coherences, a greater degree of phase migration can be acquired under magnetic field gradients, an effect we will discuss in greater detail in Chapter 11. Second, and of particular interest in the measurement of diffusion over long times, singlet states that combine zero-quantum coherence and longitudinal two-spin order can be generated, and these experience very long relaxation times, hence extending the timescale over which translational dynamics can be measured [64–66]. Finally, the selection of specific multiple-quantum coherence pathways in the evolution of the spin system, so-called 'multiple-quantum-filtering', can provide molecular selectivity based on spin interactions.

In the following sections we revisit multiple-quantum coherence in the context of the simple scalar-coupled two-spin system discussed earlier, outlining a simple way of visualising these coherences in terms of the energy level diagrams. We then turn to a brief discussion of the use of multiple quantum filtering in the selection of specific coherence pathways.

Multiple-quantum coherences in coupled spin systems

Let us analyse the scalar coupled two-spin problem discussed in Section 4.4.3 in the weak coupling limit, $Jh << \delta$. The energy levels of Fig. 4.12 can be simply represented in product state form as shown in Fig. 4.26, where we use the notation $\uparrow$ and $\downarrow$ to represent spin states $\frac{1}{2}$ and $-\frac{1}{2}$, respectively. For primary understanding, we write down the density matrix for the weakly coupled case as in eqn 4.99. The diagonal terms such as $\overline{a_{\uparrow\uparrow}a_{\uparrow\uparrow}*}$ simply represent the populations of the states and, following Levitt [18], we illustrate these as shown in part (a) of Fig. 4.26.

$$\begin{aligned}\rho &= \overline{\begin{bmatrix} a_{\uparrow\uparrow} \\ a_{\uparrow\downarrow} \\ a_{\downarrow\uparrow} \\ a_{\downarrow\downarrow} \end{bmatrix} \begin{bmatrix} a_{\uparrow\uparrow}* & a_{\uparrow\downarrow}* & a_{\downarrow\uparrow}* & a_{\downarrow\downarrow}* \end{bmatrix}} \\ &= \begin{bmatrix} \overline{a_{\uparrow\uparrow}a_{\uparrow\uparrow}*} & \overline{a_{\uparrow\uparrow}a_{\uparrow\downarrow}*} & \overline{a_{\uparrow\uparrow}a_{\downarrow\uparrow}*} & \overline{a_{\uparrow\uparrow}a_{\downarrow\downarrow}} \\ \overline{a_{\uparrow\downarrow}a_{\uparrow\uparrow}*} & \overline{a_{\uparrow\downarrow}a_{\uparrow\downarrow}*} & \overline{a_{\uparrow\downarrow}a_{\downarrow\uparrow}*} & \overline{a_{\uparrow\downarrow}a_{\downarrow\downarrow}} \\ \overline{a_{\downarrow\uparrow}a_{\uparrow\uparrow}*} & \overline{a_{\downarrow\uparrow}a_{\uparrow\downarrow}*} & \overline{a_{\downarrow\uparrow}a_{\downarrow\uparrow}*} & \overline{a_{\downarrow\uparrow}a_{\downarrow\downarrow}} \\ \overline{a_{\downarrow\downarrow}a_{\uparrow\uparrow}*} & \overline{a_{\downarrow\downarrow}a_{\uparrow\downarrow}*} & \overline{a_{\downarrow\downarrow}a_{\downarrow\uparrow}*} & \overline{a_{\downarrow\downarrow}a_{\downarrow\downarrow}} \end{bmatrix} \end{aligned} \tag{4.99}$$

These populations are responsible for states of z-magnetisation of the spin system, but are not directly observable in the receiver coil of the NMR apparatus. The NMR observable is the single quantum coherence, $p = -1$, represented by the terms $\overline{a_{\downarrow\uparrow}a_{\uparrow\uparrow}*}$, $\overline{a_{\downarrow\downarrow}a_{\downarrow\uparrow}*}$, $\overline{a_{\downarrow\downarrow}a_{\uparrow\downarrow}*}$, and $\overline{a_{\uparrow\downarrow}a_{\uparrow\uparrow}*}$, in which there exists a coherent superposition between up and down states of a single spin. Two examples of $p = \pm 1$ quantum coherences are shown in Fig. 4.26 (b), where the grey arrows indicate the coherence sign. The –1 quantum coherence involves a flip down of one spin. Notice that only one spin at a time is active, the direct detection probability for dual-spin processes being vanishingly small. In Table 3.4 these single-quantum coherences are identified by the spherical tensor operators, $T^1_{\pm 1}(10)$ and $T^1_{\pm 1}(01)$, with associated product operator forms $\mp\frac{1}{\sqrt{2}}I_{i\pm} \otimes \underline{\underline{1}}$ and $\mp\frac{1}{\sqrt{2}}\underline{\underline{1}} \otimes I_{j\pm}$.

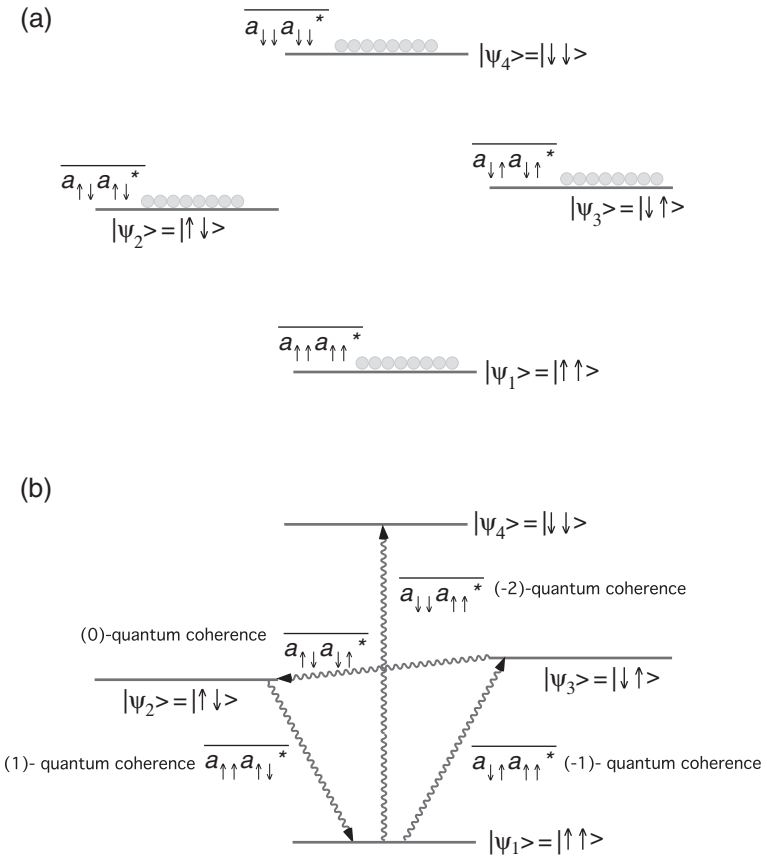

Fig. 4.26 Energy levels for scalar coupled spins in the weak coupling limit. (a) shows density matrix elements corresponding to populations (the four diagonal elements) while (b) shows a sample of multiple-quantum coherences.

Also shown in Fig. 4.26(b) is an example of a double-quantum coherence and a zero-quantum coherence. In practice, excitation of these coherent superposition states often involves the presence of two terms, for example a double-quantum coherence as $\overline{a_{\uparrow\uparrow}a_{\downarrow\downarrow}}* + \overline{a_{\downarrow\downarrow}a_{\uparrow\uparrow}}*$, or $[I_{i+}I_{j+} + I_{i-}I_{j-}]$, or a zero-quantum coherence as $\overline{a_{\uparrow\downarrow}a_{\downarrow\uparrow}}* - \overline{a_{\downarrow\uparrow}a_{\uparrow\downarrow}}*$, or $\frac{1}{\sqrt{2}}[I_{i-}I_{j+} - I_{i+}I_{j-}]$. Note that zero-quantum coherence is but one example of a $p = 0$ state, longitudinal one-spin magnetisation, I_{iz}, or longitudinal two-spin order, $I_{iz}I_{jz}$, being others.

States of the weakly coupled spin system in the product operator basis

In Chapter 2, the Liouville basis involving product operators of (I_{ix}, I_{iy}, I_{iz}) and (I_{jx}, I_{jy}, I_{jz}) was outlined, with details of the operator basis set given in Tables 3.4 and 3.5. Using this basis set, any states of the density matrix given in eqn 4.99 can be rewritten as a linear superposition of the operators from Tables 3.4 and 3.5. By

this means, the product operator basis provides a convenient language to describe the evolution of the coupled spin system.

In other words, rather than describe the spin system in terms of elements such as $\overline{a_{\downarrow\downarrow}a_{\downarrow\uparrow}*}$, this element could be re-expressed in terms of amplitudes of I_{jx}, I_{jy}, $I_{iz}I_{jx}$, and $I_{iz}I_{jy}$, as given in eqn 3.63. This product basis set can be conveniently represented pictorially, as shown by Sørensen [67] in the manner of Figs 4.26 and 4.27. The diagrams follow directly from Tables 3.4 and 3.5. States diagonal in the product operator basis are presented purely by population differences. Off-diagonal states are associated with coherences, and are represented pictorially by wavy lines, which are are solid or dashed depending on the phase of the coherence.

Multiple quantum filters

All NMR experiments starting from thermal equilibrium and ending with Faraday detection represent a transition from $p = 0$ to $p = -1$. The pathway by which this transition occurs may involve migrations through various orders of quantum coherence, depending on the actions of the spin Hamiltonian and the RF pulses [68]. In the case of uncoupled spins, quadrupolar interactions may permit the formation of coherences with $|p| > 1$, while spins coupled by the dipolar or scalar interaction may form not only $|p| > 1$ but zero-quantum coherences as well. By appropriate selection procedures it is possible to filter the evolution pathway so that only elements of the density matrix that have passed through a particular coherence state can contribute to the detected NMR signal. Such a process is known as multiple quantum filtering. The advantage of such a filter is that it permits the experimenter to screen out contributions to the signal that have not been directly associated with a particular spin Hamiltonian term. For example, a double quantum filter, in the case of a quadrupolar nucleus, will allow contributions only from spins that are experiencing non-zero quadrupole interactions, a signature for molecular ordering. Alternatively, a zero quantum filter or double quantum filter can be used to discriminate spins coupled by a bilinear interaction, such as the scalar coupling. More importantly, because the highest order of quantum coherence possible for K coupled spin-$\frac{1}{2}$ nuclei is K, a K-quantum filter acts as a spin-counting tool, allowing signals only from such a pool of interacting spins.

The standard trick used for coherence selection is the use of a phase cycle on the RF pulses [68]. Recall from eqn 3.65 that a rotation, the action of an RF pulse, may change the order but not the rank of a spherical tensor. Suppose we represent a sequence of RF pulses by evolution operators, U_i, so that each operator causes a transition of the density matrix of order p between different orders of coherence as

$$U_i\rho_p(t_{i-})U_i^{-1} = \sum_{p'} \rho_{p'}(t_{i+}) \tag{4.100}$$

where t_{i-} and t_{i+} refer to times just before and after the RF pulse evolution, respectively. For each evolution, the change in coherence order is Δp_i. The idea is illustrated schematically in Fig. 4.28. A phase shift ϕ_i in the ith RF pulse is represented by

$$U_i(\phi_i) = \exp(-i\phi_i \sum I_z)U_i(0)\exp(i\phi_i \sum I_z) \tag{4.101}$$

where $\sum I_z$ is the total z-component of angular momentum for the K coupled spins. According to eqn 3.54 we find

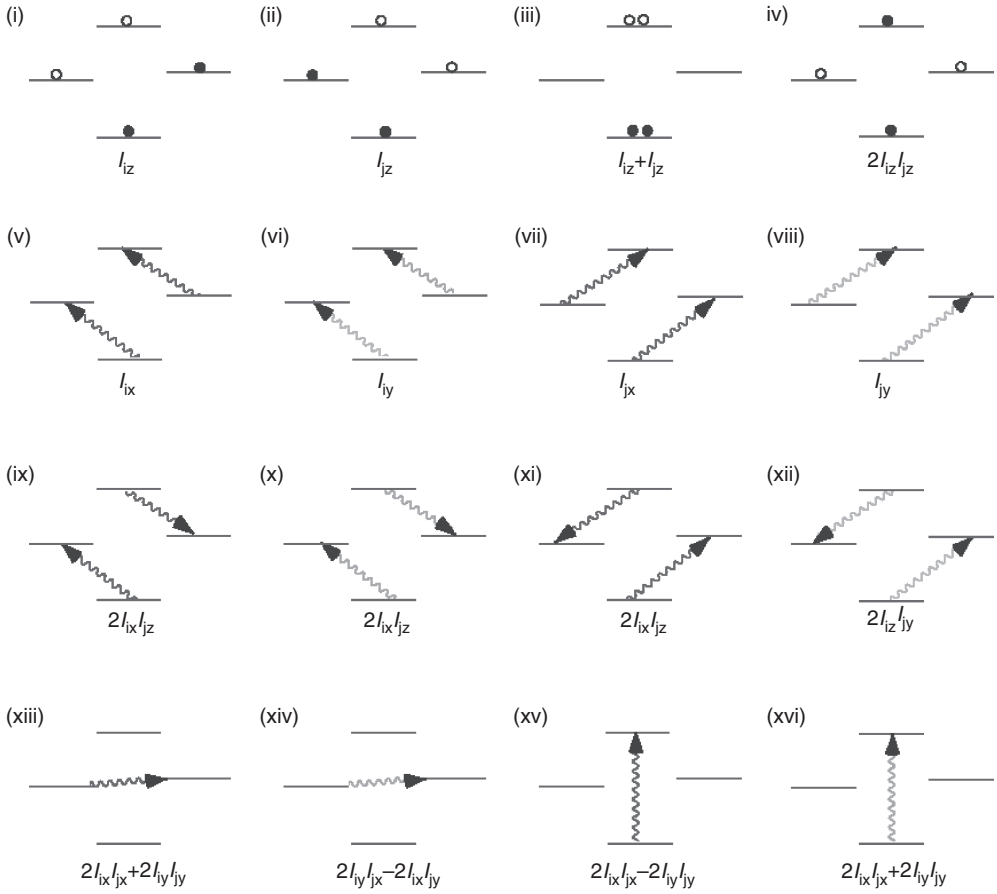

Fig. 4.27 (i) to (xii) Pictorial representations of product operators representing single quantum magnetisation and longitudinal magnetisation in a system of two coupled nuclei with $I = l/2$, after Sørensen *et al.* [67]. The x and y magnetisation components are represented by wavy lines in the energy-level diagram (dashed lines for y-components). Populations are represented by open symbols for states that are depleted, filled symbols for states that are more populated. (xiii) to (xvi) Linear combinations of product operators that represent pure zero and double-quantum coherence. The wavy lines are solid or dashed depending on the phase of the coherence. (Adapted from Sorensen *et al.* [67].)

$$U_i(\phi_i)\rho_p(t_{i-})U_i(\phi_i)^{-1} = \sum_{p'} \rho_{p'}(t_{i+}) \exp(-i\Delta p_i \phi_i) \tag{4.102}$$

These successive phase shifts are transmitted to the final signal.

Suppose we focus our attention on a particular RF pulse i and perform N_i experiments such that the phase for that pulse is successively incremented as

$$\phi_{k_i} = k_i 2\pi / N_i \tag{4.103}$$

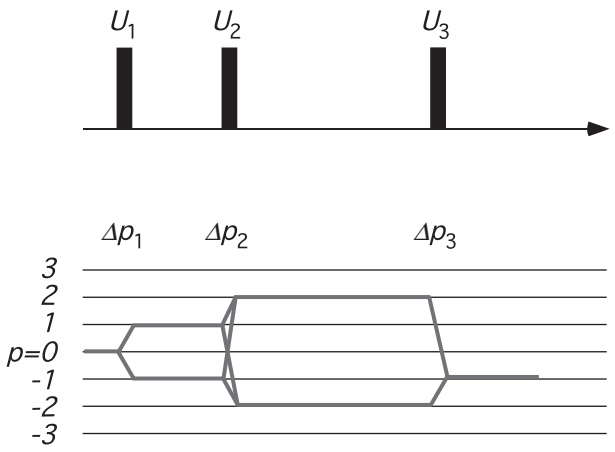

Fig. 4.28 Schematic representation of changes in coherence order during a multiple RF pulse experiment. The starting and finishing orders are $p = 0$ and $p = -1$, corresponding to thermal equilibrium magnetisation and detectable single-quantum coherence, respectively. At each RF pulse the change of coherence order is $\Delta p_i = p' - p$.

where k_i ranges from 0 to $N_i - 1$. Then if we sum the signal contributions, S_{k_i}, arising from each phase shift, each carries a phase term $\exp(-i\Delta p_i \phi_{k_i})$. Extracting the desired signal is done by a Fourier analysis as

$$S = \frac{1}{N_i} \sum_{k_i=0}^{N_i-1} S_{k_i} \exp(i\Delta p_i \phi_{k_i}) \tag{4.104}$$

Inclusion of the factor $\exp(i\Delta p_i \phi_i)$ on detection simply involves the multiplication of the signal by the appropriate complex number, in other words setting the acquisition phase. This cycle of RF pulse phase and acquisition phase selects coherence transfer pathways involving Δp_i for the ith RF pulse. To ensure a unique Δp_i is selected, N_i must at least be equal to the maximum number of changes in phase. Where the phases of each RF pulse are cycled, the successive phase change is represented by a vector, $\mathbf{\Delta p}$, where each component corresponds to an RF pulse. The basic principles of the selectivity process remain the same.

An alternative approach to multiple quantum filtering is to utilise the fact that the rate of Larmor precession of coherence order p is $p\Delta\omega$, where $\Delta\omega$ is the frequency of single-quantum coherence in the rotating frame. If a magnetic field gradient is applied, $\Delta\omega$ is spatially dependent so that, across the sample, a wide uniform distribution of phase shifts can be engendered, resulting in the sum of signal contributions being zero. This effect is known as 'homospoiling'. Since the rate of homospoiling depends on p, careful choice of gradient amplitude during the various time evolution periods of any pulse sequence can be used to select for multiple-quantum coherence order.

4.6.5 Multidimensional NMR

The complex NMR signal, $S(t)$, corresponding to coherence order $p = -1$, is collected at successive points of a time domain t. However, any pulse sequence involving more than one RF pulse contains other time intervals during which the spin density matrix may evolve. In 1971 Jean Jeener [69] suggested the possibility of using this evolution time as a second dimension for spectroscopy. The consequences of this suggestion have transformed NMR and magnetic resonance imaging (MRI) [14].

Suppose that some evolution time associated with a particular pulse sequence interval is varied in successive independent experiments so that each signal acquired now becomes a 2-D function of the evolution time t_1 and the acquisition time t_2. The idea can be extended to higher dimensions by inserting additional evolution intervals. By convention we always ascribe the highest index to the acquisition dimension, so that in 3-D spectroscopy, the two evolution dimensions are t_1 and t_2, while the acquisition dimension is t_3. Then, just as the 1-D FID, $S(t)$, can be Fourier transformed to yield a 1-D spectrum $s(\omega)$, so a 2-D array of time-domain data, $S(t_1, t_2)$ can be Fourier transformed to provide a 2-D spectrum $s(\omega_1, \omega_2)$, as

$$s(\omega_1, \omega_2) = \int_{-\infty}^{\infty} \int_{-\infty}^{\infty} S(t_1, t_2) \exp(i\omega_1 t_1) \exp(i\omega_2 t_2) dt_1 dt_2 \tag{4.105}$$

In the next chapter, where magnetic field gradients are discussed, we will see that phase evolution of the spin system can equally occur under the influence of field gradient pulses, where the equivalent to 'advancing the evolution time' will be 'advancing the gradient pulse area' [54]. In this case the Fourier spectrum directly relates to the distribution of physical displacements, in other words, the magnetic resonance image.

The schematic for a 2-D NMR spectroscopy experiment is shown in Fig. 4.29, in which separate preparation, evolution, mixing, and detection intervals are identified. The experiment is performed by collecting a succession of FIDs, sampled over time variable t_2, for a sequence of different evolution times t_1, so as to produce a 2-D matrix of time-domain data with rows labelled by t_2 and columns by t_1. This matrix may be Fourier transformed to give a 2-D spectrum. with rows labelled by f_2 and columns by f_1. Note that the preparation period is used to prepare the state of coherence whose evolution is desired to be investigated during the period t_1. While the mixing segment of the pulse sequence must be used to ultimately transform the coherence back to the detectable $p = -1$, it may also allow for possible storage of magnetisation before ultimate recall for detection.

The process of obtaining a phased 2-D spectrum is a little more subtle than in the case of 1-D NMR. In particular, if the evolution and acquisition contributions to the signal each generate a dispersive component, then absorption and dispersion become 'twisted together' in the 2-D spectrum, the real and imaginary parts of the 2-D spectrum both containing absorptive and dispersive parts, thus making the the process of 'phasing the spectrum' in 2-D intractable [18]. There are various means of avoiding this problem, for example acquiring a complete echo signal in the acquisition domain, comprising both negative and positive time intervals, avoids dispersion in acquisition. Alternatively, by a clever sampling in the evolution domain in which 1-D spectra from

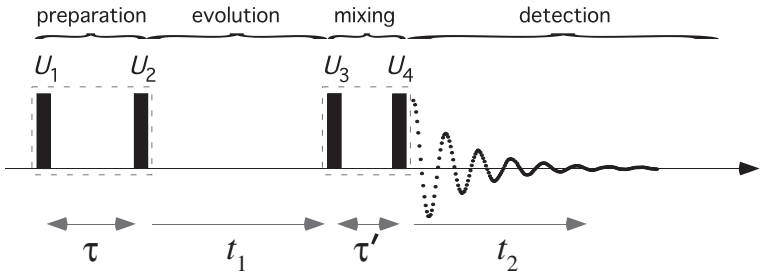

Fig. 4.29 Schematic representation of a 2-D NMR experiment. The preparation period in the first dashed box is represented, for simplicity, by two RF pulses with evolution operations U_1 and U_2 separated by time period τ. The first of these would normally be a 90° RF pulse. The period marked 'evolution' is the particular evolution singled out to be the variable time period, separate experiments being performed at different values of t_1. During the mixing period, the spin system goes through a further evolution, perhaps a transfer of coherence, or simply kept 'on hold' by storage as z-magnetisation, before the final recall as $p = -1$ coherence and FID detection over the time variable t_2.

separate cosine and sine amplitude modulations are subsequently combined to form a complex signal, dispersion twist can be avoided at the second Fourier transform. These matters are discussed in a number of texts dealing with NMR spectroscopy [14, 18] and will not be commented on further here.

The power of multidimensional NMR spectroscopy is that two or more spectroscopic domains allow for the correlation of different spectral properties or for the measurement of how certain spectral properties change under time. These two possibilities are known as correlation and exchange spectroscopy, respectively. And most importantly for this book, the analysis of the time-dependencies of the two domains need not involve Fourier transformation alone. In particular, where the signal behaviour under time advance is an exponential decay, as in relaxation, as opposed to an oscillation arising from spin Hamiltonian terms, then the more appropriate means of analysis may be inverse Laplace transformation. Multidimensional inverse Laplace spectroscopy is discussed in Chapter 10.

Exchange spectroscopy

In a 2-D exchange experiment, two identical evolution processes on the same identically prepared spin system are compared after allowing for an interval between the evolution in which spin magnetisation is kept 'in storage'. This storage interval is known as the mixing time τ_m, and the purpose of the exchange experiment is to determine if some spectral property changes with time. It is therefore a probe of geometric or structural dynamics of molecules or molecular assemblies [14].

Figure 4.30 shows an example of a simple exchange spectroscopy pulse sequence in the case of a spectrum comprising two lines, each of which corresponds to sites which chemically exchange. Below the pulse sequence are representations of the 2-D matrices for the time and frequency domain, in the first case where the mixing time

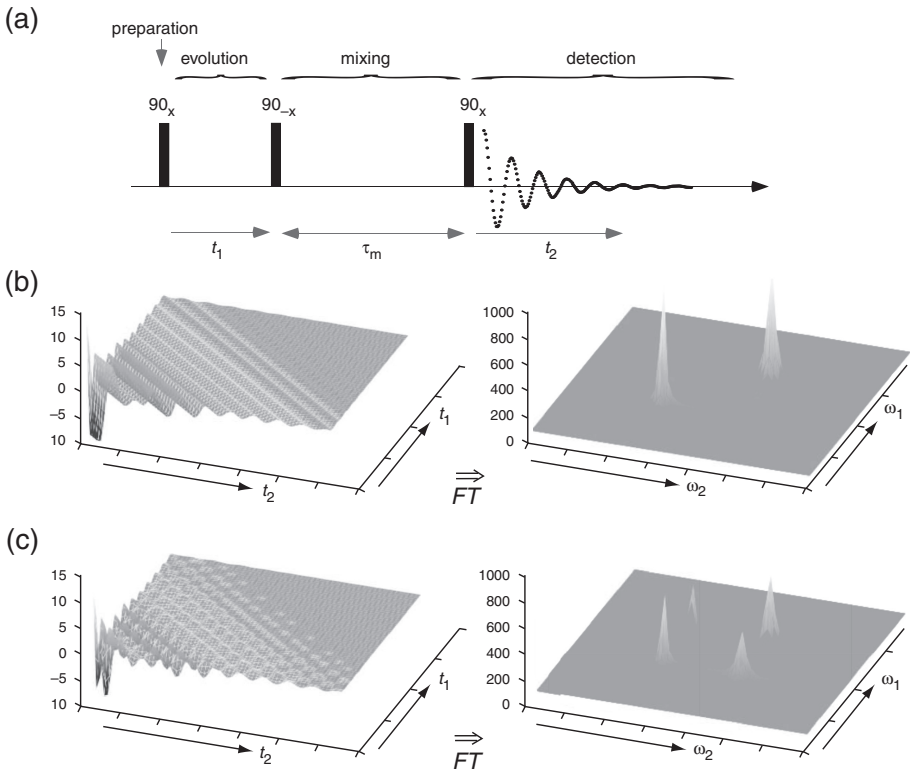

Fig. 4.30 (a) Pulse sequence for a simple 2-D exchange spectroscopy experiment in which the transverse magnetisation produced by a 90°_x RF pulse is allowed to evolve in the spin Hamiltonian during the evolution interval t_1, before being stored along the z-axis for later recall after a mixing time τ_m. (b) The time-domain data and frequency-domain 2-D spectrum for a system with two frequencies associated with sites A and B, for which τ_m is sufficiently short that no exchange between A and B occurs. (c) For longer τ_m with exchange evident as off-diagonal peaks in the 2-D spectrum.

is short compared with the exchange time, and in the second where the times are comparable. The appearance of off-diagonal peaks in the 2-D spectrum is the indication that site exchange has occurred. Such exchange experiments can be generalised to any spectral property indicative of chemical site, translational position, or orientation, where changes in site occupancy, position, or orientation lead to a spectral change. In each case the evolution and detection components of the pulse sequence must be tailored to the desired spectral feature.

Correlation spectroscopy

The purpose of a multidimensional correlation experiment is to reveal proximity or connectivity between specific nuclei in the NMR spectrum [14]. These connectivities might be, for example, carbon–proton direct bonding (heteronuclear single-quantum

coherence spectroscopy—HSQC), protons experiencing inter-nuclear through-space dipolar interactions (nuclear Overhauser effect spectroscopy—NOESY) or protons experiencing inter-nuclear J-couplings (correlation spectroscopy—COSY). The last of these was first proposed by Jeener and first performed by Aue, Bartholdi, and Ernst in 1976. It is instructive to look at this experiment in a little more detail.

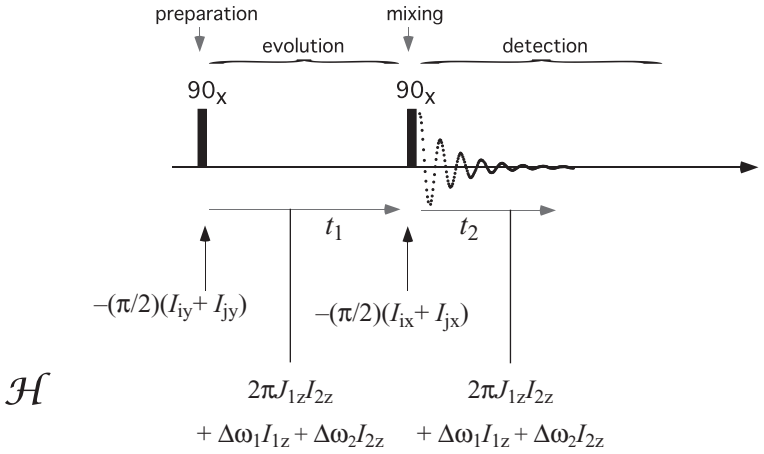

Fig. 4.31 Pulse sequence for a simple 2-D COSY spectroscopy experiment in which the transverse magnetisation produced by a 90°_x RF pulse is allowed to evolve in the spin Hamiltonian during the evolution interval t_1 before a second 90°_x RF pulse mixes and transforms coherences before a final detection period.

The COSY experiment is easy to understand in the weak coupling case represented by eqn 4.49. Here the scalar interaction is represented by $2\pi J I_{1z} I_{2z}$, and we naturally use the standpoint of the product operator formalism with the precession diagrams shown in Fig. 4.23. The scalar interaction causes precession of the initial I_{1y} state of the density matrix into $I_{1x}I_{2z}$ and hence a dephasing of I_{2y} into an admixture $-I_{2y}\cos(\pi J t_1) + 2I_{1x}I_{2z}\sin(\pi J t_1)$. Hence

$$
\begin{aligned}
&I_{1z} + I_{2z} \\
&\xrightarrow{-(\pi/2)(I_{1x}+I_{2x})} && I_{1y} + I_{2y} \\
&\xrightarrow{2\pi J I_{1z} I_{2z}} && (I_{1y} + I_{2y})\cos(\pi J t_1) - (2I_{1x}I_{2z} + 2I_{1z}I_{2x})\sin(\pi J t_1) \\
&\xrightarrow{\Delta\omega_1 I_{1z} + \Delta\omega_2 I_{2z}} && [I_{1y}\cos(\Delta\omega_1 t_1) + I_{1x}\sin(\Delta\omega_1 t_1) \\
& && +I_{2y}\cos(\Delta\omega_2 t_1) + I_{2x}\sin(\Delta\omega_2 t_1)]\cos(\pi J t_1) \\
& && -[2(I_{1x}\cos(\Delta\omega_1 t_1) - I_{1y}\sin(\Delta\omega_1 t_1))I_{2z} \\
& && +2I_{1z}(I_{2x}\cos(\Delta\omega_2 t_1) - I_{2y}\sin(\Delta\omega_2 t_1))]\sin(\pi J t_1) \\
&\xrightarrow{-(\pi/2)(I_{1x}+I_{2x})} && [-I_{1z}\cos(\Delta\omega_1 t_1) + I_{1x}\sin(\Delta\omega_1 t_1) \\
& && -I_{2z}\cos(\Delta\omega_2 t_1) + I_{2x}\sin(\Delta\omega_2 t_1)]\cos(\pi J t_1)
\end{aligned}
$$

$$
\begin{aligned}
&-[2(I_{1x}\cos(\Delta\omega_1 t_1)+I_{1z}\sin(\Delta\omega_1 t_1))I_{2y}\\
&+2I_{1y}(I_{2x}\cos(\Delta\omega_2 t_1)+I_{2z}\sin(\Delta\omega_2 t_1))]\sin(\pi J t_1)\\
\xrightarrow{retaining\ detectable}\ &[I_{1x}\sin(\Delta\omega_1 t_1)+I_{2x}\sin(\Delta\omega_2 t_1)]\cos(\pi J t_1)\\
&-[2I_{1z}I_{2y}\sin(\Delta\omega_1 t_1)+2I_{1y}I_{2z}\sin(\Delta\omega_2 t_1)]\sin(\pi J t_1)\\
\xrightarrow{2\pi J I_{1z}I_{2z}}\ &[I_{1x}\sin(\Delta\omega_1 t_1)+I_{2x}\sin(\Delta\omega_2 t_1)]\cos(\pi J t_1)\cos(\pi J t_2)\\
&+[2I_{1y}I_{2z}\sin(\Delta\omega_1 t_1)+2I_{1z}I_{2y}\sin(\Delta\omega_2 t_1)]\cos(\pi J t_1)\sin(\pi J t_2)\\
&-[2I_{1z}I_{2y}\sin(\Delta\omega_1 t_1)+2I_{1y}I_{2z}\sin(\Delta\omega_2 t_1)]\sin(\pi J t_1)\cos(\pi J t_2)\\
&+[I_{2x}\sin(\Delta\omega_1 t_1)+I_{1x}\sin(\Delta\omega_2 t_1)]\sin(\pi J t_1)\sin(\pi J t_2)\\
\xrightarrow{retaining\ detectable}\ &[I_{1x}\sin(\Delta\omega_1 t_1)+I_{2x}\sin(\Delta\omega_2 t_1)]\cos(\pi J t_1)\cos(\pi J t_2)\\
&+[I_{2x}\sin(\Delta\omega_1 t_1)+I_{1x}\sin(\Delta\omega_2 t_1)]\sin(\pi J t_1)\sin(\pi J t_2)\\
\xrightarrow{\Delta\omega_1 I_{1z}+\Delta\omega_2 I_{2z}}\ &[I_{1x}\sin(\Delta\omega_1 t_1)\cos(\Delta\omega_1 t_2)-I_{1y}\sin(\Delta\omega_1 t_1)\sin(\Delta\omega_1 t_2)\\
&+I_{2x}\sin(\Delta\omega_2 t_1)cos(\Delta\omega_2 t_2)-I_{2y}\sin(\Delta\omega_2 t_1)\sin(\Delta\omega_2 t_2)]\\
&\times\cos(\pi J t_1)\cos(\pi J t_2)\\
&+[I_{2x}\sin(\Delta\omega_1 t_1)\cos(\Delta\omega_2 t_2)+I_{1x}\sin(\Delta\omega_2 t_1)\cos(\Delta\omega_1 t_2)\\
&-I_{2y}\sin(\Delta\omega_1 t_1)\sin(\Delta\omega_2 t_2)-I_{1y}\sin(\Delta\omega_2 t_1)\sin(\Delta\omega_1 t_2)]\\
&\times\sin(\pi J t_1)\sin(\pi J t_2)
\end{aligned}
\tag{4.106}
$$

Note that the 'retaining detectable' steps involve removing those density matrix terms that are unable to return to observable single-quantum coherence ($p = -1$) under the spin Hamiltonian. The final terms that remain neatly divide into two parts. The first three lines involve diagonal components (ω_1, ω_1) and (ω_2, ω_2) of the spectrum, since spin 1 experiences $\Delta\omega_1$ during both the evolution (t_1) and detection (t_2) periods, while spin 2 experiences only $\Delta\omega_2$. The second three terms have spin 1 experiencing $\Delta\omega_2$ during the evolution period and $\Delta\omega_1$ during detection, with similar crossing over for spin 2. These terms lead to off-diagonal peaks at (ω_1, ω_2) and (ω_2, ω_1) and are a direct consequence of the scalar coupling between spins 1 and 2. The point in the pulse sequence at which the magnetisation transfer occurs between the two sets of spins is the mixing step associated with the second RF pulse.

References

[1] C. J. Gorter. Negative result of an attempt to detect nuclear magnetic spins. *Physica*, 3:995, 1936.

[2] C. J. Gorter and L. J. F. Broer. Negative result of an attempt to observe nuclear magnetic resonance in solids. *Physica*, 9:591, 1942.

[3] J. S. Rigden. *Rabi, Scientist and Citizen*. Sloan Foundation Series: Basic Books, New York, 1987.

[4] I. I. Rabi, J.R. Zacharias, S. Millman, and P. Kusch. A new method of measuring nuclear magnetic moment. *Phys. Rev.*, 53:318, 1938.

[5] N. F. Ramsey. Early history of magnetic resonance. *Bulletin of Magnetic Resonance*, 7:95, 1985.

[6] E. K. Zavoisky. Paramagnetic absorption for solutions in parallel fields. *Zhurn. Eksperiment. Teoret. Fiziki*, 15:253, 1945.
[7] F. Bloch, W. Hansen, and M. E. Packard. Nuclear induction. *Phys. Rev.*, 69:127, 1946.
[8] E. M. Purcell, H. G. Torrey, and R. V. Pound. Resonant absorption by nuclear magnetic moments in a solid. *Phys. Rev.*, 69:37, 1946.
[9] A. Abragam. *Principles of Nuclear Magnetism.* Clarendon Pres, Oxford, 1961.
[10] C. P. Slichter. *Principles of Magnetic Resonance (3rd edition).* Springer, New York, 1996.
[11] T. C. Farrar and E. D. Becker. *Pulse and Fourier Transform NMR.* Elsevier, Amsterdam, 1971.
[12] M. Mehring. *High Resolution NMR in Solids.* Springer, Berlin, 1982.
[13] A. Bax. *Two-Dimensional Nuclear Magnetic Resonance in Liquids.* Delft University Press, Dordrect, 1984.
[14] R. R. Ernst, G. Bodenhausen, and A. Wokaun. *Principles of Nuclear Magnetic Resonance in One and Two Dimensions.* Clarendon Press, Oxford, 1987.
[15] M. Munowitz. *Coherence and NMR.* Wiley-Interscience,New York, 1988.
[16] M. Goldman. *Quantum Description of High-Resolution NMR in Liquids.* Oxford University Press, New York, 1999.
[17] E. D. Becker. *High Resolution NMR: Theory and Chemical Applications (3rd edition).* Academic Press, New York, 1999.
[18] M. H. Levitt. *Spin Dynamics (2nd edition).* Wiley, New York, 2008.
[19] E. L. Hahn. Spin echoes. *Phys. Rev.*, 77:746, 1950.
[20] N. Bloembergen, E. M. Purcell, and R. V. Pound. Relaxation effects in nuclear magnetic resonance absorption. *Phys. Rev.*, 73:679, 1948.
[21] F. Bloch. Nuclear induction. *Phys. Rev.*, 70:460, 1946.
[22] F. Bloch and R. K. Wangsness. The differential equations of nuclear induction. *Phys. Rev.*, 78:82, 1950.
[23] H. C. Torrey. Bloch equations with diffusion terms. *Phys. Rev.*, 104:563, 1956.
[24] N. Q. Fan, M. B. Heney, J. Clarke, D. Newitt, L. L. Waard, E. L. Hahn, A. Bielecki, and A. Pines. Nuclear magnetic resonance with DC squid preamplifiers. *IEEE Transactions on Magnetics*, 25:1193, 1989.
[25] R. McDermott, A. H. Trabesinger, M. Muck, E. L. Hahn, A. Pines, and J. Clarke. Liquid-state NMR and scalar couplings in microtesla magnetic fields. *Science*, 295:2247, 2002.
[26] V. V. Yashchuk, J. Granweh, D. F. Kimball, S. M. Rochester, A. H. Trabesinger, J. T. Urban, D. Budker, and A. Pines. Hyperpolarized Xenon nuclear spins detected by optical atomic magnetometry. *Phys. Rev. Lett.*, 93:160801, 2004.
[27] S. J. Xu, V. V. Yashchuk, M. H. Donaldson, S. M. Rocheste, D. Budker, and A. Pines. Magnetic resonance imaging with an optical atomic magnetometer. *PNAS*, 103:12668, 2006.
[28] A. Abragam, M. A. H. McCausland, and F. N. H. Robinson. Dynamic nuclear polarization. *Phys. Rev. Lett.*, 2:449, 1959.
[29] T. Maly, G. T. Debelouchina, V. S. Bajaj, S. Vikram, K. N. Hu, C. G. Joo, M. L. Mak-Jurkauskas, J. R. Sirigiri, R. Jagadishwar, P. C. A. van der Wel, J. Herzfeld,

R. J. Temkinand, and R. G. Griffin. Dynamic nuclear polarization. *J. Chem. Phys.*, 128:052211, 2008.
[30] W. Happer. Optical pumping. *Rev. Mod. Phys.*, 44:169, 1972.
[31] B. C. Grover. Noble gas NMR detection through noble gas rubidium hyperfine contact interaction. *Phys. Rev. Lett.*, 40:391, 1978.
[32] D. Raftery, H. Long, T. Meersmann, P. J. Grandinetti, L. Reven, and A. Pines. High field NMR of absorbed xenon polarized by laser pumping. *Phys. Rev. Lett.*, 66:584, 1991.
[33] W. C. Proctor and F. C. Yu. The dependence of a nuclear magnetic resonance frequency on a chemical compound. *J. Chem. Phys.*, 484:3831, 1968.
[34] W. C. Dickinson. Dependence of the ^{19}F nuclear resonance position on chemical compound. *Phys. Rev.*, 77:736, 1968.
[35] L. A. Madsen, T. J. Dingemans, M. Nakata, and E. T. Samulski. Thermotropic biaxial nematic liquid crystals. *Phys. Rev. Lett.*, 92:145505, 2004.
[36] Z. Luz and S. Meiboom. Nuclear magnetic resonance studnmies of smectic liquid crystals. *J.Chem. Phys.*, 59:275, 1973.
[37] D. Wolf. *Spin-Temperature and Nuclear-Spin Relaxation in Matter.* Clarendon Press, Oxford, 1979.
[38] R. Lenk. *Fluctuations, Diffusion, and Spin Relaxation.* Elsevier, Amsterdam, 1986.
[39] B. Cowan. *Nuclear Magnetic Resonance and Relaxation.* Cambridge University Press, Cambridge, 2005.
[40] J. Kowalewski and L. Maler. *Nuclear Spin Relaxation in Liquids.* CRC Press, New York, 2006.
[41] D. C. Look and I. J. Lowe. Nuclear magnetic dipole-dipole relaxation along static and rotating magretic field-application to gypsum. *J. Chem. Phys.*, 44:2995, 1966.
[42] L. C. Hebel and C. P. Slichter. Nuclear spin relaxation in normal and superconducting aluminium. *Phys. Rev.*, 113:1504, 1959.
[43] P. W. Anderson and P. R. Weiss. Exchange narrowing in paramagnetic resonance. *Rev. Mod. Phys.*, 25:269, 1953.
[44] H. Y. Carr and E. M. Purcell. Effects of diffusion on free prcession in nuclear magnetic resonance experiments. *Phys. Rev..*, 94:630, 1954.
[45] S. Meiboom and D. Gill. Modified spin echo method for measuring nuclear relaxation times. *Rev. Sci. Instr.*, 29:688, 1958.
[46] L. K. Wanlass and J. Wakabaya. Stimulated spin echo measurement of cross relaxation times in neutron-irradiated calcite. *Phys. Rev. Lett.*, 6:271, 1961.
[47] R. Freeman and H. D. W. Hill. Fourier transform study of NMR spin-lattice relaxation by progressive saturation. *J. Chem. Phys.*, 54:3367, 1971.
[48] H. Y. Carr. Steady state free precession in nuclear magnetic resonance. *Phys. Rev.*, 112:1693, 1958.
[49] D. I. Hoult and R. E. Richards. Critical factors in design of sensitive high-resolution nuclear magnetic resonance spectrometers. *Proc. Roy. Soc. Series A*, 344:311, 1975.
[50] C. J. Turner and S. L. Patt. Artifacts in 2D NMR. *J. Magn. Reson.*, 85:492, 1989.
[51] R. L. Vold, J. S. Waugh, M. P. Klein, and D. E. Phelps. Measurement of spin relaxation in complex systems. *J. Chem. Phys.*, 484:3831, 1968.

[52] P. J. Hore. Solvent suppression in Fourier transform nuclear magnetic resonance. *J. Magn. Reson.*, 55:283, 1983.

[53] D. M. Doddrell, G. J. Galloway, W. M. Brooks, J. Field, J. M. Bulsing, M. G. Irving, and H. Baddeley. Water signal elimination in vivo using suppression by mistimed echo and repetitive gradient episodes. *J. Magn. Reson.*, 70:176, 1986.

[54] P. T. Callaghan. *Principles of Nuclear Magnetic Resonance Microscopy.* Oxford, New York, 1991.

[55] E. L. Hahn and D. E. Maxwell. Spin echo measurements of nuclear spin-spin coupling. *Phys. Rev.*, 85:7621, 1952.

[56] H. S. Gutowsky, D. W. McCall, and C. P. Slichter. Nuclear magnetic resonance multiplets in liquids. *J. Chem. Phys.*, 21:279, 1953.

[57] E. D. Ostroff and J. S. Waugh. Multiple spin echoes and spin-locking in solids. *Phys. Rev. Lett.*, 16:1097, 1966.

[58] P. Mansfield and D. Ware. Nuclear resonance line narrowing in solids by repeated short pulse RF irradiation. *Phys. Lett.*, 22:133, 1966.

[59] U. Haeberlen and J. S. Waugh. Coherent averaging effects in magnetic resonance. *Phys. Rev.*, 175:453, 1968.

[60] J. S. Waugh, L. M. Huber, and U. Haeberlen. Approach to high-resolution NMR in solids. *Phys. Rev. Lett.*, 20:180, 1968.

[61] P. Mansfield. Symmetrized pulse sequences in high resolution NMR in solids. *J. Phys. C*, 4:1444, 1971.

[62] P. Mansfield, M. J. Orchard, D. C. Stalker, and K. H. B. Richards. Symmetrized multipulse nuclear-magnetic-resonance experiments in solids—measurement of chemical shift shielding tensor in some compounds. *Phys. Rev. B*, 7:90, 1973.

[63] W. K. Rhim, D. D. Elleman, and R. W. Vaughan. Analysis of multiple pulse NMR in solids. *J. Chem. Phys.*, 59:3740, 1973.

[64] M. Carravetta, O. G. Johannessen, and M. H. Levitt. Beyond the t_1 limit: singlet nuclear spin states in low magnetic fields. *Phys. Rev. Lett.*, 92:153003, 2004.

[65] R. Sarkar, P. R. Vasos, and G. Bodenhausen. Singlet-state exchange NMR spectroscopy for the study of very slow dynamic processes. *J. Am. Chem. Soc.*, 129:328, 2007.

[66] R. Sarkar, P. Ahuja, P. R. Vasos, and G. Bodenhausen. Measurement of slow diffusion coefficients of molecules with arbitrary scalar couplings via long-lived spin states . *Chem. Phys. Chem.*, 9:2414, 2008.

[67] O. W. Sørensen, G. W. Eich, M. H. Levitt, G. Bodenhausen, and R. R. Ernst. Product operator formalism for the description of NMR pulse experiments. *Progress in NMR Spectroscopy*, 16:163, 1983.

[68] G. Bodenhausen, H. Kogler, and R. R. Ernst. Selection of coherence-transfer pathways in NMR pulse experiments. *J. Magn. Reson.*, 85:370, 1984.

[69] J. Jeener. *Ampere International Summer School.* Basko Polje, Yugoslavia, 1971.